

# Extended Skyrme effective interactions with higher-order momentum-dependence for transport models and neutron stars

Si-Pei Wang,<sup>1</sup> Xin Li,<sup>1,2</sup> Rui Wang,<sup>3</sup> Jun-Ting Ye,<sup>1</sup> and Lie-Wen Chen<sup>1,\*</sup>

<sup>1</sup>*School of Physics and Astronomy, Shanghai Key Laboratory for Particle Physics and Cosmology, and Key Laboratory for Particle Astrophysics and Cosmology (MOE), Shanghai Jiao Tong University, Shanghai 200240, China*

<sup>2</sup>*College of Physics, Henan Normal University, Xinxiang 453007, China*

<sup>3</sup>*Istituto Nazionale di Fisica Nucleare (INFN), Sezione di Catania, I-95123 Catania, Italy*

(Dated: April 18, 2025)

The recently developed extended Skyrme effective interaction based on the so-called N3LO Skyrme pseudopotential is generalized to the general  $Nn$ LO case by incorporating the derivative terms up to  $2n$ th-order into the central term of the pseudopotential. The corresponding expressions of Hamiltonian density and single-nucleon potential are derived within the Hartree-Fock approximation under general nonequilibrium conditions. The inclusion of the higher-order derivative terms provides additional higher-order momentum dependence for the single-nucleon potential, and in particular, we find that the N5LO single-nucleon potential with momentum dependent terms up to  $p^{10}$  can give a nice description for the empirical nucleon optical potential up to energy of 2 GeV. At the same time, the density-dependent terms in the extended Skyrme effective interaction are extended correspondingly in the spirit of the Fermi momentum expansion, which allows highly flexible variation of density behavior for both the symmetric nuclear matter equation of state and the symmetry energy. Based on the Skyrme pseudopotential up to N3LO, N4LO and N5LO, we construct a series of interactions with the nucleon optical potential having different high-momentum behaviors and with the symmetry potentials featuring different linear isospin-splitting coefficients for nucleon effective mass, by which we study the properties of nuclear matter and neutron stars. Furthermore, within the lattice BUU transport model, some benchmark simulations with selected interactions are performed for the Au+Au collisions at a beam energy of 1.23 GeV/nucleon, and the predicted collective flows for protons are found to nicely agree with the data measured by HADES collaboration.

## I. INTRODUCTION

The equation of state (EOS) of dense nuclear matter, which is directly related to the in-medium effective nuclear interactions, is of fundamental importance for both nuclear physics and astrophysics [1–8]. In the past four decades, the EOS of symmetric nuclear matter (SNM) from nuclear saturation density  $\rho_0$  to suprasaturation density of about  $5\rho_0$  has been relatively well constrained, based on analyses on the data from the giant monopole resonance in finite nuclei [9–14] as well as the measurements of collective flow [3, 15] and kaon production [16–19] in high energy heavy-ion collisions (HICs). For the symmetry energy  $E_{\text{sym}}(\rho)$ , which characterizes the isospin dependent part of the EOS for asymmetric nuclear matter (ANM), significant progress has been made in constraining its density dependence around and below the nuclear saturation density  $\rho_0$  by analyzing finite nuclei properties [20–32], isospin probes in HICs at energies less than about 100 MeV/nucleon [33–40] and microscopic many-body calculations (see, e.g., Refs. [41–45]), but its high density behavior remains elusive. In recent years, many works have been devoted to constraining the high density behavior of the symmetry energy by using the multimessenger data, especially the simultaneous determination of the mass and radius of neu-

tron stars by NICER as well as the gravitational wave observation in binary neutron star merger, but the uncertainty of the constraints is still very large [46–53]. Dense neutron-rich nuclear matter can be present or produced in neutron-rich nuclei, heavy-ion collisions (HICs) induced by neutron-rich nuclei, neutron stars and their mergers, as well as in core-collapse supernovae. The ongoing accumulation of experimental data from radioactive beam facilities around the world, together with multimessenger signals of neutron stars and their mergers from astrophysical observations will provide unique opportunities to pin down the EOS of dense neutron-rich matter [54, 55].

The HICs provide a unique approach to produce dense nuclear matter in terrestrial laboratories. In HICs, the state of matter produced during the collisions can be modified by adjusting the beam energy, collision geometry as well as the isospin asymmetry of the collision system. In order to describe the dynamics of the collisions and extract the EOS of dense nuclear matter from the collision products which generally involves dynamics far from thermal equilibrium, microscopic transport models such as the Boltzmann-Uehling-Uhlenbeck (BUU) equation [56] and the quantum molecular dynamics (QMD) model [57] have been developed and widely applied. In recent years, the Transport Model Evaluation Project (TMEP) has been pursued to test the robustness of transport models and then try to narrow down the uncertainties of their predictions [58–63]. One

\* Corresponding author: lwchen@sjtu.edu.cn

direct and fundamental input for the transport model is the single-nucleon potential (nuclear mean-field potential), which is generally obtained from an in-medium effective nuclear interactions based on the Hartree-Fock (HF) approach. It is directly connected to the nuclear matter EOS through the corresponding energy-density functional (EDF) [56, 57]. Therefore, probing the single-nucleon potential is a key issue of transport model simulations for HICs at intermediate energies.

The single-nucleon potential in neutron-rich matter generally depends on the density and isospin asymmetry of the medium as well as the momentum and isospin of the nucleon. The momentum/energy dependence of the single-nucleon potential plays an important role for nuclear systems at finite temperatures or in nonequilibrium conditions, including not only HICs, but also proto-neutron stars, neutron star mergers and supernovae. The effective nuclear interactions used in transport model simulations are therefore necessary to accurately describe the momentum/energy dependence of the single-nucleon potential. In previous works [64, 65], a Skyrme-like quasiloca EDF up to N3LO has been constructed by including additional higher-order derivative terms (higher-power momentum dependence) in the conventional Skyrme interaction, which is notorious with the incorrect high energy behavior of the nucleon optical potential when nucleon kinetic energy is above about 300 MeV/nucleon. Actually, the Skyrme interaction can be recognized as a low-momentum expansion of the finite-range interaction, and a quasiloca functional can be obtained from a finite-range interaction through the density-matrix expansion [66, 67]. Indeed, the construction of the quasiloca interaction based on the density-matrix expansion is quite important, as it provides a general procedure for exploring the universal EDF of nuclear systems and examining the validity of each term in an order-by-order way. Through the partial wave decomposition, it has been shown that the Skyrme pseudopotential up to N3LO provides a very good approximation of finite-range potential up to about saturation density, and thus it is flexible enough to substitute finite-range interaction in nuclear structure calculations [68].

Moreover, the additional higher-order derivatives in the effective interaction extend the momentum-dependent (MD) terms and density-gradient terms in the corresponding nuclear EDF, which could be important for investigating HICs using transport models. We would like to emphasize that, one of important advantages for the polynomial form of the mean-field potential provided by the Skyrme pseudopotential is that it can significantly reduce the computational complexity of the transport model, and we will further discuss this point later. Based on the Skyrme pseudopotential up to N3LO, the extended Skyrme interactions have been built within the mean-field approximation in Ref. [69] to reproduce the empirical results on the nucleon optical potential up to energy of 1 GeV (corresponding to nucleon momentum of 1.5 GeV/c) obtained by Hama *et al.* from ana-

lyzing the proton-nucleus elastic scattering data [70, 71]. These extended Skyrme interactions have been applied in the lattice BUU transport model to successfully describe the nuclear collective dynamics (giant resonances) [72–76] and the light-nuclei production at energies of 0.25–1.0 GeV/nucleon [77] measured by the FOPI Collaboration [78]. Similar idea has also been employed in QMD-type transport models [79].

Besides the HICs experiments at intermediate and high energies in terrestrial laboratories, the neutron stars and their dynamics also provide natural laboratories to shed light on the EOS of dense nuclear matter. Recent multimessenger astrophysical observations, such as the gravitational wave signal from the binary neutron-star merger [80], the relativistic Shapiro delay measurements [81, 82], the x-ray data obtained by Neutron Star Interior Composition Explorer (NICER) and x-ray multi-mirror (XMM-Newton) telescope [83–87] have been used to determine the maximum mass ( $M_{\text{TOV}}$ ), the mass-radius relation (M-R), and the tidal deformability ( $\Lambda$ ) of neutron stars, thereby further to constrain the EOS of neutron-rich matter at suprasaturation densities. To make the Skyrme pseudopotential applicable in neutron stars, it is proposed recently in Ref. [88] to extend the density-dependent (DD) terms based on the Fermi momentum expansion, which is considered to be a model-independent parametrization of the nuclear matter EOS [89]. By this means, the density behavior of nuclear matter bulk properties, including properties of SNM and the symmetry energy, can be highly flexible. A series of extended Skyrme interactions up to N3LO with different slope parameter  $L$  of the symmetry energy have been constructed in Ref. [88]. These interactions are developed not only by fitting the empirical nucleon optical potential, but also by incorporating the empirical properties of SNM, the microscopic calculations of pure neutron matter (PNM) as well as neutron stars properties from astrophysical observations through modifying the extended DD terms.

It should be pointed out that for the Skyrme pseudopotential up to N3LO, it is failing to describe the saturated behavior of nuclear optical potential when the kinetic energy exceeds 1 GeV, although it can give a nice description of the empirical nuclear optical potential below 1 GeV [88]. As a matter of fact, the single-nucleon potential in the extended Skyrme interactions up to N3LO rises rapidly when nucleon kinetic energy exceeds 1 GeV if the empirical nuclear optical potential below 1 GeV is well reproduced [69], mainly due to its polynomial structure in the framework of Skyrme pseudopotential, and this feature may hinder the interaction from its application in transport model simulations for heavy-ion collisions when the incident energy exceeds 1 GeV. To address this problem, in the present work, we provide a general approach to extend the Skyrme pseudopotential by including derivative terms up to  $2n$ th-order in the central term of the Skyrme pseudopotential, corresponding to the Skyrme pseudopotential up to  $Nn$ LO. We derive

the corresponding expressions of Hamiltonian density as well as single-nucleon potential, whose MD part is now extended to  $p^{2n}$ . This extension provides extra flexibility of the high-momentum behavior of the single-nucleon potential, and with an optimization method we find that the N5LO Skyrme pseudopotential can provide a good description of the empirical nucleon optical potential up to energy of 2 GeV with a saturated behavior above 1 GeV. Therefore, the N5LO Skyrme pseudopotential can be applied in transport model simulations for HICs at incident energy up to 2 GeV/nucleon, such as the experiments conducted and to be conducted by HIAF [90, 91] in China, HADES [92–95] and FAIR [96, 97] at GSI in Germany, J-PARC-HI [98–100] in Japan, and NICA [101] and BM@N [102] at JINR in Russia. Note the density of the nuclear matter produced in HICs at incident energies of about 2 GeV/nucleon is expected to exceed  $3\rho_0$  during the collision process [103], and therefore the N5LO Skyrme pseudopotential can be principally applied to probe the EOS of nuclear matter with density up to  $3\rho_0$ .

Furthermore, in the present work, we follow the Fermi momentum expansion approach in Ref. [88] to construct the DD terms in the  $Nn$ LO Skyrme pseudopotential. Particularly, for the N5LO Skyrme pseudopotential, the adjustable macroscopic parameters to characterize the density behavior of the symmetry energy, which correspond to the expansion coefficients of the symmetry energy at  $\rho_0$ , shall include: the magnitude  $E_{\text{sym}}(\rho_0)$ , the slope parameter  $L$ , the curvature parameter  $K_{\text{sym}}$ , the skewness parameter  $J_{\text{sym}}$ , the kurtosis parameter  $I_{\text{sym}}$  and the hyper-skewness parameter  $H_{\text{sym}}$ . Similarly, the adjustable characteristic parameters of the SNM are also increased to six quantities: the nuclear saturation density  $\rho_0$ , the binding energy  $E_0(\rho_0)$  as well as its expansion coefficients at  $\rho_0$  from the second to the fifth order, i.e.,  $K_0$ ,  $J_0$ ,  $I_0$  and  $H_0$ .

Another important quantity in the construction of the extended Skyrme effective interaction is the (first-order) symmetry potential, which represents the isospin-dependent part of the single-nucleon potential in ANM. The uncertainty of the symmetry energy may result from our poor understanding of the symmetry potential, and this can be evidenced from the single-nucleon potential decomposition of  $E_{\text{sym}}(\rho)$  and  $L$  [104–109] based on the Hugenholtz-Van Hove (HVH) theorem [110, 111]. Similar to the structure of the single-nucleon potential, the symmetry potential also includes MD terms up to  $p^{2n}$ , with a total of  $n$  adjustable parameters to control its momentum behavior. In order to ensure that the symmetry potential behaves well in the momentum range up to 2 GeV/ $c$  (avoiding sharp changes or fluctuations), we assume a scaling between the coefficients of each  $p^{2n}$  term. In this case, we can use one physical quantity, i.e., the linear isospin splitting coefficient  $\Delta m_1^*(\rho_0)$ , to feature the different symmetry potentials.

To demonstrate the validity and clearly illustrate the comparison of the extension at different orders, we construct in this work a series of interactions based on the

Skyrme pseudopotential up to N3LO, N4LO and N5LO, respectively. The single-nucleon potentials of these three models are consistent with the empirical nucleon optical potential up to energy of 1 GeV, resulting in similar values of the isoscalar nucleon effective mass at saturation density  $m_{s,0}^*/m \approx 0.77$ , while their behaviors above 1 GeV differ significantly due to the high-order momentum dependence. At the same time, we use the parametrization to construct eight symmetry potentials with  $\Delta m_1^*(\rho_0)$  values of  $\pm 0.7$ ,  $\pm 0.5$ ,  $\pm 0.3$ , and  $\pm 0.1$ , respectively. Based on the N3LO model, a series of characteristic quantities related to nuclear matter bulk properties have been obtained by fitting various nuclear theoretical/experimental constraints and the astrophysical observations [88]. Here for demonstration, we choose one parameter set, i.e., “SP6L45” in Table II in Ref. [88], to construct the new interactions. The values of  $I_0$  and  $I_{\text{sym}}$  in N4LO and N5LO model as well as  $H_0$  and  $H_{\text{sym}}$  in N5LO model are taken to be the corresponding calculated values from the N3LO model. Thus, the properties of SNM and the symmetry energy among different models are constructed as consistent as possible, allowing for a clearer observation of the impacts caused by different models (different momentum behaviors of single-nucleon potential). Based on these new constructed extended Skyrme interactions, we investigate the properties of nuclear matter and neutron stars, and we find that these interactions can give reasonable descriptions of neutron-star properties. Furthermore, the interactions with  $\Delta m_1^*(\rho_0) = 0.3$  are applied in the lattice BUU model [72, 74] to simulate the fixed-target Au+Au collision at  $E_{\text{beam}} = 1.23$  GeV/nucleon [94, 95] (corresponding to  $\sqrt{s_{NN}} = 2.4$  GeV) conducted by HADES collaboration. Additionally, to investigate the effect of the isoscalar nucleon effective mass  $m_{s,0}^*$  on the HICs, we also introduce another single-nucleon potential constructed based on the N3LO model from Ref. [88], for which the value of  $m_{s,0}^*$  equals to  $0.83m$ . We show that these four interactions can provide good predictions of the proton collective flows in the HADES experiments. Moreover, we find that the proton elliptic flows  $v_2$  is sensitive to the single-nucleon potential as well as the  $m_{s,0}^*$ . Specifically, a larger  $m_{s,0}^*$  (indicating weaker energy dependence at low energies) predicts a smaller magnitude of  $v_2$ , while the rapidly rising single-nucleon potential, compared to the saturated ones, results in a larger magnitude of  $v_2$ .

This paper is organized as follow: In Sec. II, we introduce the Skyrme pseudopotential up to N5LO by extending the central terms and the DD terms, and display the expressions of Hamiltonian density and single-nucleon potential. Ignoring the high-order terms, these expressions in the N5LO model will reduce to the corresponding forms in the N4LO (N3LO) model. In Sec. III, we present the fitting strategy as well as the theoretical/experimental data and constraints and the parametrization used in our fitting, and we construct 24 new parameter sets of the extended Skyrme interactions. In Sec. IV, we present the bulk properties of cold nu-

clear matter, the single-nucleon potential behaviors and neutron-star properties of the 24 interactions. The cumulative contributions from the MD term up to different orders for the nuclear matter bulk properties and for the single-nucleon potential are also discussed in this section. In Sec. V, we briefly introduce the BUU equation and the lattice Hamiltonian method, by which these new interactions are used to simulate the Au+Au collisions at  $\sqrt{s_{NN}} = 2.4$  GeV. In this section, we also present the simulation result for proton collective flows and compare them with the HADES data. Finally, we summarize our conclusions and make a brief outlook in Sec. VI.

For completeness, we include several Appendices. In Appendix A, we introduce our basic assumption to extend the central term of the Skyrme interaction and give the corresponding forms up to NnLO. With HF approximation, the expressions of Hamiltonian density and single-nucleon potential are derived under general nonequilibrium conditions. We also discuss the advantage of the polynomial form of the MD part of single particle potentials in Appendix A. The expressions of the characteristic quantities of the SNM EOS and the symmetry energy are provided in Appendix B, where we also present the expressions of the fourth-order symmetry energy, the isoscalar and isovector nucleon effective masses as well as the linear isospin splitting coefficient. In Appendix C, we list the Skyrme parameters for these new interactions.

## II. THEORETICAL FRAMEWORK

### A. New extended Skyrme interaction based on N5LO pseudopotential

In the previous works [64, 65], the generalization of Skyrme interaction has been constructed up to the N3LO by including the additional fourth and sixth-order derivative terms, which is also referred to as N3LO Skyrme pseudopotential. This theoretical framework has been applied in studies of the EOS of nuclear matter [112–116] and the properties of finite nuclei [117, 118]. The Hamiltonian density and the single-nucleon potential has been derived within the HF approximation [69], and it can be seen that compared to the conventional Skyrme interaction, the higher-order derivative terms provide additional

momentum dependence for the single-nucleon potential, allowing it to better reproduce the empirical nucleon optical potential [70, 71]. Consequently, the N3LO Skyrme pseudopotential can be employed in transport models, such as the lattice BUU method, to investigate both the collective dynamics of finite nuclei [73, 76] and the HICs simulations at intermediate energies [77]. In a very recent work [88], the DD term in the N3LO Skyrme pseudopotential is extended in the spirit of Fermi momentum expansion, resulting in a highly flexible density behavior of SNM EOS and the symmetry energy. This allows for simultaneous descriptions of both the various microscopic calculations of the EOS of PNM (see Ref. [119] and references therein) and multimessenger astrophysical observations of neutron stars [80–86]. Finally, we can describe the properties of finite nuclei, neutron stars and HICs in a unified theoretical framework.

However, because the single-nucleon potential rapidly deviates from its saturated behavior when energy exceeds 1 GeV, these interactions may not be suitable for studying the HICs of incident energies beyond 1 GeV/nucleon, such as the fixed Au+Au collision at 1.23 GeV/nucleon by HADES collaboration [94, 95] and the central collisions at the energies of 1-2 GeV/nucleon measured by FOPI collaboration [78]. To solve this problem, we propose extending the central terms to provide additional momentum dependence for the single-nucleon potential. We assume that the  $2n$ th-order derivative terms in the central term come from  $(\hat{A} + \hat{B})^n$ , where:  $\hat{A} = \frac{1}{2} [\hat{k}'^2 \delta(\vec{r}_1 - \vec{r}_2) + \delta(\vec{r}_1 - \vec{r}_2) \hat{k}^2]$ ,  $\hat{B} = \hat{k}' \cdot \delta(\vec{r}_1 - \vec{r}_2) \hat{k}$ , and  $\hat{k} = -i(\hat{\nabla}_1 - \hat{\nabla}_2)/2$  is the relative momentum operator, while  $\hat{k}'$  is the conjugate operator of  $\hat{k}$ . In Appendix A, we present the general form of the extended central term up to arbitrary order, along with the derivations of the corresponding Hamiltonian density and single-nucleon potential. Compared to the N3LO model, the central term in N5LO model includes additional eighth- and tenth-order derivative terms, which ensure that single-nucleon potential remains saturated up to 2 GeV. To clearly illustrate the impact of the high-order derivative terms in an order-by-order way, we provide the forms of the central terms for the N3LO, N4LO, and N5LO models, respectively, and subsequently construct the corresponding interactions based on these.

The central term of the N3LO Skyrme pseudopotential is written as

$$\begin{aligned}
 V_{\text{N3LO}}^C = & t_0 (1 + x_0 \hat{P}_\sigma) + t_1^{[2]} (1 + x_1^{[2]} \hat{P}_\sigma) \frac{1}{2} (\hat{k}'^2 + \hat{k}^2) + t_2^{[2]} (1 + x_2^{[2]} \hat{P}_\sigma) \hat{k}' \cdot \hat{k} + t_1^{[4]} (1 + x_1^{[4]} \hat{P}_\sigma) \left[ \frac{1}{4} (\hat{k}'^2 + \hat{k}^2)^2 + (\hat{k}' \cdot \hat{k})^2 \right] \\
 & + t_2^{[4]} (1 + x_2^{[4]} \hat{P}_\sigma) (\hat{k}' \cdot \hat{k}) (\hat{k}'^2 + \hat{k}^2) + t_1^{[6]} (1 + x_1^{[6]} \hat{P}_\sigma) (\hat{k}'^2 + \hat{k}^2) \left[ \frac{1}{2} (\hat{k}'^2 + \hat{k}^2)^2 + 6 (\hat{k}' \cdot \hat{k})^2 \right] \\
 & + t_2^{[6]} (1 + x_2^{[6]} \hat{P}_\sigma) (\hat{k}' \cdot \hat{k}) \left[ 3 (\hat{k}'^2 + \hat{k}^2)^2 + 4 (\hat{k}' \cdot \hat{k})^2 \right],
 \end{aligned} \tag{1}$$

and the extensions of  $V_{\text{N3LO}}^C$  include the eighth-order term  $v^{[8]}$  and the tenth-order term  $v^{[10]}$  based on Eq. (A12) and

Eq. (A13), i.e.,

$$v^{[8]} = t_1^{[8]} \left(1 + x_1^{[8]} \hat{P}_\sigma\right) \left[ \left( \frac{\vec{k}'^2 + \vec{k}^2}{2} \right)^4 + 6 \left( \frac{\vec{k}'^2 + \vec{k}^2}{2} \right)^2 (\vec{k}' \cdot \vec{k})^2 + (\vec{k}' \cdot \vec{k})^4 \right] \\ + t_2^{[8]} \left(1 + x_2^{[8]} \hat{P}_\sigma\right) \left[ 4 \left( \frac{\vec{k}'^2 + \vec{k}^2}{2} \right)^3 (\vec{k}' \cdot \vec{k}) + 4 \left( \frac{\vec{k}'^2 + \vec{k}^2}{2} \right) (\vec{k}' \cdot \vec{k})^3 \right], \quad (2)$$

and

$$v^{[10]} = t_1^{[10]} \left(1 + x_1^{[10]} \hat{P}_\sigma\right) \left[ \left( \frac{\vec{k}'^2 + \vec{k}^2}{2} \right)^5 + 10 \left( \frac{\vec{k}'^2 + \vec{k}^2}{2} \right)^3 (\vec{k}' \cdot \vec{k})^2 + 5 \left( \frac{\vec{k}'^2 + \vec{k}^2}{2} \right) (\vec{k}' \cdot \vec{k})^4 \right] \\ + t_2^{[10]} \left(1 + x_2^{[10]} \hat{P}_\sigma\right) \left[ 5 \left( \frac{\vec{k}'^2 + \vec{k}^2}{2} \right)^4 (\vec{k}' \cdot \vec{k}) + 10 \left( \frac{\vec{k}'^2 + \vec{k}^2}{2} \right)^2 (\vec{k}' \cdot \vec{k})^3 + (\vec{k}' \cdot \vec{k})^5 \right], \quad (3)$$

where  $\hat{P}_\sigma$  is the spin-exchange operator.

Thus the central term of N4LO and N5LO Skyrme pseudopotential can be expressed as

$$V_{\text{N4LO}}^C = V_{\text{N3LO}}^C + v^{[8]}, \quad (4)$$

$$V_{\text{N5LO}}^C = V_{\text{N3LO}}^C + v^{[8]} + v^{[10]}. \quad (5)$$

Based on Fermi momentum expansion proposed in Ref. [88], the DD term can be written as

$$V_N^{\text{DD}} = \sum_{n=1}^N \frac{1}{6} t_3^{[2n-1]} \left(1 + x_3^{[2n-1]} \hat{P}_\sigma\right) \rho^{\frac{2n-1}{3}}(\vec{R}), \quad (6)$$

where  $\vec{R} = (\vec{r}_1 + \vec{r}_2)/2$ . For brevity, the factor  $\hat{\delta}(\vec{r}_1 - \vec{r}_1)$  is omitted from Eqs. (1), (2), (3) and (6). The general form of the Skyrme pseudopotential includes the spin-independent terms, the spin-orbit terms, as well as the tensor components (see, e.g., Refs. [64, 65, 113, 114]). In the present work, we focus on the spin-averaged quantities, where the spin-orbit and tensor terms make no contribution. By extending the central term and DD term systematically, the Skyrme interactions used in this work are then written as

$$v_{sk}^{\text{N3LO}} = V_{\text{N3LO}}^C + V_3^{\text{DD}}, \quad (7)$$

$$v_{sk}^{\text{N4LO}} = V_{\text{N4LO}}^C + V_4^{\text{DD}}, \quad (8)$$

$$v_{sk}^{\text{N5LO}} = V_{\text{N5LO}}^C + V_5^{\text{DD}}. \quad (9)$$

The  $t_0$ ,  $x_0$ ;  $t_i^{[n]}$ ,  $x_i^{[n]}$  ( $n = 2, 4, 6, 8, 10$  and  $i = 1, 2$ );  $t_3^{[n]}$ ,  $x_3^{[n]}$  ( $n = 1, 3, 5, 7, 9$ ) are Skyrme parameters, and the total numbers of these parameters are 20, 26 and 32 for N3LO, N4LO and N5LO interactions, respectively.

## B. Hamiltonian density and single-nucleon potential in one-body transport model

In the BUU microscopic transport model, since the system is in a nonequilibrium state, the Hamiltonian

density  $\mathcal{H}(\vec{r})$  and the single-nucleon potential  $U_\tau(\vec{r}, \vec{p})$  are expressed as functions of the phase space distribution function of nucleons (Wigner function)  $f_\tau(\vec{r}, \vec{p})$ , with  $\tau = 1$  (or n) for neutrons and  $-1$  (or p) for protons. With the HF approximation, the Hamiltonian density with the Skyrme interactions defined in Eqs. (7)-(9) can be expressed as (detailed derivation can be found in Appendix A)

$$\mathcal{H}(\vec{r}) = \mathcal{H}^{\text{kin}}(\vec{r}) + \mathcal{H}^{\text{loc}}(\vec{r}) + \mathcal{H}^{\text{MD}}(\vec{r}) + \mathcal{H}^{\text{grad}}(\vec{r}) + \mathcal{H}^{\text{DD}}(\vec{r}), \quad (10)$$

where  $\mathcal{H}^{\text{kin}}(\vec{r})$ ,  $\mathcal{H}^{\text{loc}}(\vec{r})$ ,  $\mathcal{H}^{\text{MD}}(\vec{r})$ ,  $\mathcal{H}^{\text{grad}}(\vec{r})$  and  $\mathcal{H}^{\text{DD}}(\vec{r})$  are the kinetic, local, MD, gradient (GD) and DD terms, respectively. The kinetic term and the local term are the same for N3LO, N4LO and N5LO Skyrme pseudopotential, where they are expressed as

$$\mathcal{H}^{\text{kin}}(\vec{r}) = \sum_{\tau=n,p} \int \frac{d^3p}{(2\pi\hbar)^3} \frac{p^2}{2m_\tau} f_\tau(\vec{r}, \vec{p}) \quad (11)$$

and

$$\mathcal{H}^{\text{loc}}(\vec{r}) = \frac{1}{4} t_0 \left[ (2 + x_0) \rho^2 - (2x_0 + 1) \sum_{\tau=n,p} \rho_\tau^2 \right], \quad (12)$$

respectively. The  $\rho_\tau(\vec{r}) = \int f_\tau(\vec{r}, \vec{p}) \frac{d^3p}{(2\pi\hbar)^3}$  is the nucleon density and the  $\rho(\vec{r}) = \rho_n(\vec{r}) + \rho_p(\vec{r})$  is the total nucleon density.

For N5LO interaction, the MD term is expressed as

$$\begin{aligned}\mathcal{H}^{\text{MD}}(\vec{r}) = & \frac{C^{[2]}}{16\hbar^2} \mathcal{H}^{\text{md}[2]}(\vec{r}) + \frac{D^{[2]}}{16\hbar^2} \sum_{\tau=n,p} \mathcal{H}_{\tau}^{\text{md}[2]}(\vec{r}) + \frac{C^{[4]}}{32\hbar^4} \mathcal{H}^{\text{md}[4]}(\vec{r}) + \frac{D^{[4]}}{32\hbar^4} \sum_{\tau=n,p} \mathcal{H}_{\tau}^{\text{md}[4]}(\vec{r}) \\ & + \frac{C^{[6]}}{16\hbar^6} \mathcal{H}^{\text{md}[6]}(\vec{r}) + \frac{D^{[6]}}{16\hbar^6} \sum_{\tau=n,p} \mathcal{H}_{\tau}^{\text{md}[6]}(\vec{r}) + \frac{C^{[8]}}{128\hbar^8} \mathcal{H}^{\text{md}[8]}(\vec{r}) + \frac{D^{[8]}}{128\hbar^8} \sum_{\tau=n,p} \mathcal{H}_{\tau}^{\text{md}[8]}(\vec{r}) \\ & + \frac{C^{[10]}}{256\hbar^{10}} \mathcal{H}^{\text{md}[10]}(\vec{r}) + \frac{D^{[10]}}{256\hbar^{10}} \sum_{\tau=n,p} \mathcal{H}_{\tau}^{\text{md}[10]}(\vec{r}),\end{aligned}\quad (13)$$

where  $\mathcal{H}^{\text{md}[n]}(\vec{r})$  and  $\mathcal{H}_{\tau}^{\text{md}[n]}(\vec{r})$  are defined as

$$\mathcal{H}^{\text{md}[n]}(\vec{r}) = \int \frac{d\mathbf{p}^3}{(2\pi\hbar)^3} \frac{d^3p'}{(2\pi\hbar)^3} (\vec{p} - \vec{p}')^n f(\vec{r}, \vec{p}) f(\vec{r}, \vec{p}'), \quad (14)$$

$$\mathcal{H}_{\tau}^{\text{md}[n]}(\vec{r}) = \int \frac{d\mathbf{p}^3}{(2\pi\hbar)^3} \frac{d^3p'}{(2\pi\hbar)^3} (\vec{p} - \vec{p}')^n f_{\tau}(\vec{r}, \vec{p}) f_{\tau}(\vec{r}, \vec{p}'), \quad (15)$$

with  $f(\vec{r}, \vec{p}) = f_n(\vec{r}, \vec{p}) + f_p(\vec{r}, \vec{p})$ . The gradient term can be expressed as

$$\begin{aligned}\mathcal{H}^{\text{GD}}(\vec{r}) = & \frac{1}{16} E^{[2]} \{2\rho(\vec{r}) \nabla^2 \rho(\vec{r}) - 2[\nabla \rho(\vec{r})]^2\} + \frac{1}{16} F^{[2]} \sum_{\tau=n,p} \{2\rho_{\tau}(\vec{r}) \nabla^2 \rho_{\tau}(\vec{r}) - 2[\nabla \rho_{\tau}(\vec{r})]^2\} \\ & + \frac{1}{32} E^{[4]} \{2\rho(\vec{r}) \nabla^4 \rho(\vec{r}) - 8\nabla \rho(\vec{r}) \nabla^3 \rho(\vec{r}) + 6[\nabla^2 \rho(\vec{r})]^2\} \\ & + \frac{1}{32} F^{[4]} \sum_{\tau=n,p} \{2\rho_{\tau}(\vec{r}) \nabla^4 \rho_{\tau}(\vec{r}) - 8\nabla \rho_{\tau}(\vec{r}) \nabla^3 \rho_{\tau}(\vec{r}) + 6[\nabla^2 \rho_{\tau}(\vec{r})]^2\} \\ & + \frac{1}{16} E^{[6]} \{2\rho(\vec{r}) \nabla^6 \rho(\vec{r}) - 12\nabla \rho(\vec{r}) \nabla^5 \rho(\vec{r}) + 30\nabla^2 \rho(\vec{r}) \nabla^4 \rho(\vec{r}) - 20[\nabla^3 \rho(\vec{r})]^2\} \\ & + \frac{1}{16} F^{[6]} \sum_{\tau=n,p} \{2\rho_{\tau}(\vec{r}) \nabla^6 \rho_{\tau}(\vec{r}) - 12\nabla \rho_{\tau}(\vec{r}) \nabla^5 \rho_{\tau}(\vec{r}) + 30\nabla^2 \rho_{\tau}(\vec{r}) \nabla^4 \rho_{\tau}(\vec{r}) - 20[\nabla^3 \rho_{\tau}(\vec{r})]^2\} \\ & + \frac{E^{[8]}}{128} \{2\rho(\vec{r}) \nabla^8 \rho(\vec{r}) - 16\nabla \rho(\vec{r}) \nabla^7 \rho(\vec{r}) + 56\nabla^2 \rho(\vec{r}) \nabla^6 \rho(\vec{r}) - 112\nabla^3 \rho(\vec{r}) \nabla^5 \rho(\vec{r}) + 70[\nabla^4 \rho(\vec{r})]^2\} \\ & + \frac{F^{[8]}}{128} \sum_{\tau=n,p} \{2\rho_{\tau}(\vec{r}) \nabla^8 \rho_{\tau}(\vec{r}) - 16\nabla \rho_{\tau}(\vec{r}) \nabla^7 \rho_{\tau}(\vec{r}) + 56\nabla^2 \rho_{\tau}(\vec{r}) \nabla^6 \rho_{\tau}(\vec{r}) - 112\nabla^3 \rho_{\tau}(\vec{r}) \nabla^5 \rho_{\tau}(\vec{r}) + 70[\nabla^4 \rho_{\tau}(\vec{r})]^2\} \\ & + \frac{E^{[10]}}{256} \{2\rho(\vec{r}) \nabla^{10} \rho(\vec{r}) - 20\nabla \rho(\vec{r}) \nabla^9 \rho(\vec{r}) + 90\nabla^2 \rho(\vec{r}) \nabla^8 \rho(\vec{r}) - 240\nabla^3 \rho(\vec{r}) \nabla^7 \rho(\vec{r}) \\ & \quad + 420\nabla^4 \rho(\vec{r}) \nabla^6 \rho(\vec{r}) - 252[\nabla^5 \rho(\vec{r})]^2\} \\ & + \frac{F^{[10]}}{256} \sum_{\tau=n,p} \{2\rho_{\tau}(\vec{r}) \nabla^{10} \rho_{\tau}(\vec{r}) - 20\nabla \rho_{\tau}(\vec{r}) \nabla^9 \rho_{\tau}(\vec{r}) + 90\nabla^2 \rho_{\tau}(\vec{r}) \nabla^8 \rho_{\tau}(\vec{r}) - 240\nabla^3 \rho_{\tau}(\vec{r}) \nabla^7 \rho_{\tau}(\vec{r}) \\ & \quad + 420\nabla^4 \rho_{\tau}(\vec{r}) \nabla^6 \rho_{\tau}(\vec{r}) - 252[\nabla^5 \rho_{\tau}(\vec{r})]^2\}.\end{aligned}\quad (16)$$

In Eqs. (13) and (16), we have recombined the Skyrme parameters  $t_1^{[2n]}$ ,  $x_1^{[2n]}$ ,  $t_2^{[2n]}$  and  $x_2^{[2n]}$  into the parameters  $C^{[2n]}$ ,  $D^{[2n]}$ ,  $E^{[2n]}$  and  $F^{[2n]}$ , which are defined in Eqs. (A26)-(A29). The DD term comes from  $V_5^{\text{DD}}$  in Eq. (6) of the N5LO interaction is expressed as

$$\mathcal{H}^{\text{DD}}(\vec{r}) = \sum_{n=1}^5 \frac{1}{24} t_3^{[2n-1]} \left[ \left(2 + x_3^{[2n-1]}\right) \rho^2 - \left(2x_3^{[2n-1]} + 1\right) (\rho_n^2 + \rho_p^2) \right] \rho^{\frac{2n-1}{3}}. \quad (17)$$

By ignoring the  $C^{[10]}$ ,  $D^{[10]}$ ,  $E^{[10]}$ ,  $F^{[10]}$  and  $t_3^{[9]}$  terms (or as well as the  $C^{[8]}$ ,  $D^{[8]}$ ,  $E^{[8]}$ ,  $F^{[8]}$  and  $t_3^{[7]}$  terms), Eq. (13), Eq. (16) and Eq. (17) will reduce to the expressions corresponding to N4LO (N3LO) interactions (same in the following expressions).

Based on the Landau Fermi liquid theory, the single-nucleon potential reflects the net nuclear medium effects, and it can be obtained by taking the variation of  $\mathcal{H}(\vec{r})$  with respect to  $f_{\tau}(\vec{r}, \vec{p})$ . Since  $\mathcal{H}(\vec{r})$  includes terms with density

gradients, the single-nucleon potential can be calculated as (details can be found in Ref. [120])

$$U_\tau(\vec{r}, \vec{p}) = \frac{\delta H^{\text{pot}}}{\delta f_\tau(\vec{r}, \vec{p})} = \frac{\partial [\mathcal{H}^{\text{loc}}(\vec{r}) + \mathcal{H}^{\text{DD}}(\vec{r}) + \mathcal{H}^{\text{grad}}(\vec{r})]}{\partial \rho_\tau(\vec{r})} + \sum_n (-1)^n \nabla^n \frac{\partial \mathcal{H}^{\text{grad}}(\vec{r})}{\partial [\nabla^n \rho_\tau(\vec{r})]} + \frac{\delta H^{\text{MD}}}{\delta f_\tau(\vec{r}, \vec{p})}, \quad (18)$$

where  $H^{\text{pot}} = \int d\vec{r} [\mathcal{H}^{\text{loc}}(\vec{r}) + \mathcal{H}^{\text{DD}}(\vec{r}) + \mathcal{H}^{\text{MD}}(\vec{r}) + \mathcal{H}^{\text{grad}}(\vec{r})]$  is the potential part of the Hamiltonian with  $H^{\text{MD}} = \int d\vec{r} \mathcal{H}^{\text{MD}}(\vec{r})$  being the MD part. Substitute Eq. (10) into Eq. (18), and this yields

$$\begin{aligned} U_\tau(\vec{r}, \vec{p}) = & \frac{1}{2} t_0 [(2 + x_0) \rho(\vec{r}) - (2x_0 + 1) \rho_\tau(\vec{r})] + \sum_{n=1}^5 \left\{ \frac{1}{12} t_3^{[2n-1]} \left[ (2 + x_3^{[2n-1]}) \rho(\vec{r}) - (2x_3^{[2n-1]} + 1) \rho_\tau(\vec{r}) \right] \rho(\vec{r})^{\frac{2n-1}{3}} \right\} \\ & + \sum_{n=1}^5 \left\{ \frac{t_3^{[2n-1]}}{24} \frac{2n-1}{3} \left[ (2 + x_3^{[2n-1]}) \rho(\vec{r})^2 - (2x_3^{[2n-1]} + 1) \sum_{\tau=n,p} \rho_\tau(\vec{r})^2 \right] \rho(\vec{r})^{\frac{2n-1}{3}-1} \right\} + \frac{1}{8\hbar^2} C^{[2]} U^{\text{md}[2]}(\vec{r}, \vec{p}) \\ & + \frac{1}{8\hbar^2} D^{[2]} U_\tau^{\text{md}[2]}(\vec{r}, \vec{p}) + \frac{1}{16\hbar^4} C^{[4]} U^{\text{md}[4]}(\vec{r}, \vec{p}) + \frac{1}{16\hbar^4} D^{[4]} U_\tau^{\text{md}[4]}(\vec{r}, \vec{p}) + \frac{1}{8\hbar^6} C^{[6]} U^{\text{md}[6]}(\vec{r}, \vec{p}) \\ & + \frac{1}{8\hbar^6} D^{[6]} U_\tau^{\text{md}[6]}(\vec{r}, \vec{p}) + \frac{C^{[8]}}{64\hbar^8} U^{\text{md}[8]}(\vec{r}, \vec{p}) + \frac{D^{[8]}}{64\hbar^8} U_\tau^{\text{md}[8]}(\vec{r}, \vec{p}) + \frac{C^{[10]}}{128\hbar^{10}} U^{\text{md}[10]}(\vec{r}, \vec{p}) + \frac{D^{[10]}}{128\hbar^{10}} U_\tau^{\text{md}[10]}(\vec{r}, \vec{p}) \\ & + \frac{1}{2} E^{[2]} \nabla^2 \rho(\vec{r}) + \frac{1}{2} F^{[2]} \nabla^2 \rho_\tau(\vec{r}) + E^{[4]} \nabla^4 \rho(\vec{r}) + F^{[4]} \nabla^4 \rho_\tau(\vec{r}) + 8E^{[6]} \nabla^6 \rho(\vec{r}) + 8F^{[6]} \nabla^6 \rho_\tau(\vec{r}) \\ & + 4E^{[8]} \nabla^8 \rho(\vec{r}) + 4F^{[8]} \nabla^8 \rho_\tau(\vec{r}) + 8E^{[10]} \nabla^{10} \rho(\vec{r}) + 8F^{[10]} \nabla^{10} \rho_\tau(\vec{r}), \end{aligned} \quad (19)$$

where  $U^{\text{md}[n]}(\vec{r}, \vec{p})$  and  $U_\tau^{\text{md}[n]}(\vec{r}, \vec{p})$  are defined as

$$U^{\text{md}[n]}(\vec{r}, \vec{p}) = \int \frac{d^3 p'}{(2\pi\hbar)^3} (\vec{p} - \vec{p}')^n f(\vec{r}, \vec{p}'), \quad (20)$$

$$U_\tau^{\text{md}[n]}(\vec{r}, \vec{p}) = \int \frac{d^3 p'}{(2\pi\hbar)^3} (\vec{p} - \vec{p}')^n f_\tau(\vec{r}, \vec{p}'). \quad (21)$$

### C. Equation of state of cold nuclear matter

The EOS of isospin asymmetric nuclear matter with total nucleon density  $\rho = \rho_n + \rho_p$  and isospin asymmetry  $\delta = (\rho_n - \rho_p)/\rho$  are defined as its binding energy per nucleon. In uniform infinite system, all the gradient terms ( $E^{[n]}$  and  $F^{[n]}$  terms) in the Hamiltonian density [Eq. (10)] vanish. At zero temperature,  $f_\tau(\vec{r}, \vec{p})$  becomes a step function, i.e.,  $f_\tau(\vec{r}, \vec{p}) = g_\tau \theta(p_{F_\tau} - |\vec{p}|)$ , with  $g_\tau$  being the degeneracy and  $p_{F_\tau} = \hbar(3\pi^2 \rho_\tau)^{1/3}$  being the Fermi momentum of nucleons with isospin  $\tau$ . In this case, the EOS of isospin asymmetric nuclear can be analytically expressed as

$$\begin{aligned} E(\rho, \delta) = & \frac{3}{5} \frac{\hbar^2 a^2}{2m} F_{5/3} \rho^{2/3} + \frac{1}{8} t_0 \left[ 2(x_0 + 2) - (2x_0 + 1) F_2 \right] \rho^{3/3} + \frac{1}{48} t_3^{[1]} \left[ 2(x_3^{[1]} + 2) - (2x_3^{[1]} + 1) F_2 \right] \rho^{4/3} \\ & + \frac{9a^2}{64} \left[ \frac{8}{15} C^{[2]} F_{5/3} + \frac{4}{15} D^{[2]} F_{8/3} \right] \rho^{5/3} + \frac{1}{48} t_3^{[3]} \left[ 2(x_3^{[3]} + 2) - (2x_3^{[3]} + 1) F_2 \right] \rho^{6/3} \\ & + \frac{9a^4}{128} \left[ C^{[4]} \left( \frac{68}{105} F_{7/3} + \frac{4}{15} \delta G_{7/3} + \frac{4}{15} H_{5/3} \right) + \frac{16}{35} D^{[4]} F_{10/3} \right] \rho^{7/3} + \frac{1}{48} t_3^{[5]} \left[ 2(x_3^{[5]} + 2) - (2x_3^{[5]} + 1) F_2 \right] \rho^{8/3} \\ & + \frac{9a^6}{64} \left[ C^{[6]} \left( \frac{148}{135} F_3 + \frac{4}{5} \delta G_3 + \frac{4}{5} H_{5/3} F_{2/3} \right) + \frac{128}{135} D^{[6]} F_4 \right] \rho^{9/3} + \frac{1}{48} t_3^{[7]} \left[ 2(x_3^{[7]} + 2) - (2x_3^{[7]} + 1) F_2 \right] \rho^{10/3} \\ & + \frac{9a^8}{512} \left[ C^{[8]} \left( \frac{180}{77} F_{11/3} + \frac{44}{21} \delta G_{11/3} + \frac{16}{15} H_{5/3} F_{4/3} + \frac{36}{35} H_{7/3} \right) + \frac{512}{231} D^{[8]} F_{14/3} \right] \rho^{11/3} \\ & + \frac{1}{48} t_3^{[9]} \left[ 2(x_3^{[9]} + 2) - (2x_3^{[9]} + 1) F_2 \right] \rho^{12/3} \\ & + \frac{9a^{10}}{1024} \left[ C^{[10]} \left( \frac{1564}{273} F_{13/3} + \frac{116}{21} \delta G_{13/3} + \frac{4}{3} H_{5/3} F_2 + \frac{88}{21} H_{7/3} F_{2/3} \right) + \frac{512}{91} D^{[10]} F_{16/3} \right] \rho^{13/3}, \end{aligned} \quad (22)$$

where  $a = (3\pi^2/2)^{1/3}$ , and  $m$  is nucleon rest mass in vacuum. In Eq. (22),  $F_x$ ,  $G_x$  and  $H_x$  are defined as

$$F_x = [(1 + \delta)^x + (1 - \delta)^x] / 2,$$

$$\begin{aligned} G_x &= [(1 + \delta)^x - (1 - \delta)^x] / 2, \\ H_x &= [(1 + \delta)(1 - \delta)]^x. \end{aligned}$$

The EOS can be expanded as a power series in  $\delta$ , i.e.,

$$E(\rho, \delta) = E_0(\rho) + E_{\text{sym}}(\rho)\delta^2 + E_{\text{sym},4}(\rho)\delta^4 + \mathcal{O}(\delta^6), \quad (23)$$

where  $E_0(\rho)$  is the EOS of the SNM. The symmetry energy  $E_{\text{sym}}(\rho)$  and the fourth-order symmetry energy  $E_{\text{sym},4}(\rho)$  are defined as

$$E_{\text{sym}}(\rho) = \frac{1}{2!} \frac{\partial^2 E(\rho, \delta)}{\partial \delta^2} \Big|_{\delta=0}, \quad (24)$$

and

$$E_{\text{sym},4}(\rho) = \frac{1}{4!} \frac{\partial^4 E(\rho, \delta)}{\partial \delta^4} \Big|_{\delta=0}, \quad (25)$$

respectively. The expressions of  $E_0(\rho)$ ,  $E_{\text{sym}}(\rho)$  and  $E_{\text{sym},4}(\rho)$  are presented in Appendix B.

The pressure of the isospin asymmetric nuclear matter can be expressed as

$$P(\rho, \delta) = \rho^2 \frac{\partial E(\rho, \delta)}{\partial \rho}. \quad (26)$$

The saturation density  $\rho_0$  is defined where the pressure of the SNM is zero (except for  $\rho = 0$ ), i.e.,

$$P(\rho_0, \delta = 0) = \rho_0^2 \frac{dE(\rho, 0)}{d\rho} \Big|_{\rho=\rho_0} = 0. \quad (27)$$

Around the saturation density  $\rho_0$ , both  $E_0(\rho)$  and  $E_{\text{sym}}(\rho)$  can be expanded as power series in a dimensionless variable  $\chi \equiv \frac{\rho - \rho_0}{3\rho_0}$ , i.e.,

$$E_0(\rho) = E_0(\rho_0) + L_0\chi + \frac{K_0}{2!}\chi^2 + \frac{J_0}{3!}\chi^3 + \frac{I_0}{4!}\chi^4 + \frac{H_0}{5!}\chi^5 + \mathcal{O}(\chi^6), \quad (28)$$

and

$$E_{\text{sym}}(\rho) = E_{\text{sym}}(\rho_0) + L\chi + \frac{K_{\text{sym}}}{2!}\chi^2 + \frac{J_{\text{sym}}}{3!}\chi^3 + \frac{I_{\text{sym}}}{4!}\chi^4 + \frac{H_{\text{sym}}}{5!}\chi^5 + \mathcal{O}(\chi^6). \quad (29)$$

The first five coefficients of  $\chi^n$  in the two expansions are

$$L_0 = 3\rho_0 \frac{dE_0(\rho)}{d\rho} \Big|_{\rho=\rho_0}, L = 3\rho_0 \frac{dE_{\text{sym}}(\rho)}{d\rho} \Big|_{\rho=\rho_0}, \quad (30)$$

$$K_0 = (3\rho_0)^2 \frac{d^2 E_0(\rho)}{d\rho^2} \Big|_{\rho=\rho_0}, K_{\text{sym}} = (3\rho_0)^2 \frac{d^2 E_{\text{sym}}(\rho)}{d\rho^2} \Big|_{\rho=\rho_0}, \quad (31)$$

$$J_0 = (3\rho_0)^3 \frac{d^3 E_0(\rho)}{d\rho^3} \Big|_{\rho=\rho_0}, J_{\text{sym}} = (3\rho_0)^3 \frac{d^3 E_{\text{sym}}(\rho)}{d\rho^3} \Big|_{\rho=\rho_0}, \quad (32)$$

$$I_0 = (3\rho_0)^4 \frac{d^4 E_0(\rho)}{d\rho^4} \Big|_{\rho=\rho_0}, I_{\text{sym}} = (3\rho_0)^4 \frac{d^4 E_{\text{sym}}(\rho)}{d\rho^4} \Big|_{\rho=\rho_0}, \quad (33)$$

$$H_0 = (3\rho_0)^5 \frac{d^5 E_0(\rho)}{d\rho^5} \Big|_{\rho=\rho_0}, H_{\text{sym}} = (3\rho_0)^5 \frac{d^5 E_{\text{sym}}(\rho)}{d\rho^5} \Big|_{\rho=\rho_0}, \quad (34)$$

respectively. Obviously, we have  $L_0 = 0$  by the definition of  $\rho_0$  in Eq. (27).  $K_0$  is the incompressibility coefficient of SNM which characterizes the curvature of  $E_0(\rho)$  at  $\rho_0$ .  $J_0$ ,  $I_0$  and  $H_0$  represent higher-order contributions and are commonly referred to as the skewness, kurtosis and hyper-skewness coefficients of SNM.  $L$ ,  $K_{\text{sym}}$ ,  $J_{\text{sym}}$ ,  $I_{\text{sym}}$  and  $H_{\text{sym}}$  are the slope coefficient, curvature coefficient, skewness coefficient, kurtosis coefficient and hyper-skewness coefficient of the symmetry energy at  $\rho_0$ . The expressions of these characteristic parameters are presented in Appendix B.



### D. Single-nucleon potential, symmetry potential, nucleon effective masses and linear isospin splitting coefficient in cold nuclear matter

In the case of zero-temperature and uniform nuclear matter, the single-nucleon potential [Eq. (19)] reduces to an analytical function of  $\rho$ ,  $\delta$ , and the magnitude of nucleon momentum  $p = |\vec{p}|$ , i.e.,

$$\begin{aligned}
U_\tau(\rho, \delta, p) = & \frac{1}{4} t_0 [2(x_0 + 2) - (2x_0 + 1)(1 + \tau\delta)] \rho \\
& + \sum_{n=1}^5 \frac{1}{24} t_3^{[2n-1]} \left[ \left( \frac{2n-1}{3} + 2 \right) (x_3^{[2n-1]} + 2) - (2x_3^{[2n-1]} + 1) \left( \frac{1}{2} \frac{2n-1}{3} F_2 + 1 + \tau\delta \right) \right] \rho^{\frac{2n-1}{3}+1} \\
& + \frac{1}{4} C^{[2]} \left[ \frac{1}{3} \frac{k_F^3}{\pi^2} \left( \frac{p}{\hbar} \right)^2 + \frac{1}{5} \frac{k_F^5}{\pi^2} F_{5/3} \right] + \frac{1}{8} D^{[2]} \left[ \frac{1}{3} \frac{k_F^3}{\pi^2} \left( \frac{p}{\hbar} \right)^2 (1 + \tau\delta) + \frac{1}{5} \frac{k_F^5}{\pi^2} (1 + \tau\delta)^{5/3} \right] \\
& + \frac{1}{8} C^{[4]} \left[ \frac{1}{3} \frac{k_F^3}{\pi^2} \left( \frac{p}{\hbar} \right)^4 + \frac{2}{3} \frac{k_F^5}{\pi^2} \left( \frac{p}{\hbar} \right)^2 F_{5/3} + \frac{1}{7} \frac{k_F^7}{\pi^2} F_{7/3} \right] \\
& + \frac{1}{16} D^{[4]} \left[ \frac{1}{3} \frac{k_F^3}{\pi^2} \left( \frac{p}{\hbar} \right)^4 (1 + \tau\delta) + \frac{2}{3} \frac{k_F^5}{\pi^2} \left( \frac{p}{\hbar} \right)^2 (1 + \tau\delta)^{5/3} + \frac{1}{7} \frac{k_F^7}{\pi^2} (1 + \tau\delta)^{7/3} \right] \\
& + \frac{1}{4} C^{[6]} \left[ \frac{1}{3} \frac{k_F^3}{\pi^2} \left( \frac{p}{\hbar} \right)^6 + \frac{7}{5} \frac{k_F^5}{\pi^2} \left( \frac{p}{\hbar} \right)^4 F_{5/3} + \frac{k_F^7}{\pi^2} \left( \frac{p}{\hbar} \right)^2 F_{7/3} + \frac{1}{9} \frac{k_F^9}{\pi^2} F_3 \right] \\
& + \frac{1}{8} D^{[6]} \left[ \frac{1}{3} \frac{k_F^3}{\pi^2} \left( \frac{p}{\hbar} \right)^6 (1 + \tau\delta) + \frac{7}{5} \frac{k_F^5}{\pi^2} \left( \frac{p}{\hbar} \right)^4 (1 + \tau\delta)^{5/3} + \frac{k_F^7}{\pi^2} \left( \frac{p}{\hbar} \right)^2 (1 + \tau\delta)^{7/3} + \frac{1}{9} \frac{k_F^9}{\pi^2} (1 + \tau\delta)^3 \right] \\
& + \frac{1}{32} C^{[8]} \left[ \frac{1}{3} \frac{k_F^3}{\pi^2} \left( \frac{p}{\hbar} \right)^8 + \frac{12}{5} \frac{k_F^5}{\pi^2} \left( \frac{p}{\hbar} \right)^6 F_{5/3} + \frac{18}{5} \frac{k_F^7}{\pi^2} \left( \frac{p}{\hbar} \right)^4 F_{7/3} + \frac{4}{3} \frac{k_F^9}{\pi^2} \left( \frac{p}{\hbar} \right)^2 F_3 + \frac{1}{11} \frac{k_F^{11}}{\pi^2} F_{11/3} \right] \\
& + \frac{1}{64} D^{[8]} \left[ \frac{1}{3} \frac{k_F^3}{\pi^2} \left( \frac{p}{\hbar} \right)^8 (1 + \tau\delta) + \frac{12}{5} \frac{k_F^5}{\pi^2} \left( \frac{p}{\hbar} \right)^6 (1 + \tau\delta)^{5/3} + \frac{18}{5} \frac{k_F^7}{\pi^2} \left( \frac{p}{\hbar} \right)^4 (1 + \tau\delta)^{7/3} \right. \\
& \quad \left. + \frac{4}{3} \frac{k_F^9}{\pi^2} \left( \frac{p}{\hbar} \right)^2 (1 + \tau\delta)^3 + \frac{1}{11} \frac{k_F^{11}}{\pi^2} F_{11/3} (1 + \tau\delta)^{11/3} \right] \\
& + \frac{1}{64} C^{[10]} \left[ \frac{1}{3} \frac{k_F^3}{\pi^2} \left( \frac{p}{\hbar} \right)^{10} + \frac{11}{3} \frac{k_F^5}{\pi^2} \left( \frac{p}{\hbar} \right)^8 F_{5/3} + \frac{66}{7} \frac{k_F^7}{\pi^2} \left( \frac{p}{\hbar} \right)^6 F_{7/3} + \frac{22}{3} \frac{k_F^9}{\pi^2} \left( \frac{p}{\hbar} \right)^4 F_3 \right. \\
& \quad \left. + \frac{5}{3} \frac{k_F^{11}}{\pi^2} \left( \frac{p}{\hbar} \right)^2 F_{11/3} + \frac{1}{13} \frac{k_F^{13}}{\pi^2} F_{13/3} \right] \\
& + \frac{1}{128} D^{[10]} \left[ \frac{1}{3} \frac{k_F^3}{\pi^2} \left( \frac{p}{\hbar} \right)^{10} (1 + \tau\delta) + \frac{11}{3} \frac{k_F^5}{\pi^2} \left( \frac{p}{\hbar} \right)^8 (1 + \tau\delta)^{5/3} + \frac{66}{7} \frac{k_F^7}{\pi^2} \left( \frac{p}{\hbar} \right)^6 (1 + \tau\delta)^{7/3} \right. \\
& \quad \left. + \frac{22}{3} \frac{k_F^9}{\pi^2} \left( \frac{p}{\hbar} \right)^4 (1 + \tau\delta)^3 + \frac{5}{3} \frac{k_F^{11}}{\pi^2} \left( \frac{p}{\hbar} \right)^2 (1 + \tau\delta)^{11/3} + \frac{1}{13} \frac{k_F^{13}}{\pi^2} (1 + \tau\delta)^{13/3} \right], \tag{35}
\end{aligned}$$

where  $\tau$  equals 1 [-1] for neutrons [proton] and  $k_F = (3\pi^2\rho/2)^{1/3}$  is the Fermi wave number of nucleons in the SNM. Expanding  $U_\tau(\rho, \delta, p)$  as a power series in  $\tau\delta$ , we can obtain

$$U_\tau(\rho, \delta, p) = U_0(\rho, p) + \sum_{i=1,2,\dots} U_{\text{sym},i}(\rho, p)(\tau\delta)^i = U_0(\rho, p) + U_{\text{sym},1}(\rho, p)(\tau\delta) + U_{\text{sym},2}(\rho, p)(\tau\delta)^2 + \dots, \tag{36}$$

where

$$\begin{aligned}
U_0(\rho, p) \equiv & U_\tau(\rho, \delta = 0, p) \\
= & \frac{3}{4} t_0 \rho + \sum_{n=1}^5 \frac{t_3^{[2n-1]}}{16} \left( \frac{2n-1}{3} + 2 \right) \rho^{\frac{2n-1}{3}+1} + \frac{1}{8} (2C^{[2]} + D^{[2]}) \left[ \frac{1}{3} \frac{k_F^3}{\pi^2} \left( \frac{p}{\hbar} \right)^2 + \frac{1}{5} \frac{k_F^5}{\pi^2} \right] \\
& + \frac{1}{16} (2C^{[4]} + D^{[4]}) \left[ \frac{1}{3} \frac{k_F^3}{\pi^2} \left( \frac{p}{\hbar} \right)^4 + \frac{2}{3} \frac{k_F^5}{\pi^2} \left( \frac{p}{\hbar} \right)^2 + \frac{1}{7} \frac{k_F^7}{\pi^2} \right] \\
& + \frac{1}{8} (2C^{[6]} + D^{[6]}) \left[ \frac{1}{3} \frac{k_F^3}{\pi^2} \left( \frac{p}{\hbar} \right)^6 + \frac{7}{5} \frac{k_F^5}{\pi^2} \left( \frac{p}{\hbar} \right)^4 + \frac{k_F^7}{\pi^2} \left( \frac{p}{\hbar} \right)^2 + \frac{1}{9} \frac{k_F^9}{\pi^2} \right] \\
& + \frac{1}{64} (2C^{[8]} + D^{[8]}) \left[ \frac{1}{3} \frac{k_F^3}{\pi^2} \left( \frac{p}{\hbar} \right)^8 + \frac{12}{5} \frac{k_F^5}{\pi^2} \left( \frac{p}{\hbar} \right)^6 + \frac{18}{5} \frac{k_F^7}{\pi^2} \left( \frac{p}{\hbar} \right)^4 + \frac{4}{3} \frac{k_F^9}{\pi^2} \left( \frac{p}{\hbar} \right)^2 + \frac{1}{11} \frac{k_F^{11}}{\pi^2} \right] \\
& + \frac{1}{128} (2C^{[10]} + D^{[10]}) \left[ \frac{1}{3} \frac{k_F^3}{\pi^2} \left( \frac{p}{\hbar} \right)^{10} + \frac{11}{3} \frac{k_F^5}{\pi^2} \left( \frac{p}{\hbar} \right)^8 + \frac{66}{7} \frac{k_F^7}{\pi^2} \left( \frac{p}{\hbar} \right)^6 + \frac{22}{3} \frac{k_F^9}{\pi^2} \left( \frac{p}{\hbar} \right)^4 + \frac{5}{3} \frac{k_F^{11}}{\pi^2} \left( \frac{p}{\hbar} \right)^2 + \frac{1}{13} \frac{k_F^{13}}{\pi^2} \right] \tag{37}
\end{aligned}$$

is the single-nucleon potential in SNM and  $U_{\text{sym},i}$  can be expressed as

$$U_{\text{sym},i}(\rho, p) \equiv \frac{1}{i!} \frac{\partial^i U_n(\rho, \delta, p)}{\partial \delta^i} \Big|_{\delta=0} = \frac{(-1)^i}{i!} \frac{\partial^i U_p(\rho, \delta, p)}{\partial \delta^i} \Big|_{\delta=0}. \quad (38)$$

Neglecting higher-order terms ( $\delta^2, \delta^3, \dots$ ) in Eq. (36) leads to the well-known Lane potential [121]:

$$U_\tau(\rho, \delta, p) \approx U_0(\rho, p) + U_{\text{sym}}(\rho, p)(\tau\delta). \quad (39)$$

In the following, we abbreviate the first-order symmetry potential  $U_{\text{sym},1}$  as  $U_{\text{sym}}$ , and it can be expressed as

$$\begin{aligned} U_{\text{sym}}(\rho, p) = & -\frac{1}{4}t_0(2x_0+1)\rho - \sum_{n=1}^5 \frac{1}{24}t_3^{[2n-1]} \left(2x_3^{[2n-1]}+1\right) \rho^{\frac{2n-1}{3}+1} + \frac{D^{[2]}}{8} \left[ \frac{1}{3} \frac{k_F^3}{\pi^2} \left(\frac{p}{\hbar}\right)^2 + \frac{1}{3} \frac{k_F^5}{\pi^2} \right] \\ & + \frac{D^{[4]}}{16} \left[ \frac{1}{3} \frac{k_F^3}{\pi^2} \left(\frac{p}{\hbar}\right)^4 + \frac{10}{9} \frac{k_F^5}{\pi^2} \left(\frac{p}{\hbar}\right)^2 + \frac{1}{3} \frac{k_F^7}{\pi^2} \right] + \frac{D^{[6]}}{8} \left[ \frac{1}{3} \frac{k_F^3}{\pi^2} \left(\frac{p}{\hbar}\right)^6 + \frac{7}{3} \frac{k_F^5}{\pi^2} \left(\frac{p}{\hbar}\right)^4 + \frac{7}{3} \frac{k_F^7}{\pi^2} \left(\frac{p}{\hbar}\right)^2 + \frac{1}{3} \frac{k_F^9}{\pi^2} \right] \\ & + \frac{D^{[8]}}{64} \left[ \frac{1}{3} \frac{k_F^3}{\pi^2} \left(\frac{p}{\hbar}\right)^8 + 4 \frac{k_F^5}{\pi^2} \left(\frac{p}{\hbar}\right)^6 + \frac{42}{5} \frac{k_F^7}{\pi^2} \left(\frac{p}{\hbar}\right)^4 + 4 \frac{k_F^9}{\pi^2} \left(\frac{p}{\hbar}\right)^2 + \frac{1}{3} \frac{k_F^{11}}{\pi^2} \right] \\ & + \frac{D^{[10]}}{128} \left[ \frac{1}{3} \frac{k_F^3}{\pi^2} \left(\frac{p}{\hbar}\right)^{10} + \frac{55}{9} \frac{k_F^5}{\pi^2} \left(\frac{p}{\hbar}\right)^8 + 22 \frac{k_F^7}{\pi^2} \left(\frac{p}{\hbar}\right)^6 + 22 \frac{k_F^9}{\pi^2} \left(\frac{p}{\hbar}\right)^4 + \frac{55}{9} \frac{k_F^{11}}{\pi^2} \left(\frac{p}{\hbar}\right)^2 + \frac{1}{3} \frac{k_F^{13}}{\pi^2} \right]. \end{aligned} \quad (40)$$

The nucleon effective mass is used to characterize the momentum dependence of the single-nucleon potential, and in nonrelativistic models, it can be expressed as [122, 123]

$$\frac{m_\tau^*(\rho, \delta)}{m} = \left[ 1 + \frac{m}{p} \frac{dU_\tau(\rho, \delta, p)}{dp} \Big|_{p=p_{F\tau}} \right]^{-1}. \quad (41)$$

The isoscalar nucleon effective mass  $m_s^*$  is the nucleon effective mass in SNM, and the isovector nucleon effective mass  $m_v^*$  is the effective mass of proton (neutron) in pure neutron (proton) matter, and their expressions are provided in Appendix B. Additionally, a subscript “0” denotes that the nucleon effective mass is defined at the saturation density  $\rho_0$ , e.g.,  $m_{s,0}^*$  and  $m_{v,0}^*$ . The nucleon effective mass splitting, denoted as  $m_{n-p}^*(\rho, \delta) \equiv [m_n^*(\rho, \delta) - m_p^*(\rho, \delta)]/m$ , is extensively used in nuclear physics.  $m_{n-p}^*(\rho, \delta)$  can be expanded as a power series in  $\delta$ , i.e.,

$$m_{n-p}^*(\rho, \delta) = \sum_{n=1}^{\infty} \Delta m_{2n-1}^*(\rho) \delta^{2n-1}, \quad (42)$$

where  $\Delta m_{2n-1}^*(\rho)$  are the isospin splitting coefficients (of the nucleon effective mass). The first coefficient  $\Delta m_1^*(\rho)$  is usually referred to as the linear isospin splitting coefficient, whose expression is presented in Appendix B.

### III. FITTING STRATEGY AND NEW INTERACTIONS

The gradient terms make no contribution to the properties of uniform nuclear matter, thus the parameters  $E^{[n]}$  and  $F^{[n]}$  ( $n = 2, 4, 6, 8, 10$ ) are irrelevant to the following discussions about the nuclear matter. However, the gradient terms are important for transport model and nuclear structure, and the values of  $E^{[n]}$  and  $F^{[n]}$  could be determined by the finite nuclei calculation, which is beyond the scope of this work.

The construction of interactions with the N3LO model has been discussed in detail in Ref. [88], and we briefly outline the similar process carried out in this work for completeness. To clearly demonstrate the fitting process,  $U_0(\rho_0, p)$  [Eq. (37)] and  $U_{\text{sym}}(\rho_0, p)$  [Eq. (40)] can

be expressed as

$$\begin{aligned} U_0(\rho_0, p) \equiv & a_0 + a_2 \left(\frac{p}{\hbar}\right)^2 + a_4 \left(\frac{p}{\hbar}\right)^4 \\ & + a_6 \left(\frac{p}{\hbar}\right)^6 + a_8 \left(\frac{p}{\hbar}\right)^8 + a_{10} \left(\frac{p}{\hbar}\right)^{10}, \end{aligned} \quad (43)$$

and

$$\begin{aligned} U_{\text{sym}}(\rho_0, p) \equiv & b_0 + b_2 \left(\frac{p}{\hbar}\right)^2 + b_4 \left(\frac{p}{\hbar}\right)^4 \\ & + b_6 \left(\frac{p}{\hbar}\right)^6 + b_8 \left(\frac{p}{\hbar}\right)^8 + b_{10} \left(\frac{p}{\hbar}\right)^{10}, \end{aligned} \quad (44)$$

where  $a_n$  and  $b_n$  ( $n = 0, 2, 4, 6, 8, 10$ ) take the following

forms

$$\begin{aligned}
a_0 = & \frac{3}{4}t_0\rho_0 + \sum_{n=1}^5 \frac{t_3^{[2n-1]}}{16} \left( \frac{2n-1}{3} + 2 \right) \rho_0^{\frac{2n-1}{3}+1} \\
& + \frac{k_{F_0}^5}{40\pi^2} (2C^{[2]} + D^{[2]}) + \frac{k_{F_0}^7}{112\pi^2} (2C^{[4]} + D^{[4]}) \\
& + \frac{k_{F_0}^9}{72\pi^2} (2C^{[6]} + D^{[6]}) + \frac{k_{F_0}^{11}}{704\pi^2} (2C^{[8]} + D^{[8]}) \\
& + \frac{k_{F_0}^{13}}{1664\pi^2} (2C^{[10]} + D^{[10]}), \tag{45}
\end{aligned}$$

$$\begin{aligned}
a_2 = & \frac{k_{F_0}^3}{24\pi^2} (2C^{[2]} + D^{[2]}) + \frac{k_{F_0}^5}{24\pi^2} (2C^{[4]} + D^{[4]}) \\
& + \frac{k_{F_0}^7}{8\pi^2} (2C^{[6]} + D^{[6]}) + \frac{k_{F_0}^9}{48\pi^2} (2C^{[8]} + D^{[8]}) \\
& + \frac{5k_{F_0}^{11}}{384\pi^2} (2C^{[10]} + D^{[10]}), \tag{46}
\end{aligned}$$

$$\begin{aligned}
a_4 = & \frac{k_{F_0}^3}{48\pi^2} (2C^{[4]} + D^{[4]}) + \frac{7k_{F_0}^5}{40\pi^2} (2C^{[6]} + D^{[6]}) \\
& + \frac{9k_{F_0}^7}{160\pi^2} (2C^{[8]} + D^{[8]}) + \frac{11k_{F_0}^9}{192\pi^2} (2C^{[10]} + D^{[10]}), \tag{47}
\end{aligned}$$

$$\begin{aligned}
a_6 = & \frac{k_{F_0}^3}{24\pi^2} (2C^{[6]} + D^{[6]}) + \frac{3k_{F_0}^5}{80\pi^2} (2C^{[8]} + D^{[8]}) \\
& + \frac{33k_{F_0}^7}{448\pi^2} (2C^{[10]} + D^{[10]}), \tag{48}
\end{aligned}$$

$$a_8 = \frac{k_{F_0}^3}{192\pi^2} (2C^{[8]} + D^{[8]}) + \frac{11k_{F_0}^5}{384\pi^2} (2C^{[10]} + D^{[10]}), \tag{49}$$

$$a_{10} = \frac{k_{F_0}^3}{384\pi^2} (2C^{[10]} + D^{[10]}), \tag{50}$$

and

$$\begin{aligned}
b_0 = & -\frac{1}{4}t_0(2x_0 + 1)\rho_0 \\
& - \sum_{n=1}^5 \frac{1}{24}t_3^{[2n-1]} \left( 2x_3^{[2n-1]} + 1 \right) \rho_0^{\frac{2n-1}{3}+1} \\
& + \frac{k_{F_0}^5}{24\pi^2} D^{[2]} + \frac{k_{F_0}^7}{48\pi^2} D^{[4]} + \frac{k_{F_0}^9}{24\pi^2} D^{[6]} \\
& + \frac{k_{F_0}^{11}}{192\pi^2} D^{[8]} + \frac{k_{F_0}^{13}}{384\pi^2} D^{[10]}, \tag{51}
\end{aligned}$$

$$\begin{aligned}
b_2 = & \frac{k_{F_0}^3}{24\pi^2} D^{[2]} + \frac{5k_{F_0}^5}{72\pi^2} D^{[4]} + \frac{7k_{F_0}^7}{24\pi^2} D^{[6]} \\
& + \frac{k_{F_0}^9}{16\pi^2} D^{[8]} + \frac{55k_{F_0}^{11}}{1152\pi^2} D^{[10]}, \tag{52}
\end{aligned}$$

TABLE I. The independent model parameters, the adjustable quantities and the total number (t.n.) of them for different models.

Models	Parameters	Quantities	t.n.
N3LO	$t_0, x_0, t_3^{[1]}, x_3^{[1]}, t_3^{[3]}, x_3^{[3]}, t_3^{[5]}, x_3^{[5]}, C^{[2]}, D^{[2]}, C^{[4]}, D^{[4]}, C^{[6]}, D^{[6]}$	$\rho_0, E_0(\rho_0), K_0, J_0, E_{\text{sym}}(\rho_0), L, K_{\text{sym}}, J_{\text{sym}}, a_2, a_4, a_6, b_2, b_4, b_6$	14
N4LO	N3LO + $t_3^{[7]}, x_3^{[7]}, C^{[8]}, D^{[8]}$	N3LO + $I_0, I_{\text{sym}}, a_8, b_8$	18
N5LO	N4LO + $t_3^{[9]}, x_3^{[9]}, C^{[10]}, D^{[10]}$	N4LO + $H_0, H_{\text{sym}}, a_{10}, b_{10}$	22

$$\begin{aligned}
b_4 = & \frac{k_{F_0}^3}{48\pi^2} D^{[4]} + \frac{7k_{F_0}^5}{24\pi^2} D^{[6]} + \frac{21k_{F_0}^7}{160\pi^2} D^{[8]} \\
& + \frac{11k_{F_0}^9}{64\pi^2} D^{[10]}, \tag{53}
\end{aligned}$$

$$b_6 = \frac{k_{F_0}^3}{24\pi^2} D^{[6]} + \frac{k_{F_0}^5}{16\pi^2} D^{[8]} + \frac{11k_{F_0}^7}{64\pi^2} D^{[10]} \tag{54}$$

$$b_8 = \frac{k_{F_0}^3}{192\pi^2} D^{[8]} + \frac{55k_{F_0}^5}{1152\pi^2} D^{[10]}, \tag{55}$$

$$b_{10} = \frac{k_{F_0}^3}{384\pi^2} D^{[10]}. \tag{56}$$

In Table I, we list the independent model parameters and the adjustable quantities in the N3LO, N4LO and N5LO models, respectively. The number of parameters equals to the number of characteristic quantities, which are also listed in Table I. The values of all adjustable parameters must be provided in order to fully construct an interaction, i.e., determine all the model parameters. It is worth emphasizing again that these parameters and quantities are related to the properties of uniform nuclear matter. Only when the values of  $E^{[n]}$  and  $F^{[n]}$  are determined through finite nuclei calculations can all the Skyrme parameters in Eqs. (7)-(9) be completely obtained.

In N3LO, N4LO, and N5LO models, we set the values of  $\rho_0$ ,  $E_0(\rho_0)$  and  $K_0$  to be  $0.16 \text{ fm}^{-3}$ ,  $-16 \text{ MeV}$ , and  $230 \text{ MeV}$ , respectively. Next, we use GEKKO optimization suite [124] to minimize the weighted squared difference  $\chi^2$  between  $U_0$  in Eq. (37) and the nucleon optical potential data  $U_{\text{opt}}$  [70, 71] and its extrapolation above 1 GeV:

$$\chi^2 = \sum_{i=1}^{N_d} \left( \frac{U_{0,i} - U_{\text{opt},i}}{\sigma_i} \right)^2, \tag{57}$$

with constraint of the HVH theorem [110, 111], i.e.,

$$E_0(\rho_0) = \frac{p_{F_0}^2}{2m} + U_0(\rho_0, p_{F_0}). \tag{58}$$

The  $N_d$  is the number of the experimental data points. Since there are actually no practical errors  $\sigma_i$  here, we

TABLE II. The isoscalar nucleon effective mass at saturation density ( $m_{s,0}^*$ ) and the  $a_n$  parameters related to the momentum dependence of the single-nucleon potential.

	N3LO	N4LO	N5LO
$m_{s,0}^*/m$	0.773	0.761	0.760
$a_0$ (MeV)	-64.03	-64.88	-64.97
$a_2$ (MeV fm <sup>2</sup> )	6.518	7.044	7.104
$a_4$ (MeV fm <sup>4</sup> )	-0.1260	-0.1545	-0.1628
$a_6$ (MeV fm <sup>6</sup> )	$8.133 \times 10^{-4}$	$1.428 \times 10^{-3}$	$1.731 \times 10^{-3}$
$a_8$ (MeV fm <sup>8</sup> )	-	$-4.703 \times 10^{-6}$	$-8.614 \times 10^{-6}$
$a_{10}$ (MeV fm <sup>10</sup> )	-	-	$1.621 \times 10^{-8}$

assign equal weights to each data point within the range of the nucleon momentum up to 1.5 GeV/c, 2.0 GeV/c, and 2.5 GeV/c (approximately corresponding to nucleon kinetic energy of 1 GeV, 1.5 GeV and 2 GeV) for N3LO, N4LO and N5LO models, respectively. The values of  $a_n$  parameters and the isoscalar nucleon effective mass at saturation density  $m_{s,0}^*$  are presented in Table II. In N3LO model, the last independent quantity related to SNM,  $J_0$ , is constrained by the flow data in HICs [3], and it is set to be the maximum allowed value, i.e., -383 MeV. In N4LO (N5LO) model,  $I_0$  (as well as  $H_0$ ) are adjustable, and we set them to their corresponding values calculated from N3LO model, i.e.,  $I_0 = 1818.9$  MeV and  $H_0 = -12065$  MeV.

Considering its significant uncertainty, we construct eight kinds of symmetry potential (i.e., 8 different  $b_n$  parameter sets), with  $\Delta m_1^*(\rho_0)$  values of -0.7, -0.5, -0.3, -0.1, 0.1, 0.3, 0.5, and 0.7. To avoid too many degrees of freedom and ensure that symmetry potential behaves well within the momentum range up to 2 GeV/c, the values of  $b_n$  are given by analogy the Taylor expansion of the cosine function, i.e.,

$$b_n = A \frac{(-1)^{n/2}}{n!} \left( \frac{\pi}{10} \right)^n \quad (\text{MeV fm}^n), \quad (59)$$

where  $A$  is the only adjustable parameter to provide the corresponding  $\Delta m_1^*(\rho_0)$  value, and  $n = 2, 4, 6$  for N3LO model,  $n = 2, 4, 6, 8$  for N4LO model, and  $n = 2, 4, 6, 8, 10$  for N5LO model. The values of  $A$  corresponding to 8 different  $\Delta m_1^*(\rho_0)$  values (8 different momentum dependencies of the symmetry potential) are listed in Table. III, and the corresponding  $b_n$  can be obtained through Eq. (59). It is worth noting that the value of  $b_0$  is determined by the theorem of the symmetry energy decomposition [104–109]:

$$E_{\text{sym}}(\rho_0) = \frac{1}{3} \frac{p_{F_0}^2}{2m_{s,0}^*} + \frac{1}{2} U_{\text{sym}}(\rho_0, p_{F_0}), \quad (60)$$

once the value of  $E_{\text{sym}}(\rho_0)$  is given. The quantities related to the symmetry energy in N3LO model have been discussed in detail in Ref. [88]. We set  $E_{\text{sym}}(\rho_0)$ ,  $L$ ,  $K_{\text{sym}}$ , and  $J_{\text{sym}}$  to their values in parameter set “SP6L45” from Ref. [88], namely  $E_{\text{sym}}(\rho_0) = 30$  MeV,  $L = 45$  MeV,

TABLE III. The values of  $A$  in Eq. (59) used in the parametrization of the symmetry potential, corresponding to different models and different  $\Delta m_1^*(\rho_0)$ . The values of  $b_n$  can be calculated through Eq. (59).

$\Delta m_1^*(\rho_0)$	$A$ (N3LO)	$A$ (N4LO)	$A$ (N5LO)
0.1	30.17	30.08	29.84
-0.1	-42.19	-44.61	-45.04
0.3	102.5	104.8	104.7
-0.3	-114.6	-119.3	-119.9
0.5	174.9	179.5	179.6
-0.5	-186.9	-194.0	-194.8
0.7	247.2	254.2	254.5
-0.7	-259.3	-268.7	-269.7

TABLE IV. The values of characteristic quantities related to SNM, and non-adjustable quantities are enclosed in “ ”.

	SP6	SP8	SP10
$\rho_0$ (fm <sup>-3</sup> )	0.160	0.160	0.160
$E_0(\rho_0)$ (MeV)	-16.0	-16.0	-16.0
$K_0$ (MeV)	230.0	230.0	230.0
$J_0$ (MeV)	-383.0	-383.0	-383.0
$I_0$ (MeV)	“1818.9”	1818.9	1818.9
$H_0$ (MeV)	“-12065”	“-12090”	-12065

$K_{\text{sym}} = -110$  MeV, and  $J_{\text{sym}} = 700$  MeV, to simultaneously satisfy the theoretical prediction of the EOS of PNM and various neutron star observations. The values of  $I_{\text{sym}}$  in N4LO models as well as  $H_{\text{sym}}$  in N5LO model are set to their corresponding values calculated from N3LO model, which will vary due to the differences in  $\Delta m_1^*(\rho_0)$ .

Finally, the combination of the 3 different models namely, N3LO, N4LO and N5LO and 8 different symmetry potentials forms a parameter set family consisting of 24 parameter sets. These parameters have similar density behavior of the SNM EOS and the symmetry energy by construction. We name these parameter sets as SPNL45X, where: “SP” indicates the framework of the Skyrme pseudopotential, and N represents the highest power of momentum, with N taking values of 6, 8, and 10 for N3LO, N4LO, and N5LO models, respectively; “L45” indicates that their  $L$  value is 45 MeV; “X” denotes the value of  $\Delta m_1^*(\rho_0)$ , i.e., X=Dm07, Dm05, Dm03, Dm01, D01, D03, D05, and D07 respectively indicate that the values of  $\Delta m_1^*(\rho_0)$  is -0.7, -0.5, -0.3, -0.1, 0.1, 0.3, 0.5, and 0.7. In Tables VII-IX at Appendix C, we list the Skyrme parameters for these 24 new interactions.

TABLE V. The values of high-order characteristic quantities of symmetry energy, including the kurtosis coefficient ( $I_{\text{sym}}$ ) and the hyper-skewness coefficient ( $H_{\text{sym}}$ ) corresponding to different linear isospin splitting coefficients [ $\Delta m_1^*(\rho_0)$ ] for different models. Also listed are the values of the isovector effective mass ( $m_{v,0}^*$ ) and the fourth-order symmetry energy [ $E_{\text{sym},4}(\rho_0)$ ]. Note that all the models share the common lower-order symmetry energy parameters of  $E_{\text{sym}}(\rho_0) = 30$  MeV,  $L = 45$  MeV,  $K_{\text{sym}} = -110$  MeV and  $J_{\text{sym}} = 700$  MeV.

SP6L45	Dm07	Dm05	Dm03	Dm01	D01	D03	D05	D07
$\Delta m_1^*(\rho_0)$	-0.7	-0.5	-0.3	-0.1	0.1	0.3	0.5	0.7
$I_{\text{sym}}$ (MeV)	-2241.3	-2284.7	-2328.2	-2371.6	-2415.1	-2458.5	-2502.0	-2545.5
$H_{\text{sym}}$ (MeV)	18845	19011	19177	19343	19509	19676	19842	20008
$m_{v,0}^*/m$	1.464	1.169	0.972	0.833	0.728	0.647	0.582	0.529
$E_{\text{sym},4}(\rho_0)$ (MeV)	-0.333	-0.0916	0.150	0.392	0.633	0.875	1.117	1.358
SP8L45	Dm07	Dm05	Dm03	Dm01	D01	D03	D05	D07
$\Delta m_1^*(\rho_0)$	-0.7	-0.5	-0.3	-0.1	0.1	0.3	0.5	0.7
$I_{\text{sym}}$ (MeV)	-2241.3	-2284.7	-2328.2	-2371.6	-2415.1	-2458.5	-2502.0	-2545.5
$H_{\text{sym}}$ (MeV)	18799	18972	19145	19318	19491	19663	19836	20009
$m_{v,0}^*/m$	1.464	1.161	0.962	0.812	0.716	0.635	0.571	0.518
$E_{\text{sym},4}(\rho_0)$ (MeV)	-0.366	-0.117	0.133	0.382	0.632	0.881	1.131	1.380
SP10L45	Dm07	Dm05	Dm03	Dm01	D01	D03	D05	D07
$\Delta m_1^*(\rho_0)$	-0.7	-0.5	-0.3	-0.1	0.1	0.3	0.5	0.7
$I_{\text{sym}}$ (MeV)	-2241.3	-2284.7	-2328.2	-2371.6	-2415.1	-2458.5	-2502.0	-2545.5
$H_{\text{sym}}$ (MeV)	18845	19011	19177	19343	19509	19676	19842	20008
$m_{v,0}^*/m$	1.465	1.161	0.962	0.821	0.716	0.635	0.570	0.517
$E_{\text{sym},4}(\rho_0)$ (MeV)	-0.372	-0.121	0.129	0.379	0.628	0.879	1.129	1.379

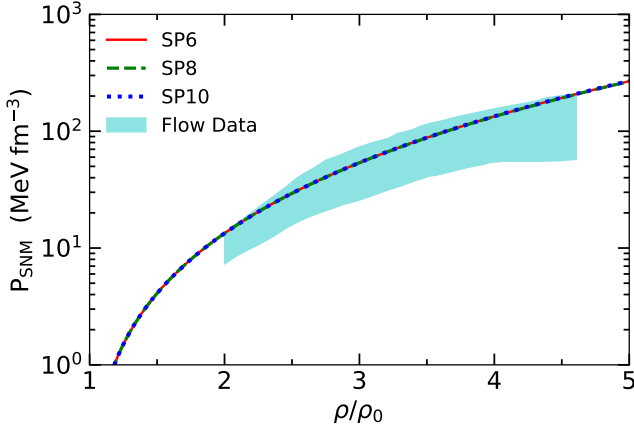


FIG. 1. The pressure of SNM [ $P_{\text{SNM}}(\rho)$ ] as a function of nucleon density given by the SP6, SP8 and SP10 models. Also included are the constraints from flow data in HICs [3].

#### IV. THE PROPERTIES OF COLD NUCLEAR MATTER

##### A. Bulk properties of cold nuclear matter

The values of characteristic quantities related to SNM of the three models are listed in Table IV, and non-adjustable quantities are denoted by “-”. In Fig. 1, we present the pressure of SNM [ $P_{\text{SNM}}(\rho)$ ] as a function of nucleon density given by SP6, SP8, and SP10 models, respectively. Also shown in Fig. 1 are the constraints from flow data in HICs [3]. It can be seen that the SNM pressure given by the three models is almost the same by the

construction, and all conform to the constraints given by the flow data.

For all interactions, the values of  $E_{\text{sym}}(\rho_0)$ ,  $L$ ,  $K_{\text{sym}}$  and  $J_{\text{sym}}$  are taken as 30 MeV, 45 MeV, -110 MeV and 700 MeV, respectively. Once these quantities are fixed: the values of  $I_{\text{sym}}$  and  $H_{\text{sym}}$  are determined in SP6 model; the values of  $I_{\text{sym}}$  remains adjustable, but  $H_{\text{sym}}$  is not independent in SP8 model; both  $I_{\text{sym}}$  and  $H_{\text{sym}}$  remain free to vary in SP10 model. To minimize the influence of the symmetry energy and thereby focus on the effects of different models (different momentum behaviors of the single-nucleon potential at high energies) and different symmetry potentials (different effective mass splitting), we set the values of  $I_{\text{sym}}$  in SP8 model, as well as  $I_{\text{sym}}$  and  $H_{\text{sym}}$  in SP10 model, to the values calculated in SP6 model. Table. V presents the values of  $I_{\text{sym}}$  and  $H_{\text{sym}}$  for different interactions corresponding to various  $\Delta m_1^*(\rho_0)$ . Also listed in Table V are the values of the isovector nucleon effective mass  $m_{v,0}^*$  and the fourth-order symmetry energy  $E_{\text{sym},4}(\rho_0)$ .

Shown in Fig. 2 is the EOS of PNM as a function of density predicted by different interactions and the result from combined microscopic calculations (see Ref. [119] and its references for details). It can be seen that all interactions are consistent with the microscopic theoretical calculations. Shown in Fig. 3 is the density dependence of the symmetry energy predicted by different interactions. It can be observed from each panel in Fig. 3 that the impact of different  $\Delta m_1^*(\rho_0)$  on the symmetry energy becomes apparent only at high densities. Moreover, for the same  $\Delta m_1^*(\rho_0)$ , the symmetry energy predicted by the three models are almost identical by construction.

To demonstrate the convergence of the high-order

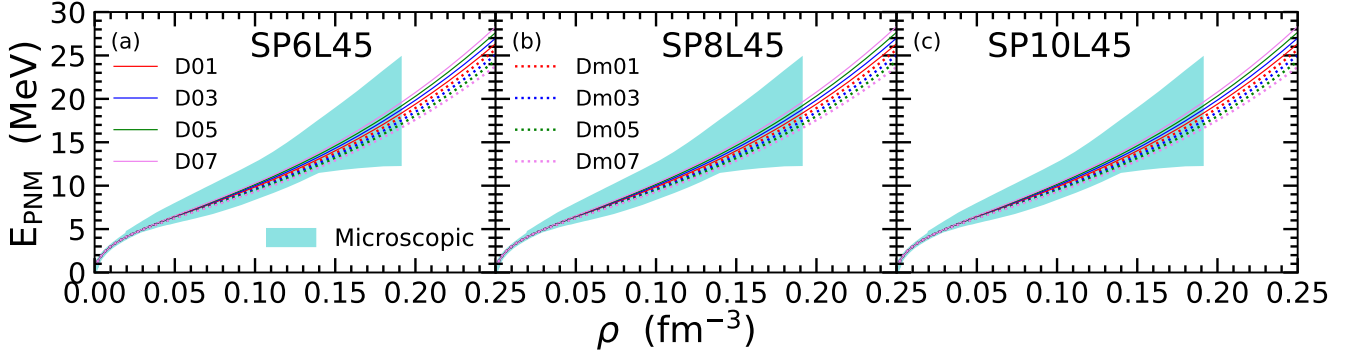


FIG. 2. The EOS of PNM predicted by different interactions, categorized according to different models. The band represents the microscopic calculation results [119] (see text for the details).

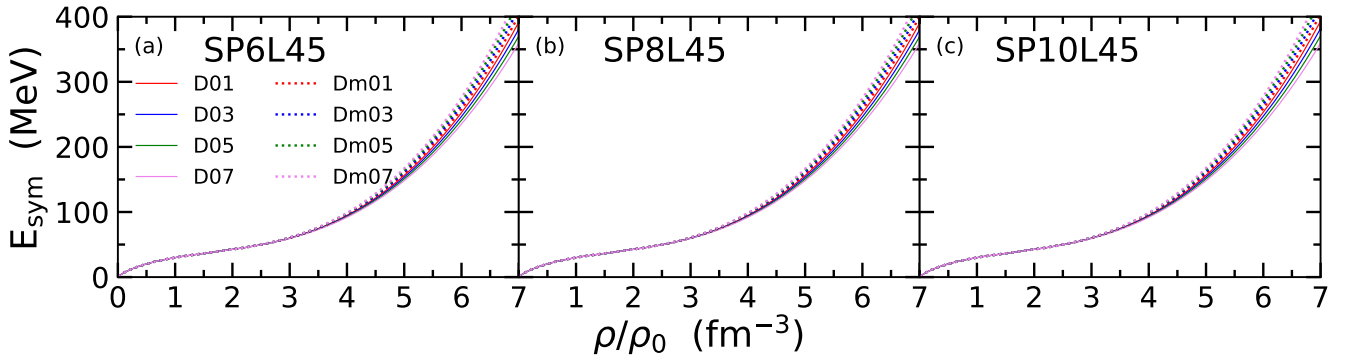


FIG. 3. The energy dependence of the symmetry energy predicted by different interactions, categorized according to different models (see text for the details).

derivatives, we further present the cumulative contributions of the MD term for the nuclear matter bulk properties. In Fig. 4, we display the SNM EOS from the momentum-independent (MID) part as well as from the sum of the MID part and the MD part up to different orders in the SP10 model. The result for the PNM EOS are presented in Fig. 5, using the SP10L45D03 model as an example. From Figs. 4 and 5, it can be seen that the SNM EOS converges up to  $p^4$ , while the PNM EOS converges up to  $p^6$ , with higher-order terms contributing negligibly. This is consistent with the conclusions in Ref. [68].

### B. Single-nucleon potential and symmetry potential

The momentum dependence of single-nucleon potential is characterized by isoscalar nucleon effective mass ( $m_s^*$ ), and it is also represented by parameters  $a_n$  in the three models. The values of  $m_{s,0}^*$  and  $a_n$  parameters are presented in Table II. Shown in Fig. 6 is the single-nucleon potential  $[U_0(\rho, p)]$  in cold SNM, predicted by SP6, SP8, and SP10 models, as a function of nucleon kinetic energy

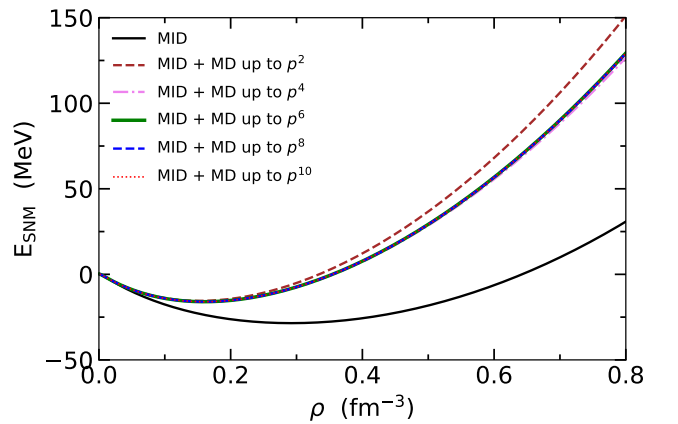


FIG. 4. The EOS of SNM as a function of nucleon density from the MID part as well as from the sum of the MID part and the MD part up to different orders in the SP10 model.

$E - m = \sqrt{p^2 + m^2} + U_0(\rho, p) - m$ , at  $\rho = 0.5\rho_0$ ,  $\rho_0$  and  $2\rho_0$ , respectively. Also shown in Fig. 6(a) is the real part of nucleon optical potential (Schrödinger equivalent potential) in SNM at  $\rho_0$  at the energy range up to 1 GeV

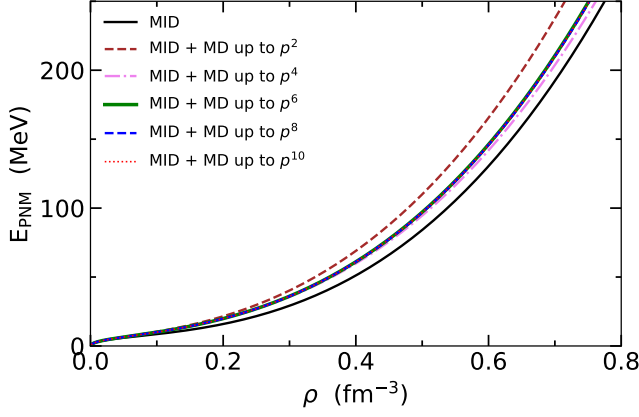


FIG. 5. The EOS of PNM as a function of nucleon density from the MID part as well from the sum of the MID part and the MD part up to different orders in the SP10L45D03 model.

obtained by Hama *et al.* [70, 71], from Dirac phenomenology of nucleon-nucleus scattering data. The extrapolation of Hama's data are also plotted in Fig. 6(a). It can be seen from Fig. 6(a) that through the optimization process we have performed in Sec. III,  $U_0(\rho, p)$  conforms rather well to the empirical nucleon optical potential (and its extrapolation) for nucleon kinetic energy up to 1 GeV, 1.5 GeV, and 2 GeV, with SP6, SP8, and SP10 models, respectively.

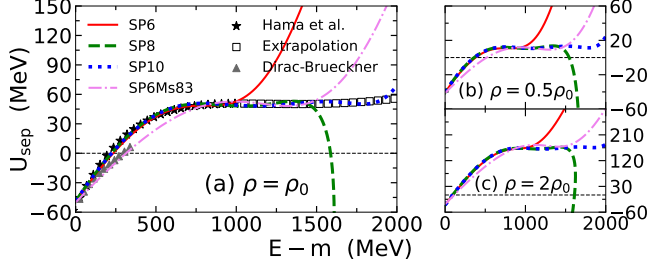


FIG. 6. The energy dependence of the single-nucleon potential in cold SNM predicted by SP6, SP8, SP10 and SP6Ms83. Also shown are the nucleon optical potential (Schrödinger equivalent potential,  $U_{\text{sep}}$ ) in SNM at  $\rho_0$  obtained by Hama *et al.* [70, 71] and the Dirac-Brueckner calculation [125].

The momentum dependence of the symmetry potential is determined by  $b_n$  parameters, whose values can be obtained through the parametrization in Eq. (59) and the  $A$  values listed in Table III. Figure 7 displays the symmetry potential  $U_{\text{sym}}(\rho_0, p)$  as a function of momentum for different interactions. For the same  $\Delta m_1^*(\rho_0)$ ,  $U_{\text{sym}}(\rho_0, p)$  obtained from SP6, SP8 and SP10 models are almost consistent within the momentum range up to 2 GeV/c. Also shown in Fig. 7 is the momentum dependence of  $U_{\text{sym}}(\rho_0, p)$  obtained from a global optical model analyses of the nucleon-nucleus scattering data at beam energies from 0.05 to 200 MeV [107, 126], and the value of  $m_{n-p}^*(\rho_0, \delta)$  is predicted to be  $(0.41 \pm 0.15)\delta$ . It

can be seen from Fig. 7 that, through this parametrization method, the predicted  $U_{\text{sym}}(\rho_0, p)$  for interactions with  $\Delta m_1^*(\rho_0)$  values being 0.3 and 0.5, i.e., SP6L45D03, SP8L45D03, SP10L45D03 and SP6L45D05, SP8L45D05, SP10L45D05 are consistent with the results from the optical model. The isovector nucleon effective mass  $m_v^*$  is

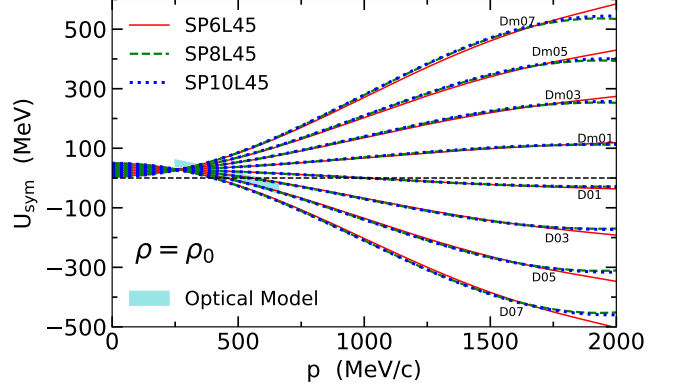


FIG. 7. The momentum dependence of the symmetry potential at saturation density with various interactions. Also included are the results from global optical model analyses [107, 126].

commonly used to describe the momentum dependence of  $U_{\text{sym}}(\rho, p)$ . In the conventional Skyrme interaction, the linear isospin splitting coefficient  $\Delta m_1^*(\rho)$  and the fourth-order symmetry energy  $E_{\text{sym},4}(\rho)$  have straightforward and interesting relations with  $m_s^*(\rho)$  and  $m_v^*(\rho)$  [127, 128]. However, in the N3LO (as well as N4LO and N5LO) Skyrme pseudopotential, since  $m_s(\rho, p)$  and  $m_v(\rho, p)$  are momentum-dependent, these relations become more complex [88]. In Table V, we present the values of  $m_{v,0}^*$  and  $E_{\text{sym},4}(\rho_0)$  of the different interactions.

Shown in Fig. 8 are the cumulative contributions from the MD terms up to different orders for the single-nucleon potential in the SP10 model. Also included in Fig. 8 are the nucleon optical potential obtained by Hama *et al.* [70, 71]. It can be seen from Fig. 8 that the contribution from  $p^{10}$  becomes significant when the nucleon momentum exceeds 1.5 GeV/c. The results for the symmetry potential with the SP10L45D03 model are presented in Fig. 9, where it can be observed that  $p^8$  is necessary for the symmetry potential to converge up to 2 GeV/c. It can be seen from Figs 8 and 9 that the higher-order momentum-dependence is crucial for the single-nucleon potential of high-momentum nucleons, although their contributions to the nuclear matter bulk properties around the saturation density are negligible.

### C. Neutron star properties

In the present work, we assume the core of neutron stars consists of free neutrons, protons, electrons and possible muons ( $npe\mu$  matter) without phase transition



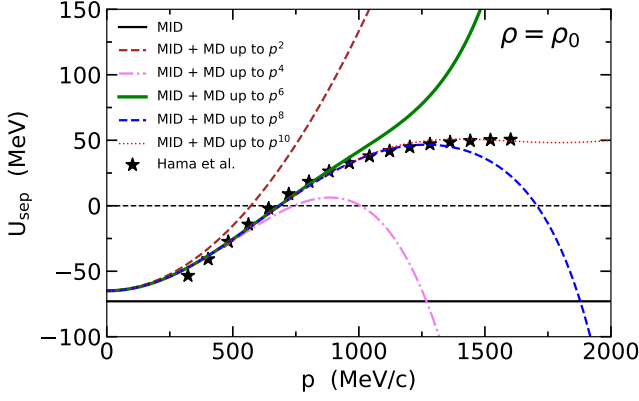


FIG. 8. The momentum dependence of the single-nucleon potential at saturation density from the MID part as well from the sum of the MID part and the MD part up to different orders in the SP10 model. Also shown are the nucleon optical potential obtained by Hama *et al.* [70, 71].

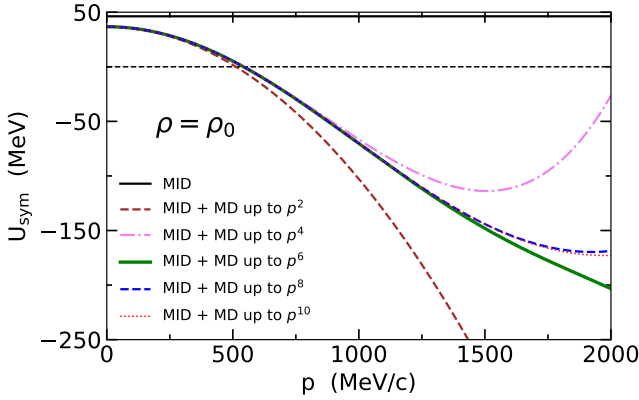


FIG. 9. The momentum dependence of the symmetry potential at saturation density from the MID part as well from the sum of the MID part and the MD part up to different orders in the SP10L45D03 model.

and other degrees of freedom at high densities. The EOS of the  $\beta$ -equilibrium and charge-neutral neutron star core is derived based on the different interactions previously constructed in this paper. The core-crust transition density  $\rho_t$  is obtained self-consistently using the dynamical methods [129], and the critical density separating the inner and the outer crust is taken to be  $\rho_{\text{out}} = 2.46 \times 10^{-4} \text{ fm}^{-3}$  [129–131]. For the outer crust, where  $\rho < \rho_{\text{out}}$ , we use the EOS of BPS (FMT) [132]; for the inner crust, where  $\rho_{\text{out}} < \rho < \rho_t$ , we construct the EOS by interpolation with the form [129–131]:

$$P = a + b\epsilon^{4/3}. \quad (61)$$

With the EOS of neutron star matter  $P(\epsilon)$ , one can obtain the mass-radius (M-R) relation of static neutron stars by solving the famous Tolman-Oppenheimer-Volkoff (TOV) equation [133, 134]. Shown in Fig. 10 are

the mass-radius relations of neutron stars obtained using different interactions. The simultaneous mass-radius determinations for PSR J0030+0451 [83, 84] and PSR J0437-4715 [87], both with a mass around  $1.4 M_\odot$ , as well as for PSR J0740+6620 [85, 86] with a mass around  $2.0 M_\odot$ , obtained from NICER (XMM-Newton) are also plotted for 68.3% credible intervals (CI) in Fig. 10 for comparison. As shown in Fig. 10, all of the 24 interactions are compatible with the constraint for PSR J0030+0451, PSR J0437-4715 and PSR J0740+6620, falling within the 68.3% CI. From Figs. 2 and 10, it can be observed that interactions with smaller  $\Delta m_1^*(\rho_0)$  predict smaller radii for low-mass neutron stars due to their smaller symmetry energy around and below saturation density.

Table. VI summarizes the core-crust transition density  $\rho_t$ , the central density  $\rho_{\text{cen}}^{\text{TOV}}$  and mass  $M_{\text{TOV}}$  of the maximum mass neutron-star configuration and the dimensionless tidal deformability  $\Lambda_{1.4}$  of  $1.4 M_\odot$  neutron stars obtained with different interactions. It can be seen from Table. VI that within the range of  $-0.7$  to  $0.7$ , the nucleon effective mass splitting have little impact on these properties of neutron stars, and  $\Lambda_{1.4}$  in all interactions complies with the limit of  $\Lambda_{1.4} \leq 580$  from the gravitational wave signal GW170817 [80].

The sound speed has widely used to characterize the properties of dense matter. Figure 11 shows the squared sound speed  $C_s^2 \equiv dP/d\epsilon$  of the neutron star matter as a function of nucleon density for the different interactions. Also shown in Fig. 11 is the central density of maximum mass neutron star configuration with different interactions, and it can be seen that the causality condition  $C_s^2 \leq c^2$  is satisfied by all the interactions. From Fig. 11, it can be observed that the nucleon effective mass splitting has negligible impact on the  $C_s^2 \equiv dP/d\epsilon$  of the neutron star matter, and the effect of different single-nucleon potentials is even more insignificant.

## V. MICROSCOPIC TRANSPORT MODEL SIMULATIONS OF HICS

These new constructed  $Nn\text{LO}$  interactions can be employed into BUU equations to study the HICs. In this section, we briefly outline the methods we adopt to solve the BUU equation, including the lattice Hamiltonian method to deal with the mean-field evolution and the stochastic approach to handle the collision term. As a benchmark, we select a series of interactions to simulate the fixed-target Au+Au collisions at  $E_{\text{beam}} = 1.23 \text{ GeV/nucleon}$  (corresponding to  $\sqrt{s_{NN}} = 2.4 \text{ GeV}$ ), and compare the predicted proton flows with the experimental data measured by the HADES collaboration. We would like to mention that a series of studies has been conducted recently to simulate the HADES experiment using various transport models [135–145].



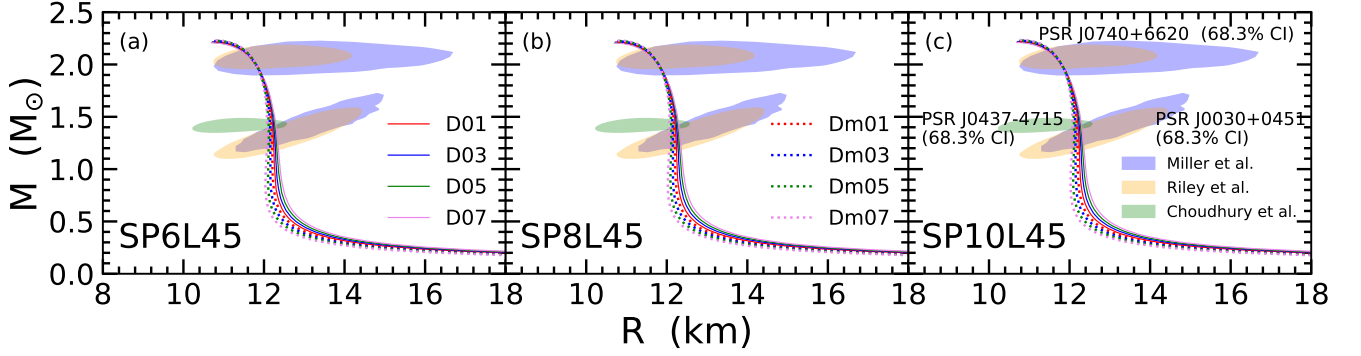


FIG. 10. M-R relation for static neutron stars from different interactions, categorized according to different models (see text for the details). The NICER (XMM-Newton) constraints for PSR J0030+0451 [83, 84], PSR J0740+6620 [85, 86] and PSR J0437-4715 [87] are also included for comparison. All contours are plotted for 68.3% CI.

TABLE VI. Core-crust transition density ( $\rho_t$ ), the central density ( $\rho_{\text{cen}}^{\text{TOV}}$ ) and mass ( $M_{\text{TOV}}$ ) of the maximum mass neutron star configuration and the dimensionless tidal deformability ( $\Lambda_{1.4}$ ) of  $1.4M_{\odot}$  neutron star for different interactions.

SP6L45	Dm07	Dm05	Dm03	Dm01	D01	D03	D05	D07
$\rho_t$ ( $\text{fm}^{-3}$ )	0.0821	0.0817	0.0813	0.0809	0.0806	0.0802	0.0799	0.0796
$\rho_{\text{cen}}^{\text{TOV}}$ ( $\text{fm}^{-3}$ )	1.03	1.03	1.03	1.04	1.04	1.04	1.05	1.05
$M_{\text{TOV}}/M_{\odot}$	2.23	2.23	2.22	2.22	2.22	2.21	2.21	2.21
$\Lambda_{1.4}$	380.4	383.2	385.8	388.0	390.0	391.8	393.4	394.8
SP8L45	Dm07	Dm05	Dm03	Dm01	D01	D03	D05	D07
$\rho_t$ ( $\text{fm}^{-3}$ )	0.0822	0.0817	0.0813	0.0809	0.0805	0.0802	0.0798	0.0795
$\rho_{\text{cen}}^{\text{TOV}}$ ( $\text{fm}^{-3}$ )	1.03	1.03	1.03	1.04	1.04	1.05	1.05	1.05
$M_{\text{TOV}}/M_{\odot}$	2.23	2.23	2.22	2.22	2.21	2.21	2.21	2.20
$\Lambda_{1.4}$	379.4	382.5	385.2	387.6	389.7	391.6	393.2	394.8
SP10L45	Dm07	Dm05	Dm03	Dm01	D01	D03	D05	D07
$\rho_t$ ( $\text{fm}^{-3}$ )	0.0822	0.0817	0.0813	0.0809	0.0805	0.0802	0.0798	0.0795
$\rho_{\text{cen}}^{\text{TOV}}$ ( $\text{fm}^{-3}$ )	1.03	1.03	1.03	1.04	1.04	1.05	1.05	1.05
$M_{\text{TOV}}/M_{\odot}$	2.23	2.23	2.23	2.22	2.22	2.22	2.21	2.21
$\Lambda_{1.4}$	379.6	382.7	385.4	387.8	389.9	391.7	393.4	394.9

### A. The lattice BUU transport model

The time evolution of the one-body phase-space distribution function (Wigner function)  $f_{\tau} = f_{\tau}(\vec{r}, \vec{p}, t)$  satisfies the BUU equation. In the present work, we solve the following BUU equation with a momentum-dependent mean-field potential, i.e.,

$$(\partial_t + \vec{\nabla}_p \epsilon_{\tau} \cdot \vec{\nabla}_r - \vec{\nabla}_r \epsilon_{\tau} \cdot \vec{\nabla}_p) f_{\tau} = I_{\tau}^{\text{coll}}[f_n, f_p, f_{\Delta}, f_{\pi}], \quad (62)$$

where  $\tau$  represent different particle species, i.e., neutrons  $n$ , protons  $p$ ,  $\Delta$ -resonances and  $\pi$ -mesons. The  $\epsilon_{\tau}$  is the single-particle energy of the particle species  $\tau$ , and it contains the kinetic part and MD mean-field potential  $U(\vec{r}, \vec{p})$ . Note  $U(\vec{r}, \vec{p})$  should be treated as a functional of  $f_{\tau}$ . The  $I_{\tau}^{\text{coll}}$  is the collision integral, which takes into account the effect of quantum statistics, i.e., Pauli blocking for Fermions and Bose enhancement for Bosons. It consists of the gain term ( $<$ ) and the loss term ( $>$ ), i.e.,

$$I_{\tau}^{\text{coll}} = \mathcal{K}_{\tau}^{<}[f_n, f_p, f_{\Delta}, f_{\pi}](1 \pm f_{\tau}) - \mathcal{K}_{\tau}^{>}[f_n, f_p, f_{\Delta}, f_{\pi}]f_{\tau}. \quad (63)$$

The factor  $1 \pm f_{\tau}$  in the gain term represents the effect from quantum statistics, and the plus sign is for Bosons while the minus sign for Fermions. In practice, since the  $f_{\tau}$  for Bosons is usually very small, we omit the effect of Bose enhancement. The gain term and loss term contain contributions from different scatterings, namely, two-body elastic scatterings,  $NN \leftrightarrow N\Delta$  and  $\Delta(N^*, \Delta^*) \leftrightarrow N\pi$ , whose scattering matrix can be deduced from their measured cross sections.

Based on the test particle method [146], the  $f$  can be mimicked by  $A \times N_E$  test particles with a form factor  $S$  in the coordinate space, i.e.,

$$f_{\tau}(\vec{r}, \vec{p}, t) = \frac{(2\pi\hbar)^3}{N_E} \sum_i^{AN_E} S[\vec{r}_i(t) - \vec{r}] \delta[\vec{p}_i(t) - \vec{p}], \quad (64)$$

where  $A$  is the mass number of the system and  $N_E$  is the number of ensembles or number of test particles. The sum in the above expression runs over all test particles with isospin  $\tau$ .

The mean-field evolution of the BUU equation is solved

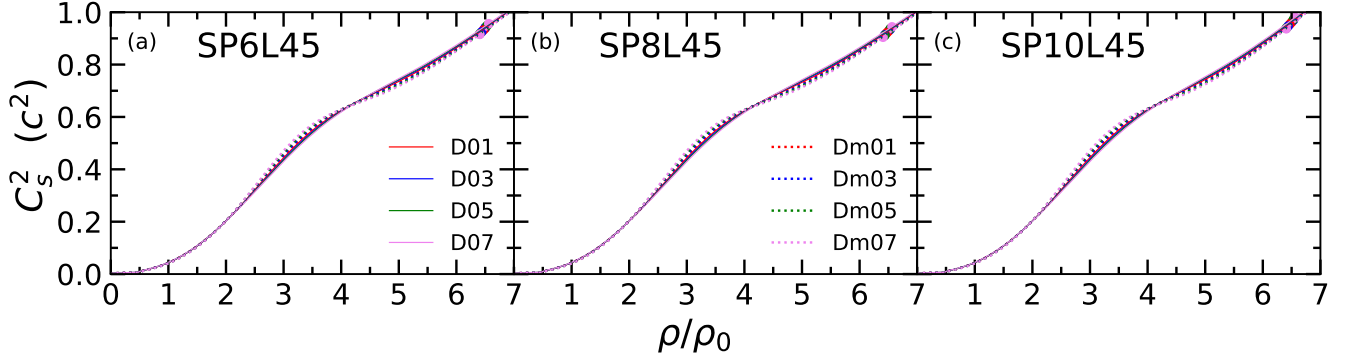


FIG. 11. The squared sound speed ( $C_s^2 \equiv dP/d\epsilon$ ) of neutron star matter as a function of nucleon density predicted by different interactions, categorized according to different models (see text for the details). The central density of maximum mass neutron star configuration is indicated by “•”.

by the lattice Hamiltonian method [72, 147], where the total Hamiltonian  $H$  can be approximated by the lattice Hamiltonian  $H_L$ , i.e.,

$$H = \int \mathcal{H}(\vec{r}) d\vec{r} \approx l^3 \sum_{\alpha} \mathcal{H}(\vec{r}_{\alpha}) \equiv H_L, \quad (65)$$

where  $\vec{r}_{\alpha}$  represents the coordinate of certain lattice site  $\alpha$ , and  $l$  is the lattice spacing. In the above expression,  $\mathcal{H}$  is the Hamiltonian density including both nuclear interaction [Eq. (10)] and Coulomb interaction. By substituting Eq. (64) into Eq. (10) and then into Eq. (65), the coordinates  $\vec{r}_i$  and momenta  $\vec{p}_i$  of test particles can be treated as canonical variables of the lattice Hamiltonian  $H_L$ , and the time evolution of  $\vec{r}_i(t)$  and  $\vec{p}_i(t)$  are then governed by the Hamilton equation of total lattice Hamiltonian of all ensembles. It therefore ensures the conservation of energy during the dynamic process. With Eq. (64), the time evolution of  $\vec{r}_i(t)$  and  $\vec{p}_i(t)$  then give the time evolution of  $f(\vec{r}, \vec{p}, t)$ , from which one obtains expectations of certain quantities.

Within the test particle method, the integral when calculating the MD part of the single-particle potential, i.e., Eqs. (20) and (21), can be converted to a summation over test particles, for  $U^{\text{md}[2n]}(\vec{r}, \vec{p})$  one has

$$\begin{aligned} U^{\text{md}[2n]}(\vec{r}, \vec{p}) &= \int \frac{d^3 p'}{(2\pi\hbar)^3} (\vec{p} - \vec{p}')^{2n} f(\vec{r}, \vec{p}') \\ &= \frac{1}{N_E} \sum_i^{AN_E} (\vec{p} - \vec{p}_i)^{2n} S(\vec{r}_i - \vec{r}), \end{aligned} \quad (66)$$

and for  $U_{\tau}^{\text{md}[2n]}(\vec{r}, \vec{p})$  the summation only applies to test particles of the given  $\tau$ . One of the advantages of the polynomial form of the MD part of the single-particle potential with NnLO, compared with the logarithm form (see, e.g., Refs. [148–152]) or Lorentzian form (see, e.g., Refs. [33, 153–158]) used in various transport models, is that its  $\vec{p}$ -dependence can be factored out from the integral or summation, as shown in Appendix A 2. This

feature significantly reduces the computational complexity of the transport model when calculating the MD part of single-particle potentials, if a very large  $N_E$  is adopted. Note that a sufficiently large  $N_E$  is essential when calculating certain quantities, e.g. the width of giant dipole resonance [73]. It should be noted that, also in the QMD models, the single-particle potential with forms as Eqs. (20) and (21) helps to reduce the computational complexity compared with the logarithm form and Lorentzian form [79].

We adopt the stochastic approach [74, 159] to deal with the collision terms  $I_{\tau}^{\text{coll}}$ . The collision probability  $P_{ij}$  of the  $i$ -th and  $j$ -th test particles during a time interval  $\Delta t$  can be derived directly from the lost term of  $I_{\tau}^{\text{coll}}$ . For example, for nucleon-nucleon elastic scatterings, one has

$$P_{ij} = v_{\text{rel}} \sigma_{\text{NN}}^* S(\vec{r}_i - \vec{r}_{\alpha}) S(\vec{r}_j - \vec{r}_{\alpha}) l^3 \Delta t, \quad (67)$$

where  $v_{\text{rel}}$  is the relative velocity of the test particles and  $\sigma_{\text{NN}}^*$  is the in-medium nucleon-nucleon cross-section. The factor  $[1 - f(\vec{r}_{\alpha}, \vec{p}_i')][1 - f(\vec{r}_{\alpha}, \vec{p}_j')]$  is calculated according to their final state  $\vec{p}_i'$  and  $\vec{p}_j'$  to determine whether the collision is blocked by the Pauli principle.

The Thomas-Fermi initialization is applied to obtain the ground state of the nuclei (see Refs. [72, 74] and the references therein for the details). The gradient parameter  $E^{[2]}$  is modified for each interaction to reproduce the experiment binding energy of the ground state nuclei. For simplicity, we omit the higher-order  $E^{[n]}$  parameters and all  $F^{[n]}$  parameters. The Thomas-Fermi method actually provides a static solution of the BUU equation, it therefore ensures the stability of the ground state evolution.

## B. Comparisons to HADES collective flow data

As mentioned above, we extend the central term of the Skyrme effective interactions to provide additional momentum/energy dependence of the single-nucleon po-

tential, which is displayed in Fig. 6. To focus on the effects of the momentum dependence of the single-nucleon potential, we fix  $\Delta m_1^*(\rho_0) = 0.3$  (i.e., fix the shape of the symmetry potential in Fig. 7) for the interactions used in the simulations, namely we choose SP6L45D03, SP8L45D03 and SP10L45D03. For brevity, in the following text and figures, these interactions will be referred to SP6, SP8 and SP10, respectively. The values of  $m_{s,0}^*$  given by these three interactions are all approximately  $0.77m$  (see Table II), because their single-nucleon potentials have similar behaviors below 1 GeV. Additionally, to investigate the effect of  $m_{s,0}^*$ , we also employ another single-nucleon potential constructed based on the N3LO model from Ref. [88], for which the value of  $m_{s,0}^*$  equals to  $0.83m$ , and we label the corresponding interaction as SP6Ms83. The  $a_n$  parameters of SP6Ms83 are listed in Table IV in Ref. [88], while other adjustable quantities are the same as those in the SP6 interaction. The single-nucleon potential of SP6Ms83 is shown in Fig. 6, and it can be seen that SP6Ms83 predicts a weaker energy dependence than other three interactions and Hama's data, while aligning with the Dirac-Brueckner calculations [125].

To evaluate the validity and establish a benchmark, we solve the BUU equation with those four interactions to simulate the fixed-target Au+Au collisions at  $E_{\text{beam}} = 1.23$  GeV/nucleon (corresponding to  $\sqrt{s_{NN}} = 2.4$  GeV) conducted by HADES collaboration [94, 95]. Some details of the simulations are as follow: the values of  $E^{[2]}$  for SP6, SP8, SP10 and SP6Ms83 are  $-305$ ,  $-300$ ,  $-310$  and  $-310$  MeV fm<sup>5</sup>, respectively, obtained by fitting the experimental binding energy of <sup>197</sup>Au; the number of test particles is set to be  $N_E = 100000$ ; the factor  $S(\vec{r}_i - \vec{r})$  in Eq. (64) is chosen to be triangle form [72, 74]; the end of the time evolution is set to 60 fm/c, with a time step of 0.2 fm/c; a fixed impact parameter  $b = 7.4$  fm is adopted for the centrality class of 20%-30% [93]; the free nucleon-nucleon cross section  $\sigma_{NN}^{\text{free}}$  is adopted based on the parametrization of experimental nucleon-nucleon scattering data as in Ref. [160], and we have tested that the in-medium correction to  $\sigma_{NN}$  has very limited impact on the simulation results; the nucleon resonances and  $\Delta$  resonances are included up to  $N(1720)$  and  $\Delta(1950)$ , respectively; the scatterings related to  $\Delta$  resonances and pions, i.e.,  $NN \leftrightarrow N\Delta$  and  $\Delta \leftrightarrow N\pi$ , as well as  $N^*(\Delta^*) \leftrightarrow N\pi$  are included with the standard cross sections and decay width taken from Refs. [63, 161]. When solving the BUU equation, we omit the single-particle potential of  $\pi$  and all other resonances except  $\Delta$ . It should be noted that the isospin dependence of the  $\Delta$  single-particle potentials is still very elusive [162–165], and there are two popular forms in the transport model simulations for heavy-ion collisions, with one proposed in Ref. [166] and the other in Refs. [103, 167], and both are expressed as a liner scaling from those of  $n$  and  $p$ . In this work, we assume the former form for the single-particle potentials of  $\Delta$  [166], i.e.,  $U_{\Delta^{++}} = -U_n + 2U_p$ ,  $U_{\Delta^+} = U_p$ ,  $U_{\Delta^0} = U_n$  and  $U_{\Delta^-} = 2U_n - U_p$ . Note that the above

$\Delta$  potentials do not cause a difference in the potential energy between the initial and final states of the scattering  $NN \leftrightarrow N\Delta$ , while their effects on the energy conservation of the scattering  $\Delta \leftrightarrow N\pi$ , i.e., the threshold effects [158, 168–170], should be taken into account when solving the BUU equation.

The particles transverse momentum  $p_t$  anisotropy is resulted from the pressure anisotropy of the compressed matter formed during the noncentral HICs, and is thus sensitive to the EOS of dense nuclear matter from the collision products. The anisotropic flows  $v_n$  of particles are the Fourier coefficients in the decomposition of their  $p_t$  spectra in the azimuthal angle  $\phi$  with respect to the reaction plane [171], i.e.,

$$E \frac{d^3N}{dp^3} = \frac{1}{2\pi} \frac{d^2N}{p_t dp_t dy} \left[ 1 + \sum_{n=1}^{\infty} 2v_n(p_t, y) \cos(n\phi) \right]. \quad (68)$$

The anisotropic flows  $v_n$  generally depend on particle transverse momentum  $p_t$  as well as rapidity  $y$ , and for a given  $y$  the anisotropic flows at  $p_t$  can be evaluated according to

$$v_n(p_t) = \langle \cos(n\phi) \rangle, \quad (69)$$

where  $\langle \dots \rangle$  denotes average over the azimuthal distribution of particles with transverse momentum  $p_t$ . The anisotropic flows  $v_n$  can further be expressed in terms of the single-particle averages [172, 173]:

$$v_1(p_t) = \left\langle \frac{p_x}{p_t} \right\rangle, \quad (70)$$

$$v_2(p_t) = \left\langle \frac{p_x^2 - p_y^2}{p_t^2} \right\rangle, \quad (71)$$

$$v_3(p_t) = \left\langle \frac{p_x^3 - 3p_x p_y^2}{p_t^3} \right\rangle, \quad (72)$$

$$v_4(p_t) = \left\langle \frac{p_x^4 - 6p_x^2 p_y^2 + p_y^4}{p_t^4} \right\rangle, \quad (73)$$

where  $p_x$  and  $p_y$  are, respectively, the projections of particle momentum in and perpendicular to the reaction plane.

We present in Fig. 12 the lattice BUU results for directed flow  $v_1$ , elliptic flow  $v_2$ , triangular flow  $v_3$  and quadrangular flow  $v_4$  for protons as function of transverse momentum  $p_t$ . All of these predictions are generally in good agreement with the HADES data. It is seen from Fig. 12(b) that SP6Ms83 predicts a smaller magnitude of  $v_2$ , whereas SP6 predicts a larger magnitude of  $v_2$ , while SP8 and SP10 are nearly identical. This difference is due to the different energy dependencies of the single-nucleon potential. It is seen from Fig. 6 that SP6Ms83 predicts a larger range of negative single-nucleon potential, and the attractive potential will weaken the  $v_2$ . In contrast, SP6 shows a rapid increase in the single-nucleon potential above 1 GeV, leading to a stronger repulsive potential for

high-energy particles and, consequently, a larger magnitude of  $v_2$  at high  $p_t$ . In Fig. 13, we show the predicted proton flows, including  $v_1$ ,  $v_2$ ,  $v_3$  and  $v_4$ , as a function of center-of-mass rapidity  $y_{cm}$ , and all of them are generally in good agreement with the HADES data. It is seen from Fig. 13(b) that at mid-rapidity, SP6Ms83 predicts the smallest magnitude of  $v_2$ , SP6 predicts the largest, and the predictions of SP8 and SP10 are almost identical and fall in between. This is consistent with the results presented in Fig. 12(b).

It should be noted that these results serve as a benchmark and broadly illustrate the impact of the single-nucleon potential. In fact, the predicted proton flows can also be affected by the nuclear EOS, which is fixed in these interactions by construction. Particularly, the stiffness of the SNM EOS could directly affect the matter densities produced during collisions, thereby influencing the single-nucleon potential in the dynamic process. Considering the joint effects of both nuclear EOS and the single-nucleon potential, extracting them from HICs will rely on future large-scale simulations.

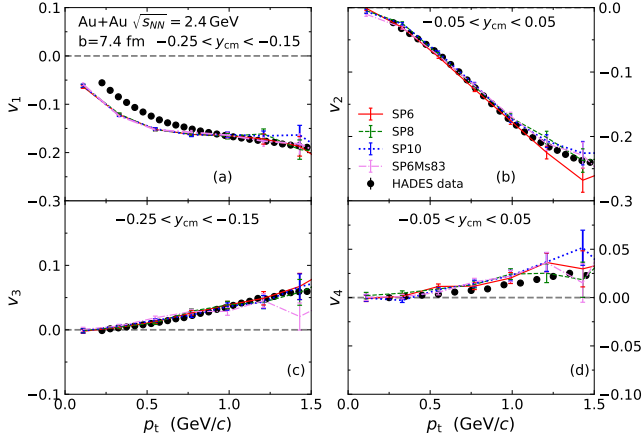


FIG. 12. Directed ( $v_1$ ), elliptic ( $v_2$ ), triangular ( $v_3$ ) and quadrangular ( $v_4$ ) flows as function of transverse momentum ( $p_t$ ) for free protons in Au+Au collisions at  $E_{beam} = 1.23$  GeV/nucleon (corresponding to  $\sqrt{s_{NN}} = 2.4$  GeV) predicted by lattice BUU model with SP6, SP8, SP10 and SP6Ms83 interactions. Also included are the HADES data [94, 95].

Finally, we would like to mention that in the LBUU transport model, the momentum-dependent Skyrme pseudopotential is non-relativistic, although the kinematics in Hamiltonian equations of motion is treated relativistically. To the best of our knowledge, for transport model simulations for heavy-ion collisions at energies up to about 2 GeV/nucleon, the non-relativistic mean-field potentials are still widely used in some popular transport model codes, e.g., IBUU [103, 137, 174], updated ART [175], UrQMD [152, 176–179], QMD [79], and LQMD [140, 180]. Furthermore, in the present LBUU model, instead of the commonly used geometric method, the stochastic collision method is implemented for the

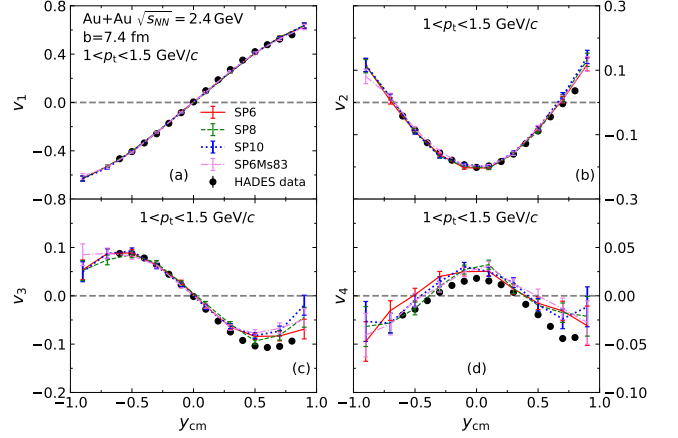


FIG. 13. Directed ( $v_1$ ), elliptic ( $v_2$ ), triangular ( $v_3$ ) and quadrangular ( $v_4$ ) flows as function of center-of-mass rapidity ( $y_{cm}$ ) for free protons in Au+Au collisions at  $E_{beam} = 1.23$  GeV/nucleon (corresponding to  $\sqrt{s_{NN}} = 2.4$  GeV) predicted by lattice BUU model with SP6, SP8, SP10 and SP6Ms83 interactions. Also included are the HADES data [94, 95].

two-body collision term in the BUU equation, and in this way the collision probability of two test nucleons can be derived directly from the two-body collision term in the BUU equation, and it thus significantly weakens the relativistic covariance effects which are very important in the geometric method where accurate distance of two scattering particles is necessary and the mean free path of a test particle should be much larger than the interaction length between the two scattering test particles. As shown in this paper, the LBUU transport model with empirical parameters can successfully reproduce the HADES experimental data, suggesting that at HADES energy (1.23 GeV/nucleon), the relativistic correction to the mean-field potential may not be so significant. Of course, a detailed and quantitative check on the relativistic effects of mean-field potential will be definitely interesting and important, although it is not trivial at all (see, e.g., Ref. [154]).

## VI. SUMMARY AND OUTLOOK

Based on a general approach conforming to the basic symmetry principles, we have extended the central terms of the conventional Skyrme interactions by incorporating specific higher-order derivative terms and obtain the general form of the Skyrme pseudopotential up to  $NnLO$ . The corresponding expressions of Hamiltonian density and single-nucleon potential are derived within the Hartree-Fock approach under general non-equilibrium conditions. The higher-order derivative terms can provide additional momentum dependence for the single-nucleon potential, especially affecting its behavior at high energies. In particular, for the Skyrme

pseudopotential up to N3LO, N4LO and N5LO, the corresponding single-nucleon potential can describe the empirical nucleon optical potential up to the energy of 1 GeV, 1.5 GeV and 2 GeV, respectively. The density-dependent term is also extended in the spirit of Fermi momentum expansion, enabling significant freedom to adjust the density dependence of the symmetry energy as well as the high-density behavior of the isospin symmetric nuclear matter. Consequently, the corresponding nuclear EOS can simultaneously fit the empirical properties of symmetric nuclear matter, the microscopic calculations of pure neutron matter and the properties of neutron stars from astrophysical observations. It is worth noting that the density behavior of the EOS corresponding to N3LO Skyrme pseudopotential is sufficiently flexible to satisfy the current constraints, and the introduction of higher-order characteristic parameters may help to extract the nuclear EOS at suprasaturation densities based on new available experimental probes in the future. Specifically, for the Skyrme pseudopotential up to N5LO, the adjustable characteristic parameters will be extended up to  $H_0$  and  $H_{\text{sym}}$ , which correspond to the fifth-order expansion coefficients of  $E_0(\rho)$  and  $E_{\text{sym}}(\rho)$ , respectively. Considering the large uncertainty in the symmetry potential, we construct eight symmetry potentials with different momentum dependencies, corresponding to the values of the linear isospin splitting coefficient  $\Delta m_1^*(\rho_0)$  ranging from  $-0.7$  to  $0.7$ . Combining three single-nucleon potential featuring different high-momentum behaviors obtained from the Skyrme pseudopotential up to N3LO, N4LO and N5LO, respectively, with the eight symmetry potentials, we have constructed a parameter sets, by which we study the properties of nuclear matter and neutron stars. Our results indi-

cate that these interactions can well describe the neutron star mass-radius relation from NICER and the tidal deformability extracted from gravitational wave signal GW170817.

Furthermore, these interactions with  $\Delta m_1^*(\rho_0) = 0.3$  have been applied in the lattice BUU model to simulate the Au+Au collisions at 1.23 GeV/nucleon conducted by HADES collaboration. Another interaction with larger  $m_{s,0}^*$  has been also used for the simulation. We find that these interactions can provide good predictions of the proton collective flows in the HADES experiments. Moreover, we find that the proton elliptic flow  $v_2$  is sensitive to the single-nucleon potential as well as  $m_{s,0}^*$ . A larger  $m_{s,0}^*$ , which indicates a more attractive potential at low energies, will weaken the  $v_2$  effects, while a stronger repulsive potential at high energies will result in a larger magnitude of  $v_2$  at high  $p_t$ .

In future, we will conduct large-scale simulations to extract the single-nucleon potential as well as the nuclear matter EOS at suprasaturation densities. Considering that the hyperons production may be significant in heavy-ion collisions at higher energies, we will incorporate the hyperon degrees of freedom in the lattice BUU model in the next step.

#### ACKNOWLEDGMENTS

This work was supported in part by the National Natural Science Foundation of China under Grant No 12235010, the National SKA Program of China (Grant No. 2020SKA0120300), and the Science and Technology Commission of Shanghai Municipality (Grant No. 23JC1402700).

### Appendix A: THE SKYRME PSEUDOPOTENTIAL UP TO $N_n$ LO

#### 1. Hamiltonian density with the extended Skyrme interaction in one-body transport model of HICs

In the transport model, considering the system being out of equilibrium, the Hamiltonian density needs to be expressed as a function of the Wigner function  $f(\vec{r}, \vec{p})$ , which can be thought as the quantum analogy of classical phase-space distribution function. The Wigner function  $f(\vec{r}, \vec{p})$  is defined as the Fourier transform of the density matrix, i.e.,

$$f(\vec{r}, \vec{p}) = \int \exp\left(-i\frac{\vec{p}}{\hbar} \cdot \vec{s}\right) \rho(\vec{r} + \vec{s}/2, \vec{r} - \vec{s}/2) d^3s \quad (\text{A1})$$

in coordinate configuration, and

$$f(\vec{r}, \vec{p}) = \int \exp\left(i\frac{\vec{q}}{\hbar} \cdot \vec{r}\right) g(\vec{p} + \vec{q}/2, \vec{p} - \vec{q}/2) d^3q \quad (\text{A2})$$

in momentum configuration, where  $\rho(\vec{r} + \vec{s}/2, \vec{r} - \vec{s}/2)$  and  $g(\vec{p} + \vec{q}/2, \vec{p} - \vec{q}/2)$  are the matrix elements of the density matrices in coordinate and momentum representations, respectively. With HF approximation, the density matrix of the system is expressed as  $\hat{\rho} = \sum_i |\phi_i\rangle \langle \phi_i|$ , and thus we have

$$\rho(\vec{r} + \vec{s}/2, \vec{r} - \vec{s}/2) = \langle \vec{r} + \vec{s}/2 | \hat{\rho} | \vec{r} - \vec{s}/2 \rangle = \sum_i \phi_i^*(\vec{r} + \vec{s}/2) \phi_i(\vec{r} - \vec{s}/2), \quad (\text{A3})$$

$$g(\vec{p} + \vec{q}/2, \vec{p} - \vec{q}/2) = \langle \vec{p} + \vec{q}/2 | \hat{\rho} | \vec{p} - \vec{q}/2 \rangle = \sum_i \phi_i^*(\vec{p} + \vec{q}/2) \phi_i(\vec{p} - \vec{q}/2), \quad (\text{A4})$$

where  $\phi_i(\vec{r})$  and  $\phi_i(\vec{p})$  are the one particle wave functions in coordinate and momentum configuration, respectively.

The central part of the standard Skyrme interaction is written as

$$v_{sk} = t_0 \left( 1 + x_0 \hat{P}_\sigma \right) \delta(\vec{r}_1 - \vec{r}_2) + t_1^{[2]} \left( 1 + x_1^{[2]} \hat{P}_\sigma \right) \frac{1}{2} \left[ \hat{k}'^2 \delta(\vec{r}_1 - \vec{r}_2) + \delta(\vec{r}_1 - \vec{r}_2) \hat{k}^2 \right] + t_2^{[2]} \left( 1 + x_2^{[2]} \hat{P}_\sigma \right) \hat{k}' \cdot \delta(\vec{r}_1 - \vec{r}_2) \hat{k}, \quad (\text{A5})$$

which is also recognized as pseudopotential up to NLO, since it includes not only the local term ( $t_0$  term), but also the spatial derivative operators up to the first order, i.e.,  $\hat{A} = \frac{1}{2} \left[ \hat{k}'^2 \delta(\vec{r}_1 - \vec{r}_2) + \delta(\vec{r}_1 - \vec{r}_2) \hat{k}^2 \right]$  and  $\hat{B} = \hat{k}' \cdot \delta(\vec{r}_1 - \vec{r}_2) \hat{k}$ . The HF calculations of the expectation values of  $\hat{A}$  and  $\hat{B}$  are considered as the starting point, which can be calculated as (detailed derivation can be found in Ref. [69])

$$\begin{aligned} \sum_{i,j} \langle ij | \hat{A} | ij \rangle &= \sum_{i,j} \langle ij | \frac{1}{2} \left[ \vec{k}'^2 \delta(\vec{r}_1 - \vec{r}_2) + \delta(\vec{r}_1 - \vec{r}_2) \vec{k}^2 \right] | ij \rangle \\ &= \int d^3r \int \frac{d^3p}{(2\pi\hbar)^3} \frac{d^3p'}{(2\pi\hbar)^3} \frac{d^3q}{(2\pi\hbar)^3} \frac{d^3q'}{(2\pi\hbar)^3} \left( \frac{1}{2\hbar} \right)^2 \left[ (\vec{p} - \vec{p}')^2 + \left( \frac{\vec{q} - \vec{q}'}{2} \right)^2 \right] \\ &\quad \times \exp\left(\frac{i\vec{q} \cdot \vec{r}}{\hbar}\right) \exp\left(\frac{i\vec{q}' \cdot \vec{r}}{\hbar}\right) \left[ g(\vec{p} + \frac{\vec{q}}{2}, \vec{p} - \frac{\vec{q}}{2}) g(\vec{p}' + \frac{\vec{q}'}{2}, \vec{p}' - \frac{\vec{q}'}{2}) \right] \end{aligned} \quad (\text{A6})$$

being the even parity term (even order of  $\hat{B}$ ), and

$$\begin{aligned} \sum_{i,j} \langle ij | \hat{B} | ij \rangle &= \sum_{i,j} \langle ij | \left[ \vec{k}' \cdot \delta(\vec{r}_1 - \vec{r}_2) \vec{k} \right] | ij \rangle \\ &= \int d^3r \int \frac{d^3p}{(2\pi\hbar)^3} \frac{d^3p'}{(2\pi\hbar)^3} \frac{d^3q}{(2\pi\hbar)^3} \frac{d^3q'}{(2\pi\hbar)^3} \left( \frac{1}{2\hbar} \right)^2 \left[ (\vec{p} - \vec{p}')^2 - \left( \frac{\vec{q} - \vec{q}'}{2} \right)^2 \right] \\ &\quad \times \exp\left(\frac{i\vec{q} \cdot \vec{r}}{\hbar}\right) \exp\left(\frac{i\vec{q}' \cdot \vec{r}}{\hbar}\right) \left[ g(\vec{p} + \frac{\vec{q}}{2}, \vec{p} - \frac{\vec{q}}{2}) g(\vec{p}' + \frac{\vec{q}'}{2}, \vec{p}' - \frac{\vec{q}'}{2}) \right] \end{aligned} \quad (\text{A7})$$

being with odd parity. The integral of  $\frac{1}{4\hbar^2} (\vec{p} - \vec{p}')^2$  becomes the MD terms, i.e.,

$$\frac{1}{4\hbar^2} \int d^3r \int \frac{d^3p}{(2\pi\hbar)^3} \frac{d^3p'}{(2\pi\hbar)^3} (\vec{p} - \vec{p}')^2 f(\vec{r}, \vec{p}) f(\vec{r}, \vec{p}'), \quad (\text{A8})$$

while the integral of  $\frac{1}{4\hbar^2} \left( \frac{\vec{q} - \vec{q}'}{2} \right)^2$  will become the gradient (GD) terms (see Ref. [69] for details), i.e.,

$$\frac{1}{4\hbar^2} \frac{\vec{q}^2 + \vec{q}'^2}{4} \implies \frac{1}{4} \left( \frac{i}{2} \right)^2 [2\rho \nabla^2 \rho], \quad (\text{A9})$$

$$\frac{1}{4\hbar^2} \frac{-2\vec{q} \cdot \vec{q}'}{4} \implies \frac{1}{4} \left( \frac{i}{2} \right)^2 [-2(\nabla \rho)^2], \quad (\text{A10})$$

where  $i$  is the imaginary unit.

The Skyrme pseudopotential up to N3LO (including derivative terms up to the sixth-order) is constructed by combining  $\hat{A}$ ,  $\hat{B}$  as well as the spin part through the so-called LS-coupling [64, 65], and the corresponding expressions in Cartesian representation have been derived in Refs. [113, 114]. It is seen that this potential is invariant under space rotation, space and time reversal and Hermitian conjugation by construction, and the coupling constants can be further constrained by the Galilean symmetry and the gauge symmetry. In the present work, we only keep the central term and ignore the spin-dependent component since they do not contribute to spin-averaged quantities, on which we are focusing here. We assume that the  $2n$ th-order derivative term in the central term of the Skyrme pseudopotential

can be constructed by using the binomial expansion of  $(\hat{A} + \hat{B})^n$  (one can see  $[\hat{A}, \hat{B}] = 0$ , and the Dirac delta function  $\delta(\vec{r}_1 - \vec{r}_2)$  is omitted here for clarity), i.e.,

$$(\hat{A} + \hat{B})^n = \sum_{m=0}^n \binom{n}{m} \hat{A}^{n-m} \hat{B}^m. \quad (\text{A11})$$

This assumption complies with the aforementioned symmetry principles and is consistent with corresponding forms in N3LO model Ref. [113, 114].

We partition Eq. (A11) into two groups according to the parity of the powers of  $\hat{B} = \vec{k}' \cdot \vec{k}$  with the corresponding Skyrme parameters  $t_1^{[2n]}$  and  $t_2^{[2n]}$ , and the  $Nn$ LO pseudopotential central term  $v^{[2n]}$  can be written as:

$$v^{[2n]} = t_1^{[2n]} \left(1 + x_1^{[2n]} \hat{P}_\sigma\right) v_{\text{even}}^{[2n]} + t_2^{[2n]} \left(1 + x_2^{[2n]} \hat{P}_\sigma\right) v_{\text{odd}}^{[2n]}, \quad (\text{A12})$$

where the even-parity term  $v_{\text{even}}^{[2n]}$  and odd-parity term  $v_{\text{odd}}^{[2n]}$  take the following forms:

$$v_{\text{P}}^{[2n]} = \sum_{\substack{m=0 \\ (m \in \text{P})}}^n \binom{n}{m} \left(\frac{\vec{k}'^2 + \vec{k}^2}{2}\right)^{n-m} (\vec{k}' \cdot \vec{k})^m, \quad (\text{A13})$$

with P being even or odd according to the parity. And the contribution of the  $2n$ th-order derivative terms with certain parity P can be calculated through HF approximation  $\frac{1}{2} \sum_{i,j} \langle ij | v_{\text{P}}^{[2n]} (1 - \hat{P}_\sigma \hat{P}_\tau \hat{P}_M) | ij \rangle$ .

One can see that for arbitrary natural numbers  $n$  and  $m$ ,

$$\begin{aligned} \langle ij | \left(\frac{\vec{k}'^2 + \vec{k}^2}{2}\right)^n (\vec{k}' \cdot \vec{k})^m | ij \rangle &= \int d^3r \int \frac{d^3p_1}{(2\pi\hbar)^3} \frac{d^3p_2}{(2\pi\hbar)^3} \cdots \frac{d^3p_{2n+1}}{(2\pi\hbar)^3} \frac{d^3p_{2n+2}}{(2\pi\hbar)^3} \cdots \frac{d^3p_{2(n+m)+1}}{(2\pi\hbar)^3} \frac{d^3p_{2(n+m)+2}}{(2\pi\hbar)^3} \\ &\times \langle ij | p_1 p_2 \rangle \exp \left[ \frac{-i(\vec{p}_1 + \vec{p}_2 - \vec{p}_3 - \vec{p}_4)}{\hbar} \cdot \vec{r} \right] \langle p_1 p_2 | \left(\frac{\vec{k}'^2 + \vec{k}^2}{2}\right)_1 | p_3 p_4 \rangle \\ &\times \dots \times \exp \left[ \frac{-i(\vec{p}_{2n-1} + \vec{p}_{2n} - \vec{p}_{2n+1} - \vec{p}_{2n+2})}{\hbar} \cdot \vec{r} \right] \langle p_{2n-1} p_{2n} | \left(\frac{\vec{k}'^2 + \vec{k}^2}{2}\right)_n | p_{2n+1} p_{2n+2} \rangle \\ &\times \exp \left[ \frac{-i(\vec{p}_{2n+1} + \vec{p}_{2n+2} - \vec{p}_{2n+3} - \vec{p}_{2n+4})}{\hbar} \cdot \vec{r} \right] \langle p_{2n+1} p_{2n+2} | (\vec{k}' \cdot \vec{k})_1 | p_{2n+3} p_{2n+4} \rangle \\ &\times \dots \times \exp \left[ \frac{-i(\vec{p}_{2(n+m)-1} + \vec{p}_{2(n+m)} - \vec{p}_{2(n+m)+1} - \vec{p}_{2(n+m)+2})}{\hbar} \cdot \vec{r} \right] \\ &\times \langle p_{2(n+m)-1} p_{2(n+m)} | (\vec{k}' \cdot \vec{k})_m | p_{2(n+m)+1} p_{2(n+m)+2} \rangle \langle p_{2(n+m)+1} p_{2(n+m)+2} | ij \rangle. \end{aligned} \quad (\text{A14})$$

Based on Eq. (A6), Eq. (A7), Eq. (A13) and Eq. (A14), we can obtain  $V_{\text{P}}^{[2n]}$ , i.e., the expectation value of  $v_{\text{P}}^{[2n]}$  without the exchange term, as

$$\begin{aligned} V_{\text{P}}^{[2n]} &= \frac{1}{2} \sum_{i,j} \langle ij | v_{\text{P}}^{[2n]} | ij \rangle = \frac{1}{2} \frac{1}{(2\hbar)^{2n}} \int d^3r \int \frac{d^3p}{(2\pi\hbar)^3} \frac{d^3p'}{(2\pi\hbar)^3} \frac{d^3q}{(2\pi\hbar)^3} \frac{d^3q'}{(2\pi\hbar)^3} \exp \left( \frac{i\vec{q} \cdot \vec{r}}{\hbar} \right) \exp \left( \frac{i\vec{q}' \cdot \vec{r}}{\hbar} \right) \\ &\times \left[ g(\vec{p} + \frac{\vec{q}}{2}, \vec{p} - \frac{\vec{q}}{2}) g(\vec{p}' + \frac{\vec{q}'}{2}, \vec{p}' - \frac{\vec{q}'}{2}) \right] \\ &\times \sum_{\substack{m=0 \\ (m \in \text{P})}}^n \binom{n}{m} \left[ (\vec{p} - \vec{p}')^2 + \left(\frac{\vec{q} - \vec{q}'}{2}\right)^2 \right]^{n-m} \left[ (\vec{p} - \vec{p}')^2 - \left(\frac{\vec{q} - \vec{q}'}{2}\right)^2 \right]^m. \end{aligned} \quad (\text{A15})$$

With the two identities:

$$\sum_{\substack{m=0 \\ (m \in \text{even})}}^n \binom{n}{m} (a+b)^{n-m} (a-b)^m = 2^{n-1} (a^n + b^n), \quad (\text{A16})$$

$$\sum_{\substack{m=0 \\ (m \in \text{odd})}}^n \binom{n}{m} (a+b)^{n-m} (a-b)^m = 2^{n-1} (a^n - b^n), \quad (\text{A17})$$

Eq. (A15) becomes:

$$\begin{aligned} V_P^{[2n]} = & \frac{1}{2} \frac{1}{(2\hbar)^{2n}} \int d^3r \int \frac{d^3p}{(2\pi\hbar)^3} \frac{d^3p'}{(2\pi\hbar)^3} \frac{d^3q}{(2\pi\hbar)^3} \frac{d^3q'}{(2\pi\hbar)^3} \exp\left(\frac{i\vec{q} \cdot \vec{r}}{\hbar}\right) \exp\left(\frac{i\vec{q}' \cdot \vec{r}}{\hbar}\right) \\ & \times \left[ g(\vec{p} + \frac{\vec{q}}{2}, \vec{p} - \frac{\vec{q}}{2}) g(\vec{p}' + \frac{\vec{q}'}{2}, \vec{p}' - \frac{\vec{q}'}{2}) \right] 2^{n-1} \left[ (\vec{p} - \vec{p}')^{2n} \pm \left(\frac{\vec{q} - \vec{q}'}{2}\right)^{2n} \right], \end{aligned} \quad (\text{A18})$$

where the even (odd) parity term take the  $+$  ( $-$ ) sign. One can see that there are no cross terms in Eq. (A18), and the integrals of  $(\vec{p} - \vec{p}')^{2n}$  and  $\left(\frac{\vec{q} - \vec{q}'}{2}\right)^{2n}$  become the MD term and GD term, respectively. Next, we consider the contribution of the exchange term, i.e.,

$$\frac{1}{2} \sum_{i,j} \langle ij | v_P^{[2n]} (-\hat{P}_\sigma \hat{P}_\tau \hat{P}_M) | ij \rangle. \quad (\text{A19})$$

The Majorana operator  $\hat{P}_M$  can be replaced by  $\hat{1} (-\hat{1})$  for even-parity (odd-parity) terms. Assuming that there is no isospin mixing of the HF states, the isospin exchange operator  $\hat{P}_\tau$  can be replaced by a Kronecker delta function  $\delta_{\tau_i \tau_j}$  with  $\tau_i$  being the isospin of the  $i$ th state. We assume the collision system is spin-averaged, and thus the spin exchange operator  $\hat{P}_\sigma$  is simply replaced by a factor of  $\frac{1}{2}$ . By incorporating the exchange terms and summing the contributions from the odd and even terms, we can obtain the Hamiltonian density of the  $n$ th-order MD term  $\mathcal{H}_{[2n]}^{\text{MD}}$  as

$$\begin{aligned} \mathcal{H}_{[2n]}^{\text{MD}}(\vec{r}) = & \frac{2^n}{8} \frac{1}{(2\hbar)^{2n}} \left[ t_1^{[2n]} \left( 2 + x_1^{[2n]} \right) + t_2^{[2n]} \left( 2 + x_2^{[2n]} \right) \right] \mathcal{H}^{\text{md}[n]}(\vec{r}) \\ & + \frac{2^n}{8} \frac{1}{(2\hbar)^{2n}} \left[ -t_1^{[2n]} \left( 2x_1^{[2n]} + 1 \right) + t_2^{[2n]} \left( 2x_2^{[2n]} + 1 \right) \right] \sum_{\tau=n,p} \mathcal{H}_\tau^{\text{md}[n]}(\vec{r}), \end{aligned} \quad (\text{A20})$$

where

$$\mathcal{H}^{\text{md}[2n]}(\vec{r}) = \int \frac{d^3p}{(2\pi\hbar)^3} \frac{d^3p'}{(2\pi\hbar)^3} (\vec{p} - \vec{p}')^{2n} f(\vec{r}, \vec{p}) f(\vec{r}, \vec{p}'), \quad (\text{A21})$$

$$\mathcal{H}_\tau^{\text{md}[2n]}(\vec{r}) = \int \frac{d^3p}{(2\pi\hbar)^3} \frac{d^3p'}{(2\pi\hbar)^3} (\vec{p} - \vec{p}')^{2n} f_\tau(\vec{r}, \vec{p}) f_\tau(\vec{r}, \vec{p}'). \quad (\text{A22})$$

On the other side, notice that  $\vec{q}^{2n-m} \cdot \vec{q}'^m$  and  $\vec{q}^m \cdot \vec{q}'^{2n-m}$  contribute equally in the integral of  $\left(\frac{\vec{q} - \vec{q}'}{2}\right)^{2n}$  in Eq. (A18), i.e., both are  $\left(\frac{\hbar}{i}\right)^{2n} \nabla^{2n-m} \rho \nabla^m \rho$  (and  $\nabla^0 \rho = \rho$ ), the Hamiltonian density of the  $n$ th-order GD term can be expressed as:

$$\begin{aligned} \mathcal{H}_{[2n]}^{\text{GD}}(\vec{r}) = & \frac{2^n}{8} \frac{1}{(2\hbar)^{2n}} \left[ t_1^{[2n]} \left( 2 + x_1^{[2n]} \right) - t_2^{[2n]} \left( 2 + x_2^{[2n]} \right) \right] \left( \frac{i\hbar}{2} \right)^{2n} \mathcal{H}^{\text{gd}[2n]}(\vec{r}) \\ & - \frac{2^n}{8} \frac{1}{(2\hbar)^{2n}} \left[ t_1^{[2n]} \left( 2x_1^{[2n]} + 1 \right) + t_2^{[2n]} \left( 2x_2^{[2n]} + 1 \right) \right] \left( \frac{i\hbar}{2} \right)^{2n} \sum_{\tau=n,p} \mathcal{H}_\tau^{\text{gd}[2n]}(\vec{r}), \end{aligned} \quad (\text{A23})$$

where

$$\begin{aligned} \mathcal{H}^{\text{gd}[2n]}(\vec{r}) = & \sum_{m=0}^{2n} (-1)^m \binom{2n}{m} \nabla^m \rho(\vec{r}) \nabla^{2n-m} \rho(\vec{r}) \\ = & 2 \sum_{m=0}^{n-1} \left[ (-1)^m \binom{2n}{m} \nabla^m \rho(\vec{r}) \nabla^{2n-m} \rho(\vec{r}) \right] + (-1)^n \binom{2n}{n} [\nabla^n \rho(\vec{r})]^2, \end{aligned} \quad (\text{A24})$$



and

$$\begin{aligned}\mathcal{H}_\tau^{\text{gd}[2n]}(\vec{r}) &= \sum_{m=0}^{2n} (-1)^m \binom{2n}{m} \nabla^m \rho_\tau(\vec{r}) \nabla^{2n-m} \rho_\tau(\vec{r}) \\ &= 2 \sum_{m=0}^{n-1} \left[ (-1)^m \binom{2n}{m} \nabla^m \rho_\tau(\vec{r}) \nabla^{2n-m} \rho_\tau(\vec{r}) \right] + (-1)^n \binom{2n}{n} [\nabla^n \rho_\tau(\vec{r})]^2.\end{aligned}\quad (\text{A25})$$

For convenience, we can recombine the Skyrme parameters in Eqs. (A20) and (A23), namely,  $t_1^{[2n]}$ ,  $t_2^{[2n]}$ ,  $x_1^{[2n]}$  and  $x_2^{[2n]}$ , into the parameters  $C^{[2n]}$ ,  $D^{[2n]}$ ,  $E^{[2n]}$  and  $F^{[2n]}$ , i.e.,

$$C^{[2n]} = t_1^{[2n]} (2 + x_1^{[2n]}) + t_2^{[2n]} (2 + x_2^{[2n]}), \quad (\text{A26})$$

$$D^{[2n]} = -t_1^{[2n]} (2x_1^{[2n]} + 1) + t_2^{[2n]} (2x_2^{[2n]} + 1), \quad (\text{A27})$$

$$E^{[2n]} = \left(\frac{i}{2}\right)^{2n} \left[ t_1^{[2n]} (2 + x_1^{[2n]}) - t_2^{[2n]} (2 + x_2^{[2n]}) \right], \quad (\text{A28})$$

$$F^{[2n]} = -\left(\frac{i}{2}\right)^{2n} \left[ t_1^{[2n]} (2x_1^{[2n]} + 1) + t_2^{[2n]} (2x_2^{[2n]} + 1) \right]. \quad (\text{A29})$$

Or we can obtain that

$$t_1^{[2n]} = \frac{1}{6} \left[ (2C^{[2n]} + D^{[2n]}) + (2i)^{2n} (2E^{[2n]} + F^{[2n]}) \right], \quad (\text{A30})$$

$$t_2^{[2n]} = \frac{1}{6} \left[ (2C^{[2n]} - D^{[2n]}) - (2i)^{2n} (2E^{[2n]} - F^{[2n]}) \right], \quad (\text{A31})$$

$$x_1^{[2n]} = -\frac{(C^{[2n]} + 2D^{[2n]}) + (2i)^{2n} (E^{[2n]} + 2F^{[2n]})}{(2C^{[2n]} + D^{[2n]}) + (2i)^{2n} (2E^{[2n]} + F^{[2n]})}, \quad (\text{A32})$$

$$x_2^{[2n]} = -\frac{(C^{[2n]} - 2D^{[2n]}) - (2i)^{2n} (E^{[2n]} - 2F^{[2n]})}{(2C^{[2n]} - D^{[2n]}) - (2i)^{2n} (2E^{[2n]} - F^{[2n]})}, \quad (\text{A33})$$

once  $C^{[2n]}$ ,  $D^{[2n]}$ ,  $E^{[2n]}$  and  $F^{[2n]}$  are given. The units for  $t_1^{[2n]}$ ,  $t_2^{[2n]}$ ,  $C^{[2n]}$ ,  $D^{[2n]}$ ,  $E^{[2n]}$  and  $F^{[2n]}$  are  $\text{MeV fm}^{2n+3}$ , while  $x_1^{[2n]}$  and  $x_2^{[2n]}$  are dimensionless.

Finally, for the  $Nn\text{LO}$  Skyrme pseudopotential central term defined in Eq. (A12), we obtain its Hamiltonian density as

$$\begin{aligned}\mathcal{H}_{[2n]}(\vec{r}) &= \frac{1}{2} \sum_{i,j} \langle ij | v^{[2n]} (1 - \hat{P}_\sigma \hat{P}_\tau \hat{P}_M) | ij \rangle = \mathcal{H}_{[2n]}^{\text{MD}}(\vec{r}) + \mathcal{H}_{[2n]}^{\text{GD}}(\vec{r}) \\ &= \frac{1}{2^{n+3}} \frac{C^{[2n]}}{\hbar^{2n}} \mathcal{H}^{\text{md}[2n]}(\vec{r}) + \frac{1}{2^{n+3}} \frac{D^{[2n]}}{\hbar^{2n}} \sum_{\tau=n,p} \mathcal{H}_\tau^{\text{md}[2n]}(\vec{r}) \\ &\quad + \frac{1}{2^{n+3}} E^{[2n]} \mathcal{H}^{\text{gd}[2n]}(\vec{r}) + \frac{1}{2^{n+3}} F^{[2n]} \sum_{\tau=n,p} \mathcal{H}_\tau^{\text{gd}[2n]}(\vec{r}).\end{aligned}\quad (\text{A34})$$

## 2. Single-nucleon potential with the extended Skyrme interaction

Within the framework of Landau Fermi liquid theory, the  $n$ th-order single-nucleon potential  $U_\tau^{[2n]}$  can be expressed as:

$$U_\tau^{[2n]}(\vec{r}, \vec{p}) = \frac{\delta \int \mathcal{H}_{[2n]}(\vec{r}) d\vec{r}}{\delta f_\tau(\vec{r}, \vec{p})} = \frac{\delta \int \mathcal{H}_{[2n]}^{\text{MD}}(\vec{r}) d\vec{r}}{\delta f_\tau(\vec{r}, \vec{p})} + \sum_{m=0}^{2n} (-1)^m \nabla^m \frac{\partial \mathcal{H}_{[2n]}^{\text{GD}}(\vec{r})}{\partial [\nabla^m \rho_\tau(\vec{r})]}. \quad (\text{A35})$$

The variation of the  $n$ th-order MD term becomes:

$$\frac{\delta \int \mathcal{H}_{[2n]}^{\text{MD}}(\vec{r}) d\vec{r}}{\delta f_\tau(\vec{r}, \vec{p})} = \frac{1}{2^{n+2}} \frac{C^{[2n]}}{\hbar^{2n}} U^{\text{md}[2n]}(\vec{r}, \vec{p}) + \frac{1}{2^{n+2}} \frac{D^{[2n]}}{\hbar^{2n}} U_\tau^{\text{md}[2n]}(\vec{r}, \vec{p}), \quad (\text{A36})$$

where

$$U^{\text{md}[2n]}(\vec{r}, \vec{p}) = \int \frac{d^3 p'}{(2\pi\hbar)^3} (\vec{p} - \vec{p}')^{2n} f(\vec{r}, \vec{p}'), \quad (\text{A37})$$

$$U_\tau^{\text{md}[2n]}(\vec{r}, \vec{p}) = \int \frac{d^3 p'}{(2\pi\hbar)^3} (\vec{p} - \vec{p}')^{2n} f_\tau(\vec{r}, \vec{p}'). \quad (\text{A38})$$

Substitute Eq. (A24) and Eq. (A25) into Eq. (A35), and note that every term in Eq. (A24) and Eq. (A25) (take  $\nabla^k \rho(\vec{r}) \nabla^{2n-k} \rho(\vec{r})$  as an example) will contribute twice with the partial derivative  $\partial/\partial[\nabla^m \rho_\tau(\vec{r})]$  (when  $m = k$  and  $m = 2n - k$ ), i.e.,

$$\begin{aligned} & \sum_{m=0}^{2n} (-1)^m \nabla^m \frac{\partial [(-1)^k \binom{2n}{k} \nabla^k \rho(\vec{r}) \nabla^{2n-k} \rho(\vec{r})]}{\partial [\nabla^m \rho_\tau(\vec{r})]} \\ &= (-1)^{2k} \binom{2n}{k} \nabla^k [\nabla^{2n-k} \rho(\vec{r})] + (-1)^{2n} \binom{2n}{k} \nabla^{2n-k} [\nabla^k \rho(\vec{r})] \\ &= 2 \binom{2n}{k} \nabla^{2n} \rho(\vec{r}). \end{aligned} \quad (\text{A39})$$

Then we can obtain that

$$\begin{aligned} \sum_{m=0}^{2n} (-1)^m \nabla^m \frac{\partial \mathcal{H}_{[2n]}^{\text{GD}}(\vec{r})}{\partial [\nabla^m \rho_\tau(\vec{r})]} &= \frac{1}{2^{n+3}} E^{[2n]} 2^{2n+1} \nabla^{2n} \rho(\vec{r}) + \frac{1}{2^{n+3}} F^{[2n]} 2^{2n+1} \nabla^{2n} \rho_\tau(\vec{r}) \\ &= 2^{n-2} E^{[2n]} \nabla^{2n} \rho(\vec{r}) + 2^{n-2} F^{[2n]} \nabla^{2n} \rho_\tau(\vec{r}), \end{aligned} \quad (\text{A40})$$

and here the identity  $\sum_{m=0}^{2n} \binom{2n}{m} = 2^{2n}$  is used. Finally, the  $n$ th-order single-nucleon potential can be expressed as

$$\begin{aligned} U_\tau^{[2n]}(\vec{r}, \vec{p}) &= \frac{1}{2^{n+2}} \frac{C^{[2n]}}{\hbar^{2n}} U^{\text{md}[2n]}(\vec{r}, \vec{p}) + \frac{1}{2^{n+2}} \frac{D^{[2n]}}{\hbar^{2n}} U_\tau^{\text{md}[2n]}(\vec{r}, \vec{p}) \\ &\quad + 2^{n-2} E^{[2n]} \nabla^{2n} \rho(\vec{r}) + 2^{n-2} F^{[2n]} \nabla^{2n} \rho_\tau(\vec{r}). \end{aligned} \quad (\text{A41})$$

As mentioned in the main text, one of the advantages of the polynomial form of the MD term in Eqs. (A37) and (A38) [also for Eqs. (A21) and (A22)] is that their  $\vec{p}$  dependence can be factored out from the integral. For Eq. (A37) one has

$$\begin{aligned} U^{\text{md}[2n]}(\vec{r}, \vec{p}) &= \int \frac{d^3 p'}{(2\pi\hbar)^3} (\vec{p} - \vec{p}')^{2n} f(\vec{r}, \vec{p}') \\ &= \int \frac{d^3 p'}{(2\pi\hbar)^3} (p^2 - 2p_x p'_x - 2p_y p'_y - 2p_z p'_z + p'^2)^n f(\vec{r}, \vec{p}') \\ &= \sum_{\substack{n_1+n_2+\dots+n_5=n \\ n_1, n_2, \dots, n_5 \geq 0}} \binom{n}{n_1, n_2, \dots, n_5} (p^2)^{n_1} (-2p_x)^{n_2} (-2p_y)^{n_3} (-2p_z)^{n_4} \left[ \int \frac{d^3 p'}{(2\pi\hbar)^3} p'_x f(\vec{r}, \vec{p}') \right]^{n_2} \\ &\quad \times \left[ \int \frac{d^3 p'}{(2\pi\hbar)^3} p'_y f(\vec{r}, \vec{p}') \right]^{n_3} \left[ \int \frac{d^3 p'}{(2\pi\hbar)^3} p'_z f(\vec{r}, \vec{p}') \right]^{n_4} \left[ \int \frac{d^3 p'}{(2\pi\hbar)^3} p'^2 f(\vec{r}, \vec{p}') \right]^{n_5} \\ &= \sum_{\substack{n_1+n_2+\dots+n_5=n \\ n_1, n_2, \dots, n_5 \geq 0}} \binom{n}{n_1, n_2, \dots, n_5} (p^2)^{n_1} (-2p_x)^{n_2} (-2p_y)^{n_3} (-2p_z)^{n_4} \langle p_x \rangle_{\vec{r}}^{n_2} \langle p_y \rangle_{\vec{r}}^{n_3} \langle p_z \rangle_{\vec{r}}^{n_4} \langle p^2 \rangle_{\vec{r}}^{n_5}. \end{aligned} \quad (\text{A42})$$

Similarly one has

$$\begin{aligned} U_\tau^{\text{md}[2n]}(\vec{r}, \vec{p}) &= \int \frac{d^3 p'}{(2\pi\hbar)^3} (\vec{p} - \vec{p}')^{2n} f_\tau(\vec{r}, \vec{p}') \\ &= \sum_{\substack{n_1+n_2+\dots+n_5=n \\ n_1, n_2, \dots, n_5 \geq 0}} \binom{n}{n_1, n_2, \dots, n_5} (p^2)^{n_1} (-2p_x)^{n_2} (-2p_y)^{n_3} (-2p_z)^{n_4} \langle p_x \rangle_{\vec{r}, \tau}^{n_2} \langle p_y \rangle_{\vec{r}, \tau}^{n_3} \langle p_z \rangle_{\vec{r}, \tau}^{n_4} \langle p^2 \rangle_{\vec{r}, \tau}^{n_5}. \end{aligned} \quad (\text{A43})$$

In the above equations,

$$\binom{n}{n_1, n_2, \dots, n_5} = \frac{n!}{n_1! n_2! \dots n_5!} \quad (\text{A44})$$

is the the multinomial coefficient, and we have defined the mean value of a quantity at  $\vec{r}$ , i.e.,

$$\langle A \rangle_{\vec{r}} = \int \frac{d^3p}{(2\pi\hbar)^3} A(\vec{p}) f(\vec{r}, \vec{p}), \quad (\text{A45})$$

$$\langle A \rangle_{\vec{r}, \tau} = \int \frac{d^3p}{(2\pi\hbar)^3} A(\vec{p}) f_\tau(\vec{r}, \vec{p}). \quad (\text{A46})$$

We notice from Eqs. (A42) and (A43) that the  $\vec{p}$  dependence of  $U^{\text{md}[2n]}(\vec{r}, \vec{p})$  and  $U_\tau^{\text{md}[2n]}(\vec{r}, \vec{p})$  are factored out from the integral over  $\vec{p}'$ . It thus enables us to eliminate a loop over test particles when calculating the momentum-dependent part of single-particle potentials in the transport model, and reduces significantly the computational complexity of the transport model if a very large  $N_E$  is adopted.

## Appendix B: THE CHARACTERISTIC QUANTITIES OF THE SNM EOS AND THE SYMMETRY ENERGY, THE FOURTH-ORDER SYMMETRY ENERGY, AND THE NUCLEON EFFECTIVE MASSES

The SNM EOS  $E_0(\rho)$ , the symmetry energy  $E_{\text{sym}}(\rho)$  along with their expansion coefficients defined in Eqs. (30)-(34) are used to characterize the density behavior of the nuclear matter, which are expressed as

$$\begin{aligned} E_0(\rho) = & \frac{3a^2\hbar^2}{10m}\rho^{2/3} + \frac{3t_0}{8}\rho^{3/3} + \frac{t_3^{[1]}}{16}\rho^{4/3} + \frac{3a^2}{80}\left(2C^{[2]} + D^{[2]}\right)\rho^{5/3} + \frac{t_3^{[3]}}{16}\rho^{6/3} + \frac{9a^4}{280}\left(2C^{[4]} + D^{[4]}\right)\rho^{7/3} \\ & + \frac{t_3^{[5]}}{16}\rho^{8/3} + \frac{2a^6}{15}\left(2C^{[6]} + D^{[6]}\right)\rho^{9/3} + \frac{t_3^{[7]}}{16}\rho^{10/3} + \frac{3a^8}{77}\left(2C^{[8]} + D^{[8]}\right)\rho^{11/3} + \frac{t_3^{[9]}}{16}\rho^{12/3} \\ & + \frac{9a^{10}}{182}\left(2C^{[10]} + D^{[10]}\right)\rho^{13/3}, \end{aligned} \quad (\text{B1})$$

$$\begin{aligned} L_0(\rho) = & \frac{3a^2\hbar^2}{5m}\rho^{2/3} + \frac{9t_0}{8}\rho^{3/3} + \frac{t_3^{[1]}}{4}\rho^{4/3} + \frac{3a^2}{16}\left(2C^{[2]} + D^{[2]}\right)\rho^{5/3} + \frac{3t_3^{[3]}}{8}\rho^{6/3} + \frac{9a^4}{40}\left(2C^{[4]} + D^{[4]}\right)\rho^{7/3} \\ & + \frac{t_3^{[5]}}{2}\rho^{8/3} + \frac{6a^6}{5}\left(2C^{[6]} + D^{[6]}\right)\rho^{9/3} + \frac{5t_3^{[7]}}{8}\rho^{10/3} + \frac{3a^8}{7}\left(2C^{[8]} + D^{[8]}\right)\rho^{11/3} + \frac{3t_3^{[9]}}{4}\rho^{12/3} \\ & + \frac{9a^{10}}{14}\left(2C^{[10]} + D^{[10]}\right)\rho^{13/3}, \end{aligned} \quad (\text{B2})$$

$$\begin{aligned} K_0(\rho) = & -\frac{3a^2\hbar^2}{5m}\rho^{2/3} + \frac{t_3^{[1]}}{4}\rho^{4/3} + \frac{3a^2}{8}\left(2C^{[2]} + D^{[2]}\right)\rho^{5/3} + \frac{9t_3^{[3]}}{8}\rho^{6/3} + \frac{9a^4}{10}\left(2C^{[4]} + D^{[4]}\right)\rho^{7/3} + \frac{5t_3^{[5]}}{2}\rho^{8/3} \\ & + \frac{36a^6}{5}\left(2C^{[6]} + D^{[6]}\right)\rho^{9/3} + \frac{35t_3^{[7]}}{8}\rho^{10/3} + \frac{24a^8}{7}\left(2C^{[8]} + D^{[8]}\right)\rho^{11/3} + \frac{27t_3^{[9]}}{4}\rho^{12/3} \\ & + \frac{45a^{10}}{7}\left(2C^{[10]} + D^{[10]}\right)\rho^{13/3}, \end{aligned} \quad (\text{B3})$$

$$\begin{aligned} J_0(\rho) = & \frac{12a^2\hbar^2}{5m}\rho^{2/3} - \frac{t_3^{[1]}}{2}\rho^{4/3} - \frac{3a^2}{8}\left(2C^{[2]} + D^{[2]}\right)\rho^{5/3} + \frac{9a^4}{10}\left(2C^{[4]} + D^{[4]}\right)\rho^{7/3} + 5t_3^{[5]}\rho^{8/3} \\ & + \frac{108a^6}{5}\left(2C^{[6]} + D^{[6]}\right)\rho^{9/3} + \frac{35t_3^{[7]}}{2}\rho^{10/3} + \frac{120a^8}{7}\left(2C^{[8]} + D^{[8]}\right)\rho^{11/3} + \frac{81t_3^{[9]}}{2}\rho^{12/3} \\ & + 45a^{10}\left(2C^{[10]} + D^{[10]}\right)\rho^{13/3}, \end{aligned} \quad (\text{B4})$$

$$\begin{aligned} I_0(\rho) = & -\frac{84a^2\hbar^2}{5m}\rho^{2/3} + \frac{5t_3^{[1]}}{2}\rho^{4/3} + \frac{3a^2}{2}\left(2C^{[2]} + D^{[2]}\right)\rho^{5/3} - \frac{9a^4}{5}\left(2C^{[4]} + D^{[4]}\right)\rho^{7/3} - 5t_3^{[5]}\rho^{8/3} \\ & + \frac{35t_3^{[7]}}{2}\rho^{10/3} + \frac{240a^8}{7}\left(2C^{[8]} + D^{[8]}\right)\rho^{11/3} + \frac{243t_3^{[9]}}{2}\rho^{12/3} + 180a^{10}\left(2C^{[10]} + D^{[10]}\right)\rho^{13/3}, \end{aligned} \quad (\text{B5})$$

$$H_0(\rho) = \frac{168a^2\hbar^2}{m}\rho^{2/3} - 20t_3^{[1]}\rho^{4/3} - \frac{21a^2}{2}\left(2C^{[2]} + D^{[2]}\right)\rho^{5/3} + 9a^4\left(2C^{[4]} + D^{[4]}\right)\rho^{7/3} \\ + 20t_3^{[5]}\rho^{8/3} - 35t_3^{[7]}\rho^{10/3} - \frac{240a^8}{7}\left(2C^{[8]} + D^{[8]}\right)\rho^{11/3} + 180a^{10}\left(2C^{[10]} + D^{[10]}\right)\rho^{13/3}, \quad (\text{B6})$$

and

$$E_{\text{sym}}(\rho) = \frac{a^2\hbar^2}{6m}\rho^{2/3} - \frac{1}{8}t_0(2x_0 + 1)\rho^{3/3} - \frac{1}{48}t_3^{[1]}\left(2x_3^{[1]} + 1\right)\rho^{4/3} + \frac{a^2}{24}\left(C^{[2]} + 2D^{[2]}\right)\rho^{5/3} \\ - \frac{1}{48}t_3^{[3]}\left(2x_3^{[3]} + 1\right)\rho^{6/3} + \frac{a^4}{24}\left(2C^{[4]} + 3D^{[4]}\right)\rho^{7/3} - \frac{1}{48}t_3^{[5]}\left(2x_3^{[5]} + 1\right)\rho^{8/3} \\ + \frac{a^6}{5}\left(3C^{[6]} + 4D^{[6]}\right)\rho^{9/3} - \frac{1}{48}t_3^{[7]}\left(2x_3^{[7]} + 1\right)\rho^{10/3} + \frac{a^8}{15}\left(4C^{[8]} + 5D^{[8]}\right)\rho^{11/3} \\ - \frac{1}{48}t_3^{[9]}\left(2x_3^{[9]} + 1\right)\rho^{12/3} + \frac{2a^{10}}{21}\left(5C^{[10]} + 6D^{[10]}\right)\rho^{13/3}, \quad (\text{B7})$$

$$L(\rho) = \frac{a^2\hbar^2}{3m}\rho^{2/3} - \frac{3}{8}t_0(2x_0 + 1)\rho^{3/3} - \frac{1}{12}t_3^{[1]}\left(2x_3^{[1]} + 1\right)\rho^{4/3} + \frac{5a^2}{24}\left(C^{[2]} + 2D^{[2]}\right)\rho^{5/3} \\ - \frac{1}{8}t_3^{[3]}\left(2x_3^{[3]} + 1\right)\rho^{6/3} + \frac{7a^4}{24}\left(2C^{[4]} + 3D^{[4]}\right)\rho^{7/3} - \frac{1}{6}t_3^{[5]}\left(2x_3^{[5]} + 1\right)\rho^{8/3} \\ + \frac{9a^6}{5}\left(3C^{[6]} + 4D^{[6]}\right)\rho^{9/3} - \frac{5}{24}t_3^{[7]}\left(2x_3^{[7]} + 1\right)\rho^{10/3} + \frac{11a^8}{15}\left(4C^{[8]} + 5D^{[8]}\right)\rho^{11/3} \\ - \frac{1}{4}t_3^{[9]}\left(2x_3^{[9]} + 1\right)\rho^{12/3} + \frac{26a^{10}}{21}\left(5C^{[10]} + 6D^{[10]}\right)\rho^{13/3}, \quad (\text{B8})$$

$$K_{\text{sym}}(\rho) = -\frac{a^2\hbar^2}{3m}\rho^{2/3} - \frac{1}{12}t_3^{[1]}\left(2x_3^{[1]} + 1\right)\rho^{4/3} + \frac{5a^2}{12}\left(C^{[2]} + 2D^{[2]}\right)\rho^{5/3} - \frac{3}{8}t_3^{[3]}\left(2x_3^{[3]} + 1\right)\rho^{6/3} \\ + \frac{7a^4}{6}\left(2C^{[4]} + 3D^{[4]}\right)\rho^{7/3} - \frac{5}{6}t_3^{[5]}\left(2x_3^{[5]} + 1\right)\rho^{8/3} + \frac{54a^6}{5}\left(3C^{[6]} + 4D^{[6]}\right)\rho^{9/3} \\ - \frac{35}{24}t_3^{[7]}\left(2x_3^{[7]} + 1\right)\rho^{10/3} + \frac{88a^8}{15}\left(4C^{[8]} + 5D^{[8]}\right)\rho^{11/3} - \frac{9}{4}t_3^{[9]}\left(2x_3^{[9]} + 1\right)\rho^{12/3} \\ + \frac{260a^{10}}{21}\left(5C^{[10]} + 6D^{[10]}\right)\rho^{13/3}, \quad (\text{B9})$$

$$J_{\text{sym}}(\rho) = \frac{4a^2\hbar^2}{3m}\rho^{2/3} + \frac{1}{6}t_3^{[1]}\left(2x_3^{[1]} + 1\right)\rho^{4/3} - \frac{5a^2}{12}\left(C^{[2]} + 2D^{[2]}\right)\rho^{5/3} + \frac{7a^4}{6}\left(2C^{[4]} + 3D^{[4]}\right)\rho^{7/3} \\ - \frac{5}{3}t_3^{[5]}\left(2x_3^{[5]} + 1\right)\rho^{8/3} + \frac{162a^6}{5}\left(3C^{[6]} + 4D^{[6]}\right)\rho^{9/3} - \frac{35}{6}t_3^{[7]}\left(2x_3^{[7]} + 1\right)\rho^{10/3} \\ + \frac{88a^8}{3}\left(4C^{[8]} + 5D^{[8]}\right)\rho^{11/3} - \frac{27}{2}t_3^{[9]}\left(2x_3^{[9]} + 1\right)\rho^{12/3} + \frac{260a^{10}}{3}\left(5C^{[10]} + 6D^{[10]}\right)\rho^{13/3}, \quad (\text{B10})$$

$$I_{\text{sym}}(\rho) = -\frac{28a^2\hbar^2}{3m}\rho^{2/3} - \frac{5}{6}t_3^{[1]}\left(2x_3^{[1]} + 1\right)\rho^{4/3} + \frac{5a^2}{3}\left(C^{[2]} + 2D^{[2]}\right)\rho^{5/3} - \frac{7a^4}{3}\left(2C^{[4]} + 3D^{[4]}\right)\rho^{7/3} \\ + \frac{5}{3}t_3^{[5]}\left(2x_3^{[5]} + 1\right)\rho^{8/3} - \frac{35}{6}t_3^{[7]}\left(2x_3^{[7]} + 1\right)\rho^{10/3} + \frac{176a^8}{3}\left(4C^{[8]} + 5D^{[8]}\right)\rho^{11/3} \\ - \frac{81}{2}t_3^{[9]}\left(2x_3^{[9]} + 1\right)\rho^{12/3} + \frac{1040a^{10}}{3}\left(5C^{[10]} + 6D^{[10]}\right)\rho^{13/3}, \quad (\text{B11})$$

$$H_{\text{sym}}(\rho) = \frac{280a^2\hbar^2}{3m}\rho^{2/3} + \frac{20}{3}t_3^{[1]}\left(2x_3^{[1]} + 1\right)\rho^{4/3} - \frac{35a^2}{3}\left(C^{[2]} + 2D^{[2]}\right)\rho^{5/3} + \frac{35a^4}{3}\left(2C^{[4]} + 3D^{[4]}\right)\rho^{7/3} \\ - \frac{20}{3}t_3^{[5]}\left(2x_3^{[5]} + 1\right)\rho^{8/3} + \frac{35}{3}t_3^{[7]}\left(2x_3^{[7]} + 1\right)\rho^{10/3} - \frac{176a^8}{3}\left(4C^{[8]} + 5D^{[8]}\right)\rho^{11/3} \\ + \frac{1040a^{10}}{3}\left(5C^{[10]} + 6D^{[10]}\right)\rho^{13/3}. \quad (\text{B12})$$

And the fourth-order symmetry energy can be expressed as

$$E_{\text{sym},4}(\rho) \equiv \frac{1}{4!} \left. \frac{\partial^4 E(\rho, \delta)}{\partial \delta^4} \right|_{\delta=0} = \frac{a^2 \hbar^2}{162m} \rho^{2/3} + \frac{a^2}{648} \left( C^{[2]} - D^{[2]} \right) \rho^{5/3} + \frac{a^4}{648} \left( 8C^{[4]} + 3D^{[4]} \right) \rho^{7/3} \\ + \frac{2a^6}{135} \left( 13C^{[6]} + 9D^{[6]} \right) \rho^{9/3} + \frac{a^8}{405} \left( 61C^{[8]} + 50D^{[8]} \right) \rho^{11/3} + \frac{2a^{10}}{81} \left( 17C^{[10]} + 15D^{[10]} \right) \rho^{13/3}. \quad (\text{B13})$$

The isoscalar nucleon effective mass  $m_s^*$  and isovector nucleon effective mass  $m_v^*$  are momentum dependent in our models. We define  $\tilde{M}_s \equiv m/m_s$  and  $\tilde{M}_v \equiv m/m_v$ . Thus, we have

$$\tilde{M}_s(\rho, p) = 1 + \frac{m}{p} \frac{dU_0(\rho, p)}{dp} \\ = 1 + \frac{m}{8\hbar^2} \rho \left( 2C^{[2]} + D^{[2]} \right) + \frac{m}{8\hbar^2} a^2 \rho^{5/3} \left( 2C^{[4]} + D^{[4]} \right) + \frac{3m}{8\hbar^2} a^4 \rho^{7/3} \left( 2C^{[6]} + D^{[6]} \right) \\ + \frac{m}{16\hbar^2} a^6 \rho^3 \left( 2C^{[8]} + D^{[8]} \right) + \frac{5m}{128\hbar^2} a^8 \rho^{11/3} \left( 2C^{[10]} + D^{[10]} \right) \\ + \frac{p^2}{\hbar^2} \left[ \frac{m}{8\hbar^2} \rho \left( 2C^{[4]} + D^{[4]} \right) + \frac{21m}{20\hbar^2} a^2 \rho^{5/3} \left( 2C^{[6]} + D^{[6]} \right) + \frac{27m}{80\hbar^2} a^4 \rho^{7/3} \left( 2C^{[8]} + D^{[8]} \right) + \frac{11m}{32\hbar^2} a^6 \rho^3 \left( 2C^{[10]} + D^{[10]} \right) \right] \\ + \frac{p^4}{\hbar^4} \left[ \frac{3m}{8\hbar^2} \rho \left( 2C^{[6]} + D^{[6]} \right) + \frac{27m}{80\hbar^2} a^2 \rho^{5/3} \left( 2C^{[8]} + D^{[8]} \right) + \frac{297m}{448\hbar^2} a^4 \rho^{7/3} \left( 2C^{[8]} + D^{[8]} \right) \right] \\ + \frac{p^6}{\hbar^6} \left[ \frac{m}{16\hbar^2} \rho \left( 2C^{[8]} + D^{[8]} \right) + \frac{11m}{32\hbar^2} a^2 \rho^{5/3} \left( 2C^{[10]} + D^{[10]} \right) \right] + \frac{p^8}{\hbar^8} \left[ \frac{5m}{128\hbar^2} \rho \left( 2C^{[10]} + D^{[10]} \right) \right], \quad (\text{B14})$$

and

$$\tilde{M}_v(\rho, p) = 1 + \frac{m}{p} \frac{dU_\tau(\rho, -\tau, p)}{dp} \\ = 1 + \frac{m}{4\hbar^2} \rho C^{[2]} + \frac{m}{4\hbar^2} 2^{2/3} a^2 \rho^{5/3} C^{[4]} + \frac{m}{2\hbar^2} 2^{1/3} a^4 \rho^{7/3} C^{[6]} + \frac{m}{2\hbar^2} a^6 \rho^3 C^{[8]} + \frac{5m}{16\hbar^2} 2^{1/3} a^8 \rho^{11/3} C^{[10]} \\ + \frac{p^2}{\hbar^2} \left[ \frac{m}{4\hbar^2} \rho C^{[4]} + \frac{21m}{20\hbar^2} 2^{2/3} a^2 \rho^{5/3} C^{[6]} + \frac{27m}{20\hbar^2} 2^{1/3} a^4 \rho^{7/3} C^{[8]} + \frac{11m}{4\hbar^2} a^6 \rho^3 C^{[10]} \right] \\ + \frac{p^4}{\hbar^4} \left[ \frac{3m}{4\hbar^2} \rho C^{[6]} + \frac{27m}{40\hbar^2} 2^{2/3} a^2 \rho^{5/3} C^{[8]} + \frac{297m}{112\hbar^2} 2^{1/3} a^4 \rho^{7/3} C^{[10]} \right] \\ + \frac{p^6}{\hbar^6} \left[ \frac{m}{8\hbar^2} \rho C^{[8]} + \frac{11m}{16\hbar^2} 2^{1/3} a^2 \rho^{5/3} C^{[10]} \right] + \frac{p^8}{\hbar^8} \left[ \frac{5m}{64\hbar^2} \rho C^{[10]} \right], \quad (\text{B15})$$

with  $\tau = 1 [-1]$  for neutron [proton]. And the linear isospin splitting coefficient can be expressed as

$$\Delta m_1^*(\rho) \equiv \left. \frac{\partial m_{\text{n-p}}^*(\rho, \delta)}{\partial \delta} \right|_{\delta=0} = -\frac{\mathcal{A}(\rho)}{\mathcal{B}(\rho)}, \quad (\text{B16})$$

where

$$\mathcal{A}(\rho) = 80m\hbar^2 \left[ 15D^{[2]} \rho^{3/3} + 10a^2 \left( 2C^{[4]} + 5D^{[4]} \right) \rho^{5/3} + 72a^4 \left( 4C^{[6]} + 7D^{[6]} \right) \rho^{7/3} \right. \\ \left. + 96a^6 \left( 2C^{[8]} + 3D^{[8]} \right) \rho^{9/3} + \frac{400}{7} a^8 \left( 8C^{[10]} + 11D^{[10]} \right) \rho^{11/3} \right], \quad (\text{B17})$$

and

$$\mathcal{B}(\rho) = 3m^2 \left[ \frac{40\hbar^2}{m} + 5 \left( 2C^{[2]} + D^{[2]} \right) \rho^{3/3} + 10a^2 \left( 2C^{[4]} + D^{[4]} \right) \rho^{5/3} + 72a^4 \left( 2C^{[6]} + D^{[6]} \right) \rho^{7/3} \right. \\ \left. + 32a^6 \left( 2C^{[8]} + D^{[8]} \right) \rho^{9/3} + \frac{400}{7} a^8 \left( 2C^{[10]} + D^{[10]} \right) \rho^{11/3} \right]^2. \quad (\text{B18})$$

Ignoring  $C^{[10]}$ ,  $D^{[10]}$ ,  $E^{[10]}$ ,  $F^{[10]}$  and  $t_3^{[9]}$  terms (or as well as the  $C^{[8]}$ ,  $D^{[8]}$ ,  $E^{[8]}$ ,  $F^{[8]}$  and  $t_3^{[7]}$  terms), these expressions in N5LO model will reduce to their corresponding forms in the N4LO (N3LO) model.

TABLE VII. The 14 parameters of the interactions SP6L45X. Here the recombination of Skyrme parameters defined in Eq. (A26) and Eq. (A27) are used. The units of parameters:  $t_0$ :  $\text{MeV fm}^3$ ;  $t_3^{[n]}$  ( $n = 1, 3, 5$ ),  $C^{[n]}$  and  $D^{[n]}$  ( $n = 2, 4, 6$ ):  $\text{MeV fm}^{n+3}$ ;  $x_0$  and  $x_3^{[n]}$  ( $n = 1, 3, 5$ ) are dimensionless.

X	Dm07	Dm05	Dm03	Dm01	D01	D03	D05	D07
$t_0$	-1840.45	-1840.45	-1840.45	-1840.45	-1840.45	-1840.45	-1840.45	-1840.45
$t_3^{[1]}$	13010.2	13010.2	13010.2	13010.2	13010.2	13010.2	13010.2	13010.2
$t_3^{[3]}$	-4036.41	-4036.41	-4036.41	-4036.41	-4036.41	-4036.41	-4036.41	-4036.41
$t_3^{[5]}$	2386.36	2386.36	2386.36	2386.36	2386.36	2386.36	2386.36	2386.36
$x_0$	0.328136	0.309276	0.290417	0.271557	0.252697	0.233838	0.214978	0.196119
$x_3^{[1]}$	0.720796	0.611729	0.502661	0.393593	0.284524	0.175457	0.066389	-0.042677
$x_3^{[3]}$	-4.69172	-3.98025	-3.26878	-2.55731	-1.84583	-1.13437	-0.422901	0.288567
$x_3^{[5]}$	-8.11908	-7.58510	-7.05111	-6.51713	-5.98314	-5.44915	-4.91517	-4.38119
$C^{[2]}$	-322.800	-135.318	52.1646	239.648	427.132	614.614	802.097	989.580
$D^{[2]}$	1343.54	968.578	593.612	218.645	-156.323	-531.287	-906.253	-1281.21
$C^{[4]}$	-2.25298	-5.30996	-8.36694	-11.4239	-14.4809	-17.5379	-20.5948	-23.6518
$D^{[4]}$	-21.9069	-15.7930	-9.67908	-3.56509	2.54890	8.66285	14.7768	20.8907
$C^{[6]}$	0.023356	0.028186	0.033017	0.037848	0.042679	0.047510	0.052341	0.057172
$D^{[6]}$	0.034618	0.024957	0.015295	0.005633	-0.004027	-0.013689	-0.023351	-0.033012

TABLE VIII. The 18 parameters of the interactions SP8L45X. Here the recombination of Skyrme parameters defined in Eq. (A26) and Eq. (A27) are used. The units of parameters:  $t_0$ :  $\text{MeV fm}^3$ ;  $t_3^{[n]}$  ( $n = 1, 3, 5, 7$ ),  $C^{[n]}$  and  $D^{[n]}$  ( $n = 2, 4, 6, 8$ ):  $\text{MeV fm}^{n+3}$ ;  $x_0$  and  $x_3^{[n]}$  ( $n = 1, 3, 5, 7$ ) are dimensionless.

X	Dm07	Dm05	Dm03	Dm01	D01	D03	D05	D07
$t_0$	-1838.65	-1838.65	-1838.65	-1838.65	-1838.65	-1838.65	-1838.65	-1838.65
$t_3^{[1]}$	12926.3	12926.3	12926.3	12926.3	12926.3	12926.3	12926.3	12926.3
$t_3^{[3]}$	-4248.13	-4248.13	-4248.13	-4248.13	-4248.13	-4248.13	-4248.13	-4248.13
$t_3^{[5]}$	2649.97	2649.97	2649.97	2649.97	2649.97	2649.97	2649.97	2649.97
$t_3^{[7]}$	-127.291	-127.291	-127.291	-127.291	-127.291	-127.291	-127.291	-127.291
$x_0$	0.331623	0.312314	0.293006	0.273698	0.254389	0.235081	0.215773	0.196464
$x_3^{[1]}$	0.746536	0.633826	0.521118	0.408409	0.295701	0.182992	0.070283	-0.042425
$x_3^{[3]}$	-4.62263	-3.91835	-3.21408	-2.50981	-1.80555	-1.10128	-0.397013	0.307262
$x_3^{[5]}$	-7.61305	-7.09574	-6.57845	-6.06115	-5.54386	-5.02656	-4.50927	-3.99196
$x_3^{[7]}$	-3.15560	-2.80526	-2.45504	-2.10484	-1.75469	-1.40438	-1.05416	-0.703829
$C^{[2]}$	-315.391	-121.836	71.7175	265.271	458.825	652.380	845.934	1039.49
$D^{[2]}$	1392.53	1005.42	618.314	231.206	-155.901	-543.011	-930.119	-1317.23
$C^{[4]}$	-5.17687	-8.33604	-11.4951	-14.6543	-17.8134	-20.9726	-24.1317	-27.2908
$D^{[4]}$	-22.7285	-16.4102	-10.0919	-3.77368	2.54458	8.86288	15.1811	21.4994
$C^{[6]}$	0.055782	0.060957	0.066131	0.071306	0.076480	0.081655	0.086829	0.092004
$D^{[6]}$	0.037228	0.026879	0.016530	0.006181	-0.004167	-0.014517	-0.024866	-0.035215
$C^{[8]}$	-0.001628	-0.001698	-0.001768	-0.001839	-0.001909	-0.001979	-0.002050	-0.002120
$D^{[8]}$	$-5.058 \times 10^{-4}$	$-3.652 \times 10^{-4}$	$-2.246 \times 10^{-4}$	$-8.399 \times 10^{-5}$	$5.663 \times 10^{-5}$	$1.972 \times 10^{-4}$	$3.378 \times 10^{-4}$	$4.785 \times 10^{-4}$

### Appendix C: PARAMETERS OF THE SKYRME INTERACTIONS

In Table VII, VIII and IX, we list the Skyrme parameters of the 24 interactions.

[1] B.-A. Li, C. M. Ko, and W. Bauer, Isospin physics in heavy ion collisions at intermediate-energies, Int. J.

Mod. Phys. E **7**, 147 (1998), arXiv:nucl-th/9707014.  
 [2] J. M. Lattimer and M. Prakash, Nuclear matter and its

TABLE IX. The 22 parameters of the interactions SP10L45X. Here the recombination of Skyrme parameters defined in Eq. (A26) and Eq. (A27) are used. The units of parameters:  $t_0$ :  $\text{MeV fm}^3$ ;  $t_3^{[n]}$  ( $n = 1, 3, 5, 7, 9$ ),  $C^{[n]}$  and  $D^{[n]}$  ( $n = 2, 4, 6, 8, 10$ ):  $\text{MeV fm}^{n+3}$ ;  $x_0$  and  $x_3^{[n]}$  ( $n = 1, 3, 5, 7, 9$ ) are dimensionless.

X	Dm07	Dm05	Dm03	Dm01	D01	D03	D05	D07
$t_0$	-1838.88	-1838.88	-1838.88	-1838.88	-1838.88	-1838.88	-1838.88	-1838.88
$t_3^{[1]}$	12927.0	12927.0	12927.0	12927.0	12927.0	12927.0	12927.0	12927.0
$t_3^{[3]}$	-4334.99	-4334.99	-4334.99	-4334.99	-4334.99	-4334.99	-4334.99	-4334.99
$t_3^{[5]}$	2898.99	2898.99	2898.99	2898.99	2898.99	2898.99	2898.99	2898.99
$t_3^{[7]}$	-477.033	-477.033	-477.033	-477.033	-477.033	-477.033	-477.033	-477.033
$t_3^{[9]}$	212.964	212.964	212.964	212.964	212.964	212.964	212.964	212.964
$x_0$	0.331118	0.311884	0.292650	0.273417	0.254183	0.234949	0.215715	0.196481
$x_3^{[1]}$	0.745822	0.633297	0.520773	0.408248	0.295723	0.183199	0.070674	-0.041850
$x_3^{[3]}$	-4.59069	-3.89277	-3.19486	-2.49695	-1.79903	-1.10112	-0.403207	0.294711
$x_3^{[5]}$	-7.21694	-6.71607	-6.21522	-5.71435	-5.21350	-4.71263	-4.21177	-3.71090
$x_3^{[7]}$	-3.14162	-2.79184	-2.44216	-2.09242	-1.74276	-1.39297	-1.04324	-0.693462
$x_3^{[9]}$	-3.17760	-2.80998	-2.44247	-2.07489	-1.70740	-1.33976	-0.972199	-0.604576
$C^{[2]}$	-313.147	-119.109	74.9264	268.964	463.002	657.040	851.077	1045.11
$D^{[2]}$	1397.65	1009.57	621.505	233.428	-154.645	-542.721	-930.795	-1318.87
$C^{[4]}$	-6.21986	-9.38697	-12.5540	-15.7211	-18.8882	-22.0553	-25.2224	-28.3895
$D^{[4]}$	-22.8126	-16.4784	-10.1442	-3.81005	2.52413	8.85835	15.1925	21.5267
$C^{[6]}$	0.073508	0.078700	0.083892	0.089084	0.094276	0.099469	0.104661	0.109853
$D^{[6]}$	0.037399	0.027014	0.016630	0.006246	-0.004138	-0.014522	-0.024906	-0.038206
$C^{[8]}$	-0.003309	-0.003382	-0.003455	-0.003528	-0.003601	-0.003674	-0.003747	-0.003820
$D^{[8]}$	$-5.258 \times 10^{-4}$	$-3.798 \times 10^{-4}$	$-2.338 \times 10^{-4}$	$-8.783 \times 10^{-5}$	$5.818 \times 10^{-5}$	$2.042 \times 10^{-4}$	$3.502 \times 10^{-4}$	$4.962 \times 10^{-4}$
$C^{[10]}$	$1.241 \times 10^{-5}$	$1.256 \times 10^{-5}$	$1.272 \times 10^{-5}$	$1.287 \times 10^{-5}$	$1.303 \times 10^{-5}$	$1.318 \times 10^{-5}$	$1.334 \times 10^{-5}$	$1.349 \times 10^{-5}$
$D^{[10]}$	$1.113 \times 10^{-6}$	$8.044 \times 10^{-7}$	$4.952 \times 10^{-7}$	$1.859 \times 10^{-7}$	$-1.232 \times 10^{-7}$	$-4.324 \times 10^{-7}$	$-7.416 \times 10^{-7}$	$-1.050 \times 10^{-6}$

- role in supernovae, neutron stars and compact object binary mergers, *Phys. Rept.* **333**, 121 (2000), arXiv:astro-ph/0002203.
- [3] P. Danielewicz, R. Lacey, and W. G. Lynch, Determination of the equation of state of dense matter, *Science* **298**, 1592 (2002), arXiv:nucl-th/0208016.
- [4] J. M. Lattimer and M. Prakash, The physics of neutron stars, *Science* **304**, 536 (2004), arXiv:astro-ph/0405262.
- [5] V. Baran, M. Colonna, V. Greco, and M. Di Toro, Reaction dynamics with exotic beams, *Phys. Rept.* **410**, 335 (2005), arXiv:nucl-th/0412060.
- [6] A. W. Steiner, M. Prakash, J. M. Lattimer, and P. J. Ellis, Isospin asymmetry in nuclei and neutron stars, *Phys. Rept.* **411**, 325 (2005), arXiv:nucl-th/0410066.
- [7] B.-A. Li, L.-W. Chen, and C. M. Ko, Recent Progress and New Challenges in Isospin Physics with Heavy-Ion Reactions, *Phys. Rept.* **464**, 113 (2008), arXiv:0804.3580 [nucl-th].
- [8] M. Oertel, M. Hempel, T. Klöhn, and S. Typel, Equations of state for supernovae and compact stars, *Rev. Mod. Phys.* **89**, 015007 (2017), arXiv:1610.03361 [astro-ph.HE].
- [9] J. P. Blaizot, Nuclear Compressibilities, *Phys. Rept.* **64**, 171 (1980).
- [10] D. H. Youngblood, H. L. Clark, and Y. W. Lui, Incompressibility of Nuclear Matter from the Giant Monopole Resonance, *Phys. Rev. Lett.* **82**, 691 (1999).
- [11] T. Li et al., Isotopic dependence of the giant monopole resonance in the even-A Sn-112 - Sn-124 isotopes and the asymmetry term in nuclear incompressibility, *Phys. Rev. Lett.* **99**, 162503 (2007), arXiv:0709.0567 [nucl-ex].
- [12] Z. Z. Li, Y. F. Niu, and G. Colò, Toward a Unified Description of Isoscalar Giant Monopole Resonances in a Self-Consistent Quasiparticle-Vibration Coupling Approach, *Phys. Rev. Lett.* **131**, 082501 (2023), arXiv:2211.01264 [nucl-th].
- [13] S. Shlomo, V. M. Kolomietz, and G. Colò, Deducing the nuclear-matter incompressibility coefficient from data on isoscalar compression modes, *Eur. Phys. J. A* **30**, 23 (2006).
- [14] U. Garg and G. Colò, The compression-mode giant resonances and nuclear incompressibility, *Prog. Part. Nucl. Phys.* **101**, 55 (2018), arXiv:1801.03672 [nucl-ex].
- [15] A. Le Fèvre, Y. Leifels, W. Reisdorf, J. Aichelin, and C. Hartnack, Constraining the nuclear matter equation of state around twice saturation density, *Nucl. Phys. A* **945**, 112 (2016), arXiv:1501.05246 [nucl-ex].
- [16] J. Aichelin and C. M. Ko, Subthreshold Kaon Production as a Probe of the Nuclear Equation of State, *Phys. Rev. Lett.* **55**, 2661 (1985).
- [17] C. Fuchs, A. Faessler, E. Zabrodin, and Y.-M. Zheng, Probing the nuclear equation of state by K+ production in heavy ion collisions, *Phys. Rev. Lett.* **86**, 1974 (2001), arXiv:nucl-th/0011102.
- [18] C. Hartnack, H. Oeschler, and J. Aichelin, Hadronic matter is soft, *Phys. Rev. Lett.* **96**, 012302 (2006), arXiv:nucl-th/0506087.
- [19] C. Fuchs, Kaon production in heavy ion reactions at intermediate energies, *Prog. Part. Nucl. Phys.* **56**, 1 (2006), arXiv:nucl-th/0507017.
- [20] L.-W. Chen, C. M. Ko, and B.-A. Li, Nuclear matter symmetry energy and the neutron skin thickness

- of heavy nuclei, *Phys. Rev. C* **72**, 064309 (2005), arXiv:nucl-th/0509009.
- [21] M. Centelles, X. Roca-Maza, X. Vinas, and M. Warda, Nuclear symmetry energy probed by neutron skin thickness of nuclei, *Phys. Rev. Lett.* **102**, 122502 (2009), arXiv:0806.2886 [nucl-th].
- [22] L.-W. Chen, C. M. Ko, B.-A. Li, and J. Xu, Density slope of the nuclear symmetry energy from the neutron skin thickness of heavy nuclei, *Phys. Rev. C* **82**, 024321 (2010), arXiv:1004.4672 [nucl-th].
- [23] B. K. Agrawal, J. N. De, and S. K. Samaddar, Determining the density content of symmetry energy and neutron skin: an empirical approach, *Phys. Rev. Lett.* **109**, 262501 (2012), arXiv:1212.0292 [nucl-th].
- [24] Z. Zhang and L.-W. Chen, Constraining the symmetry energy at subsaturation densities using isotope binding energy difference and neutron skin thickness, *Phys. Lett. B* **726**, 234 (2013), arXiv:1302.5327 [nucl-th].
- [25] B. A. Brown, Constraints on the Skyrme Equations of State from Properties of Doubly Magic Nuclei, *Phys. Rev. Lett.* **111**, 232502 (2013), arXiv:1308.3664 [nucl-th].
- [26] X. Roca-Maza, M. Brenna, B. K. Agrawal, P. F. Bortignon, G. Colò, L.-G. Cao, N. Paar, and D. Vretenar, Giant Quadrupole Resonances in 208Pb, the nuclear symmetry energy and the neutron skin thickness, *Phys. Rev. C* **87**, 034301 (2013), arXiv:1212.4377 [nucl-th].
- [27] Z. Zhang and L.-W. Chen, Constraining the density slope of nuclear symmetry energy at subsaturation densities using electric dipole polarizability in <sup>208</sup>Pb, *Phys. Rev. C* **90**, 064317 (2014), arXiv:1407.8054 [nucl-th].
- [28] P. Danielewicz and J. Lee, Symmetry Energy II: Isobaric Analog States, *Nucl. Phys. A* **922**, 1 (2014), arXiv:1307.4130 [nucl-th].
- [29] Z. Zhang and L.-W. Chen, Electric dipole polarizability in <sup>208</sup>Pb as a probe of the symmetry energy and neutron matter around  $\rho_0/3$ , *Phys. Rev. C* **92**, 031301 (2015), arXiv:1504.01077 [nucl-th].
- [30] P. Danielewicz, P. Singh, and J. Lee, Symmetry Energy III: Isovector Skins, *Nucl. Phys. A* **958**, 147 (2017), arXiv:1611.01871 [nucl-th].
- [31] J. Xu, J. Zhou, Z. Zhang, W.-J. Xie, and B.-A. Li, Constraining isovector nuclear interactions with giant resonances within a Bayesian approach, *Phys. Lett. B* **810**, 135820 (2020), arXiv:2006.05217 [nucl-th].
- [32] M. Qiu, B.-J. Cai, L.-W. Chen, C.-X. Yuan, and Z. Zhang, Bayesian model averaging for nuclear symmetry energy from effective proton-neutron chemical potential difference of neutron-rich nuclei, *Phys. Lett. B* **849**, 138435 (2024), arXiv:2312.07031 [nucl-th].
- [33] L.-W. Chen, C. M. Ko, and B.-A. Li, Determination of the stiffness of the nuclear symmetry energy from isospin diffusion, *Phys. Rev. Lett.* **94**, 032701 (2005), arXiv:nucl-th/0407032.
- [34] B.-A. Li and L.-W. Chen, Nucleon-nucleon cross sections in neutron-rich matter and isospin transport in heavy-ion reactions at intermediate energies, *Phys. Rev. C* **72**, 064611 (2005), arXiv:nucl-th/0508024.
- [35] S. Kowalski et al., Experimental determination of the symmetry energy of a low density nuclear gas, *Phys. Rev. C* **75**, 014601 (2007), arXiv:nucl-ex/0602023.
- [36] D. V. Shetty, S. J. Yennello, and G. A. Souliotis, Density dependence of the symmetry energy and the equation of state of isospin asymmetric nuclear matter, *Phys. Rev. C* **75**, 034602 (2007), arXiv:nucl-ex/0505011.
- [37] M. B. Tsang, Y. Zhang, P. Danielewicz, M. Famiano, Z. Li, W. G. Lynch, and A. W. Steiner, Constraints on the density dependence of the symmetry energy, *Phys. Rev. Lett.* **102**, 122701 (2009), arXiv:0811.3107 [nucl-ex].
- [38] R. Wada et al., The Nuclear Matter Symmetry Energy at  $0.03 \leq \rho/\rho_0 \leq 0.2$ , *Phys. Rev. C* **85**, 064618 (2012), arXiv:1110.3341 [nucl-ex].
- [39] P. Morfouace et al., Constraining the symmetry energy with heavy-ion collisions and Bayesian analyses, *Phys. Lett. B* **799**, 135045 (2019), arXiv:1904.12471 [nucl-ex].
- [40] Y. Zhang, M. Liu, C.-J. Xia, Z. Li, and S. K. Biswal, Constraints on the symmetry energy and its associated parameters from nuclei to neutron stars, *Phys. Rev. C* **101**, 034303 (2020), arXiv:2002.10884 [nucl-th].
- [41] I. Tews, T. Krüger, K. Hebeler, and A. Schwenk, Neutron matter at next-to-next-to-leading order in chiral effective field theory, *Phys. Rev. Lett.* **110**, 032504 (2013), arXiv:1206.0025 [nucl-th].
- [42] G. Wlazłowski, J. W. Holt, S. Moroz, A. Bulgac, and K. J. Roche, Auxiliary-Field Quantum Monte Carlo Simulations of Neutron Matter in Chiral Effective Field Theory, *Phys. Rev. Lett.* **113**, 182503 (2014), arXiv:1403.3753 [nucl-th].
- [43] A. Akmal, V. R. Pandharipande, and D. G. Ravenhall, The Equation of state of nucleon matter and neutron star structure, *Phys. Rev. C* **58**, 1804 (1998), arXiv:nucl-th/9804027.
- [44] M. Baldo and K. Fukukawa, Nuclear Matter from Effective Quark-Quark Interaction, *Phys. Rev. Lett.* **113**, 242501 (2014), arXiv:1409.7206 [nucl-th].
- [45] A. Carbone, A. Rios, and A. Polls, Correlated density-dependent chiral forces for infinite matter calculations within the Green's function approach, *Phys. Rev. C* **90**, 054322 (2014), arXiv:1408.0717 [nucl-th].
- [46] G. Fiorella Burgio and A. F. Fantina, Nuclear Equation of state for Compact Stars and Supernovae, *Astrophys. Space Sci. Libr.* **457**, 255 (2018), arXiv:1804.03020 [nucl-th].
- [47] N.-B. Zhang and B.-A. Li, Extracting Nuclear Symmetry Energies at High Densities from Observations of Neutron Stars and Gravitational Waves, *Eur. Phys. J. A* **55**, 39 (2019), arXiv:1807.07698 [nucl-th].
- [48] Y. Zhou, L.-W. Chen, and Z. Zhang, Equation of state of dense matter in the multimessenger era, *Phys. Rev. D* **99**, 121301 (2019), arXiv:1901.11364 [nucl-th].
- [49] Y. Zhou and L.-W. Chen, Ruling out the supersoft high-density symmetry energy from the discovery of PSR J0740+6620 with mass  $2.14^{+0.10}_{-0.09} M_\odot$ , *Astrophys. J.* **886**, 52 (2019), arXiv:1907.12284 [nucl-th].
- [50] B.-A. Li, B.-J. Cai, W.-J. Xie, and N.-B. Zhang, Progress in Constraining Nuclear Symmetry Energy Using Neutron Star Observables Since GW170817, *Universe* **7**, 182 (2021), arXiv:2105.04629 [nucl-th].
- [51] P. G. Krastev, Translating Neutron Star Observations to Nuclear Symmetry Energy via Deep Neural Networks, *Galaxies* **10**, 16 (2022), arXiv:2112.04089 [nucl-th].
- [52] T.-G. Yue, L.-W. Chen, Z. Zhang, and Y. Zhou, Constraints on the symmetry energy from PREX-II in the multimessenger era, *Phys. Rev. Res.* **4**, L022054 (2022), arXiv:2102.05267 [nucl-th].
- [53] H. Koehn et al., An overview of existing and new nuclear



- and astrophysical constraints on the equation of state of neutron-rich dense matter, (2024), arXiv:2402.04172 [astro-ph.HE].
- [54] A. Lovato et al., Long Range Plan: Dense matter theory for heavy-ion collisions and neutron stars (2022), arXiv:2211.02224 [nucl-th].
  - [55] A. Sorensen et al., Dense nuclear matter equation of state from heavy-ion collisions, Prog. Part. Nucl. Phys. **134**, 104080 (2024), arXiv:2301.13253 [nucl-th].
  - [56] G. F. Bertsch and S. Das Gupta, A Guide to microscopic models for intermediate-energy heavy ion collisions, Phys. Rept. **160**, 189 (1988).
  - [57] J. Aichelin, 'Quantum' molecular dynamics: A Dynamical microscopic n body approach to investigate fragment formation and the nuclear equation of state in heavy ion collisions, Phys. Rept. **202**, 233 (1991).
  - [58] J. Xu et al. (TMED), Understanding transport simulations of heavy-ion collisions at 100A and 400A MeV: Comparison of heavy-ion transport codes under controlled conditions, Phys. Rev. C **93**, 044609 (2016), arXiv:1603.08149 [nucl-th].
  - [59] Y.-X. Zhang et al. (TMED), Comparison of heavy-ion transport simulations: Collision integral in a box, Phys. Rev. C **97**, 034625 (2018), arXiv:1711.05950 [nucl-th].
  - [60] A. Ono et al. (TMED), Comparison of heavy-ion transport simulations: Collision integral with pions and  $\Delta$  resonances in a box, Phys. Rev. C **100**, 044617 (2019), arXiv:1904.02888 [nucl-th].
  - [61] M. Colonna et al. (TMED), Comparison of heavy-ion transport simulations: Mean-field dynamics in a box, Phys. Rev. C **104**, 024603 (2021), arXiv:2106.12287 [nucl-th].
  - [62] H. Wolter et al. (TMED), Transport model comparison studies of intermediate-energy heavy-ion collisions, Prog. Part. Nucl. Phys. **125**, 103962 (2022), arXiv:2202.06672 [nucl-th].
  - [63] J. Xu et al. (TMED), Comparing pion production in transport simulations of heavy-ion collisions at 270A MeV under controlled conditions, Phys. Rev. C **109**, 044609 (2024), arXiv:2308.05347 [nucl-th].
  - [64] B. G. Carlsson, J. Dobaczewski, and M. Kortelainen, Local nuclear energy density functional at next-to-next-to-next-to-leading order, Phys. Rev. C **78**, 044326 (2008), [Erratum: Phys.Rev.C 81, 029904 (2010)], arXiv:0807.4925 [nucl-th].
  - [65] F. Raimondi, B. G. Carlsson, and J. Dobaczewski, Effective pseudopotential for energy density functionals with higher order derivatives, Phys. Rev. C **83**, 054311 (2011), arXiv:1103.0682 [nucl-th].
  - [66] B. G. Carlsson and J. Dobaczewski, Convergence of density-matrix expansions for nuclear interactions, Phys. Rev. Lett. **105**, 122501 (2010), arXiv:1003.2543 [nucl-th].
  - [67] J. Dobaczewski, B. G. Carlsson, and M. Kortelainen, The Negele-Vautherin density matrix expansion applied to the Gogny force, J. Phys. G **37**, 075106 (2010), arXiv:1002.3646 [nucl-th].
  - [68] D. Davesne, P. Becker, A. Pastore, and J. Navarro, Infinite matter properties and zero-range limit of non-relativistic finite-range interactions, Annals Phys. **375**, 288 (2016), arXiv:1607.00835 [nucl-th].
  - [69] R. Wang, L.-W. Chen, and Y. Zhou, Extended Skyrme interactions for transport model simulations of heavy-ion collisions, Phys. Rev. C **98**, 054618 (2018), arXiv:1806.03278 [nucl-th].
  - [70] S. Hama, B. C. Clark, E. D. Cooper, H. S. Sherif, and R. L. Mercer, Global Dirac optical potentials for elastic proton scattering from heavy nuclei, Phys. Rev. C **41**, 2737 (1990).
  - [71] E. D. Cooper, S. Hama, B. C. Clark, and R. L. Mercer, Global Dirac phenomenology for proton nucleus elastic scattering, Phys. Rev. C **47**, 297 (1993).
  - [72] R. Wang, L.-W. Chen, and Z. Zhang, Nuclear collective dynamics in the lattice Hamiltonian Vlasov method, Phys. Rev. C **99**, 044609 (2019), arXiv:1902.01256 [nucl-th].
  - [73] R. Wang, Z. Zhang, L.-W. Chen, C. M. Ko, and Y.-G. Ma, Constraining the in-medium nucleon-nucleon cross section from the width of nuclear giant dipole resonance, Phys. Lett. B **807**, 135532 (2020), arXiv:2007.12011 [nucl-th].
  - [74] R. Wang, Z. Zhang, L.-W. Chen, and Y.-G. Ma, Nuclear Collective Dynamics in Transport Model With the Lattice Hamiltonian Method, Front. in Phys. **8**, 330 (2020), arXiv:2010.07790 [nucl-th].
  - [75] Y.-D. Song, R. Wang, Z. Zhang, and Y.-G. Ma, Nuclear giant quadrupole resonance within a transport approach and its constraint on the nucleon effective mass, Phys. Rev. C **104**, 044603 (2021), arXiv:2109.07092 [nucl-th].
  - [76] Y.-D. Song, R. Wang, Z. Zhang, and Y.-G. Ma, In-medium nucleon-nucleon cross sections from characteristics of nuclear giant resonances and nuclear stopping power, Phys. Rev. C **108**, 064603 (2023).
  - [77] R. Wang, Y.-G. Ma, L.-W. Chen, C. M. Ko, K.-J. Sun, and Z. Zhang, Kinetic approach of light-nuclei production in intermediate-energy heavy-ion collisions, Phys. Rev. C **108**, L031601 (2023), arXiv:2305.02988 [nucl-th].
  - [78] W. Reisdorf et al. (FOPI), Systematics of central heavy ion collisions in the 1A GeV regime, Nucl. Phys. A **848**, 366 (2010), arXiv:1005.3418 [nucl-ex].
  - [79] J. Yang, X. Chen, Y. Cui, Y. Liu, Z. Li, and Y. Zhang, Extended Skyrme momentum-dependent potential in asymmetric nuclear matter and transport models, Phys. Rev. C **109**, 054624 (2024), arXiv:2311.04026 [nucl-th].
  - [80] B. P. Abbott et al. (LIGO Scientific, Virgo), GW170817: Measurements of neutron star radii and equation of state, Phys. Rev. Lett. **121**, 161101 (2018), arXiv:1805.11581 [gr-qc].
  - [81] H. T. Cromartie et al. (NANOGrav), Relativistic Shapiro delay measurements of an extremely massive millisecond pulsar, Nature Astron. **4**, 72 (2019), arXiv:1904.06759 [astro-ph.HE].
  - [82] E. Fonseca et al., Refined Mass and Geometric Measurements of the High-mass PSR J0740+6620, Astrophys. J. Lett. **915**, L12 (2021), arXiv:2104.00880 [astro-ph.HE].
  - [83] T. E. Riley et al., A NICER View of PSR J0030+0451: Millisecond Pulsar Parameter Estimation, Astrophys. J. Lett. **887**, L21 (2019), arXiv:1912.05702 [astro-ph.HE].
  - [84] M. C. Miller et al., PSR J0030+0451 Mass and Radius from NICER Data and Implications for the Properties of Neutron Star Matter, Astrophys. J. Lett. **887**, L24 (2019), arXiv:1912.05705 [astro-ph.HE].
  - [85] T. E. Riley et al., A NICER View of the Massive Pulsar PSR J0740+6620 Informed by Radio Timing and XMM-Newton Spectroscopy, Astrophys. J. Lett. **918**, L27 (2021), arXiv:2105.06980 [astro-ph.HE].
  - [86] M. C. Miller et al., The Radius of PSR J0740+6620 from

- NICER and XMM-Newton Data, *Astrophys. J. Lett.* **918**, L28 (2021), arXiv:2105.06979 [astro-ph.HE].
- [87] D. Choudhury et al., A NICER View of the Nearest and Brightest Millisecond Pulsar: PSR J0437–4715, *Astrophys. J. Lett.* **971**, L20 (2024), arXiv:2407.06789 [astro-ph.HE].
- [88] S.-P. Wang, R. Wang, J.-T. Ye, and L.-W. Chen, Extended Skyrme effective interactions for transport models and neutron stars, *Phys. Rev. C* **109**, 054623 (2024), arXiv:2312.17105 [nucl-th].
- [89] N. K. Patra, S. M. A. Imam, B. K. Agrawal, A. Mukherjee, and T. Malik, Nearly model-independent constraints on dense matter equation of state in a Bayesian approach, *Phys. Rev. D* **106**, 043024 (2022), arXiv:2203.08521 [nucl-th].
- [90] J. C. Yang et al., High Intensity heavy ion Accelerator Facility (HIAF) in China, *Nucl. Instrum. Meth. B* **317**, 263 (2013).
- [91] Z. Xiaohong, Physics Opportunities at the New Facility HIAF, *Nucl. Phys. Rev.* **35**, 339 (2018).
- [92] G. Agakishiev et al. (HADES), The High-Acceptance Dielectron Spectrometer HADES, *Eur. Phys. J. A* **41**, 243 (2009), arXiv:0902.3478 [nucl-ex].
- [93] J. Adamczewski-Musch et al. (HADES), Centrality determination of Au + Au collisions at 1.23A GeV with HADES, *Eur. Phys. J. A* **54**, 85 (2018), arXiv:1712.07993 [nucl-ex].
- [94] J. Adamczewski-Musch et al. (HADES), Directed, Elliptic, and Higher Order Flow Harmonics of Protons, Deuterons, and Tritons in Au + Au Collisions at  $\sqrt{s_{NN}} = 2.4$  GeV, *Phys. Rev. Lett.* **125**, 262301 (2020), arXiv:2005.12217 [nucl-ex].
- [95] J. Adamczewski-Musch et al. (HADES), Proton, deuteron and triton flow measurements in Au+Au collisions at  $\sqrt{s_{NN}} = 2.4$  GeV, *Eur. Phys. J. A* **59**, 80 (2023), arXiv:2208.02740 [nucl-ex].
- [96] C. Sturm, B. Sharkov, and H. Stöcker, 1, 2, 3 ... FAIR!, *Nucl. Phys. A* **834**, 682c (2010).
- [97] T. Ablyazimov et al. (CBM), Challenges in QCD matter physics –The scientific programme of the Compressed Baryonic Matter experiment at FAIR, *Eur. Phys. J. A* **53**, 60 (2017), arXiv:1607.01487 [nucl-ex].
- [98] H. Sako et al., Towards the heavy-ion program at J-PARC, *Nucl. Phys. A* **931**, 1158 (2014).
- [99] H. Sako et al. (J-PARC Heavy-Ion), Studies of high density baryon matter with high intensity heavy-ion beams at J-PARC, *Nucl. Phys. A* **956**, 850 (2016).
- [100] H. Sako (J-PARC-HI), Studies of extremely dense matter in heavy-ion collisions at J-PARC, *Nucl. Phys. A* **982**, 959 (2019).
- [101] V. Kekelidze, A. Kovalenko, R. Lednicky, V. Matveev, I. Meshkov, A. Sorin, and G. Trubnikov, Prospects for the dense baryonic matter research at NICA, *Nucl. Phys. A* **956**, 846 (2016).
- [102] M. Kapishin (BM@N), The fixed target experiment for studies of baryonic matter at the Nuclotron (BM@N), *Eur. Phys. J. A* **52**, 213 (2016).
- [103] B.-A. Li, High density behavior of nuclear symmetry energy and high-energy heavy ion collisions, *Nucl. Phys. A* **708**, 365 (2002), arXiv:nucl-th/0206053.
- [104] K. A. Brueckner and J. Dabrowski, Symmetry Energy and the Isotopic Spin Dependence of the Single-Particle Potential in Nuclear Matter, *Phys. Rev.* **134**, B722 (1964).
- [105] J. Dabrowski and P. Haensel, Spin and isospin dependence of the single-particle potential in nuclear matter, *Phys. Lett. B* **42**, 163 (1972).
- [106] J. Dabrowski and P. Haensel, Spin and Spin-Isospin Symmetry Energy of Nuclear Matter, *Phys. Rev. C* **7**, 916 (1973).
- [107] C. Xu, B.-A. Li, and L.-W. Chen, Symmetry energy, its density slope, and neutron-proton effective mass splitting at normal density extracted from global nucleon optical potentials, *Phys. Rev. C* **82**, 054607 (2010), arXiv:1006.4321 [nucl-th].
- [108] C. Xu, B.-A. Li, L.-W. Chen, and C. M. Ko, Analytical relations between nuclear symmetry energy and single-nucleon potentials in isospin asymmetric nuclear matter, *Nucl. Phys. A* **865**, 1 (2011), arXiv:1004.4403 [nucl-th].
- [109] R. Chen, B.-J. Cai, L.-W. Chen, B.-A. Li, X.-H. Li, and C. Xu, Single-nucleon potential decomposition of the nuclear symmetry energy, *Phys. Rev. C* **85**, 024305 (2012), arXiv:1112.2936 [nucl-th].
- [110] N. M. Hugenholtz and L. van Hove, A theorem on the single particle energy in a Fermi gas with interaction, *Physica* **24**, 363 (1958).
- [111] L. Satpathy, V. Maheswari, and R. Nayak, Finite nuclei to nuclear matter: a leptodermous approach, *Physics Reports* **319**, 85 (1999).
- [112] D. Davesne, A. Pastore, and J. Navarro, Skyrme effective pseudopotential up to the next-to-next-to-leading order, *J. Phys. G* **40**, 095104 (2013), arXiv:1307.2349 [nucl-th].
- [113] D. Davesne, A. Pastore, and J. Navarro, Fitting N<sup>3</sup>LO pseudo-potentials through central plus tensor Landau parameters, *J. Phys. G* **41**, 065104 (2014), arXiv:1401.7914 [nucl-th].
- [114] D. Davesne, J. Meyer, A. Pastore, and J. Navarro, Partial wave decomposition of the N3LO equation of state, *Phys. Scripta* **90**, 114002 (2015), arXiv:1412.1934 [nucl-th].
- [115] D. Davesne, J. Navarro, P. Becker, R. Jodon, J. Meyer, and A. Pastore, Extended Skyrme pseudopotential deduced from infinite nuclear matter properties, *Phys. Rev. C* **91**, 064303 (2015), arXiv:1503.01370 [nucl-th].
- [116] D. Davesne, A. Pastore, and J. Navarro, Extended Skyrme Equation of State in asymmetric nuclear matter, *Astron. Astrophys.* **585**, A83 (2016), arXiv:1509.05744 [nucl-th].
- [117] B. G. Carlsson, J. Dobaczewski, J. Toivanen, and P. Vesely, Solution of self-consistent equations for the N3LO nuclear energy density functional in spherical symmetry. The program HOSPHE (v1.00), *Comput. Phys. Commun.* **181**, 1641 (2010), arXiv:0912.3230 [nucl-th].
- [118] P. Becker, D. Davesne, J. Meyer, J. Navarro, and A. Pastore, Solution of Hartree-Fock-Bogoliubov equations and fitting procedure using the N2LO Skyrme pseudopotential in spherical symmetry, *Phys. Rev. C* **96**, 044330 (2017), arXiv:1707.08622 [nucl-th].
- [119] Z. Zhang and L.-W. Chen, Bayesian inference of the symmetry energy and the neutron skin in Ca48 and Pb208 from CREX and PREX-2, *Phys. Rev. C* **108**, 024317 (2023), arXiv:2207.03328 [nucl-th].
- [120] V. M. Kolomietz and S. Shlomo, Bulk and isospin instabilities in hot nuclear matter, *Phys. Rev. C* **95**, 054613 (2017).

- [121] A. Lane, Isobaric spin dependence of the optical potential and quasi-elastic (p, n) reactions, *Nucl. Phys.* **35**, 676 (1962).
- [122] M. Jaminon and C. Mahaux, Effective Masses in Relativistic Approaches to the Nucleon Nucleus Mean Field, *Phys. Rev. C* **40**, 354 (1989).
- [123] B.-A. Li, B.-J. Cai, L.-W. Chen, and J. Xu, Nucleon Effective Masses in Neutron-Rich Matter, *Prog. Part. Nucl. Phys.* **99**, 29 (2018), arXiv:1801.01213 [nucl-th].
- [124] L. Beal, D. Hill, R. Martin, and J. Hedengren, Gekko optimization suite, *Processes* **6**, 106 (2018).
- [125] B. Ter Haar and R. Malfliet, Nucleons, Mesons and Deltas in Nuclear Matter. A Relativistic Dirac-Bruckner Approach, *Phys. Rept.* **149**, 207 (1987).
- [126] X.-H. Li, W.-J. Guo, B.-A. Li, L.-W. Chen, F. J. Fatoyev, and W. G. Newton, Neutron-proton effective mass splitting in neutron-rich matter at normal density from analyzing nucleon-nucleus scattering data within an isospin dependent optical model, *Phys. Lett. B* **743**, 408 (2015), arXiv:1403.5577 [nucl-th].
- [127] Z. Zhang and L.-W. Chen, Isospin splitting of the nucleon effective mass from giant resonances in  $^{208}\text{Pb}$ , *Phys. Rev. C* **93**, 034335 (2016), arXiv:1507.04675 [nucl-th].
- [128] J. Pu, Z. Zhang, and L.-W. Chen, Nuclear matter fourth-order symmetry energy in nonrelativistic mean-field models, *Phys. Rev. C* **96**, 054311 (2017), arXiv:1708.02132 [nucl-th].
- [129] J. Xu, L.-W. Chen, B.-A. Li, and H.-R. Ma, Nuclear constraints on properties of neutron star crusts, *Astrophys. J.* **697**, 1549 (2009), arXiv:0901.2309 [astro-ph.SR].
- [130] J. Carriere, C. J. Horowitz, and J. Piekarewicz, Low mass neutron stars and the equation of state of dense matter, *Astrophys. J.* **593**, 463 (2003), arXiv:nucl-th/0211015.
- [131] J. Xu, L.-W. Chen, B.-A. Li, and H.-R. Ma, Locating the inner edge of neutron star crust using terrestrial nuclear laboratory data, *Phys. Rev. C* **79**, 035802 (2009), arXiv:0807.4477 [nucl-th].
- [132] G. Baym, C. Pethick, and P. Sutherland, The Ground State of Matter at High Densities: Equation of State and Stellar Models, *Astrophys. J.* **170**, 299 (1971).
- [133] R. C. Tolman, Static solutions of Einstein's field equations for spheres of fluid, *Phys. Rev.* **55**, 364 (1939).
- [134] J. R. Oppenheimer and G. M. Volkoff, On massive neutron cores, *Phys. Rev.* **55**, 374 (1939).
- [135] P. Hillmann, J. Steinheimer, T. Reichert, V. Gaebel, M. Bleicher, S. Sombun, C. Herold, and A. Limphirat, First, second, third and fourth flow harmonics of deuterons and protons in Au+Au reactions at 1.23 AGeV, *J. Phys. G* **47**, 055101 (2020), arXiv:1907.04571 [nucl-th].
- [136] P. Parfenov, Model Study of the Energy Dependence of Anisotropic Flow in Heavy-Ion Collisions at  $\sqrt{s_{NN}} = 2\text{--}4.5$  GeV, *Particles* **5**, 561 (2022).
- [137] H. Du, G.-F. Wei, and G.-C. Yong, Directed and elliptic flows of protons and deuterons in HADES Au+Au collisions at sNN=2.4 GeV, *Phys. Lett. B* **839**, 137823 (2023), arXiv:2302.07037 [nucl-th].
- [138] L.-M. Fang, Y.-G. Ma, and S. Zhang, Simulation of collective flow of protons and deuterons in Au+Au collisions at Ebeam=1.23A GeV with the isospin-dependent quantum molecular dynamics model, *Phys. Rev. C* **107**, 044904 (2023), arXiv:2301.04279 [nucl-th].
- [139] B.-A. Li and W.-J. Xie, Bayesian inference of in-medium baryon-baryon scattering cross sections from HADES proton flow data, *Nucl. Phys. A* **1039**, 122726 (2023), arXiv:2303.10474 [nucl-th].
- [140] H.-J. Liu, H.-G. Cheng, and Z.-Q. Feng, Collective flows of clusters and pions in heavy-ion collisions at GeV energies, *Phys. Rev. C* **108**, 024614 (2023), arXiv:2304.03913 [nucl-th].
- [141] J. Mohs, S. Spies, and H. Elfner, Constraints on the Equation of State of Nuclear Matter from Systematically Comparing SMASH Calculations to HADES Data, (2024), arXiv:2409.16927 [nucl-th].
- [142] S. Lan, Z. Liu, L. Liu, and S. Shi, Elliptic and quadrangular flow of protons in the high baryon density region, (2024), arXiv:2411.06196 [nucl-th].
- [143] J. Steinheimer, T. Reichert, Y. Nara, and M. Bleicher, Momentum dependent potentials from a parity doubling CMF model in UrQMD: Results on flow and particle production, (2024), arXiv:2410.01742 [hep-ph].
- [144] V. Kireyeu, V. Voronyuk, M. Winn, S. Gläsel, J. Aichelin, C. Blume, E. Bratkovskaya, G. Coci, and J. Zhao, Constraints on the equation-of-state from low energy heavy-ion collisions within the PHQMD microscopic approach with momentum-dependent potential, (2024), arXiv:2411.04969 [nucl-th].
- [145] T. Reichert and J. Aichelin, Untangling the interplay of the Equation-of-State and the Collision Term towards the generation of Directed and Elliptic Flow at intermediate energies, (2024), arXiv:2411.12908 [nucl-th].
- [146] C.-Y. Wong, Dynamics of nuclear fluid. VIII. Time-dependent Hartree-Fock approximation from a classical point of view, *Phys. Rev. C* **25**, 1460 (1982).
- [147] R. J. Lenk and V. R. Pandharipande, Nuclear mean field dynamics in the lattice Hamiltonian Vlasov method, *Phys. Rev. C* **39**, 2242 (1989).
- [148] J. Aichelin, A. Rosenhauer, G. Peilert, H. Stoecker, and W. Greiner, Importance of Momentum Dependent Interactions for the Extraction of the Nuclear Equation of State From High-energy Heavy Ion Collisions, *Phys. Rev. Lett.* **58**, 1926 (1987).
- [149] Y. Zhang and Z. Li, Elliptic flow and system size dependence of transition energies at intermediate energies, *Phys. Rev. C* **74**, 014602 (2006), arXiv:nucl-th/0606004.
- [150] Z.-Q. Feng, Momentum dependence of the symmetry potential and its influence on nuclear reactions, *Phys. Rev. C* **84**, 024610 (2011), arXiv:1106.3797 [nucl-th].
- [151] Y. Wang, C. Guo, Q. Li, H. Zhang, Y. Leifels, and W. Trautmann, Constraining the high-density nuclear symmetry energy with the transverse-momentum dependent elliptic flow, *Phys. Rev. C* **89**, 044603 (2014), arXiv:1403.7041 [nucl-th].
- [152] Y. Liu, Y. Wang, Y. Cui, C.-J. Xia, Z. Li, Y. Chen, Q. Li, and Y. Zhang, Insights into the pion production mechanism and the symmetry energy at high density, *Phys. Rev. C* **103**, 014616 (2021), arXiv:2006.15861 [nucl-th].
- [153] C. B. Das, S. D. Gupta, C. Gale, and B.-A. Li, Momentum dependence of symmetry potential in asymmetric nuclear matter for transport model calculations, *Phys. Rev. C* **67**, 034611 (2003), arXiv:nucl-th/0212090.
- [154] M. Isse, A. Ohnishi, N. Otuka, P. K. Sahu, and Y. Nara, Mean-field effects on collective flows in high-energy heavy-ion collisions from AGS to SPS energies, *Phys.*

- Rev. C **72**, 064908 (2005), arXiv:nucl-th/0502058.
- [155] J. Rizzo, M. Colonna, V. Baran, M. Di Toro, H. H. Wolter, and M. Zielinska-Pfabe, Isospin dynamics in peripheral heavy ion collisions at Fermi energies, Nucl. Phys. A **806**, 79 (2008).
  - [156] M. D. Cozma, Y. Leifels, W. Trautmann, Q. Li, and P. Russotto, Toward a model-independent constraint of the high-density dependence of the symmetry energy, Phys. Rev. C **88**, 044912 (2013), arXiv:1305.5417 [nucl-th].
  - [157] J. Su, L. Zhu, C.-Y. Huang, W.-J. Xie, and F.-S. Zhang, Correlation between symmetry energy and effective  $k$ -mass splitting with an improved isospin- and momentum-dependent interaction, Phys. Rev. C **94**, 034619 (2016).
  - [158] N. Ikeno and A. Ono, Collision integral with momentum-dependent potentials and its impact on pion production in heavy-ion collisions, Phys. Rev. C **108**, 044601 (2023), arXiv:2307.02395 [nucl-th].
  - [159] P. Danielewicz and G. F. Bertsch, Production of deuterons and pions in a transport model of energetic heavy ion reactions, Nucl. Phys. A **533**, 712 (1991).
  - [160] J. Cugnon, J. Vandermeulen, and D. L'Hote, Simple parametrization of cross-sections for nuclear transport studies up to the GeV range, Nucl. Instrum. Meth. B **111**, 215 (1996).
  - [161] J. Weil et al. (SMASH), Particle production and equilibrium properties within a new hadron transport approach for heavy-ion collisions, Phys. Rev. C **94**, 054905 (2016), arXiv:1606.06642 [nucl-th].
  - [162] A. Drago, A. Lavagno, G. Pagliara, and D. Pigato, Early appearance of  $\Delta$  isobars in neutron stars, Phys. Rev. C **90**, 065809 (2014), arXiv:1407.2843 [astro-ph.SR].
  - [163] B.-J. Cai, F. J. Fattoyev, B.-A. Li, and W. G. Newton, Critical density and impact of  $\Delta(1232)$  resonance formation in neutron stars, Phys. Rev. C **92**, 015802 (2015), arXiv:1501.01680 [nucl-th].
  - [164] M. D. Cozma, The impact of energy conservation in transport models on the  $\pi^-/\pi^+$  multiplicity ratio in heavy-ion collisions and the symmetry energy, Phys. Lett. B **753**, 166 (2016), arXiv:1409.3110 [nucl-th].
  - [165] B.-A. Li, Symmetry potential of  $\Delta(1232)$  resonance and its effects on the  $\pi^-/\pi^+$  ratio in heavy-ion collisions near the pion-production threshold, Phys. Rev. C **92**, 034603 (2015), arXiv:1507.03279 [nucl-th].
  - [166] V. S. Uma Maheswari, C. Fuchs, A. Faessler, Z. S. Wang, and D. S. Kosov, Role of isospin dependent mean field in pion production in heavy ion reactions, Phys. Rev. C **57**, 922 (1998), arXiv:nucl-th/9708047.
  - [167] B.-A. Li, Probing the high density behavior of nuclear symmetry energy with high-energy heavy ion collisions, Phys. Rev. Lett. **88**, 192701 (2002), arXiv:nucl-th/0205002.
  - [168] G. Ferini, M. Colonna, T. Gaitanos, and M. Di Toro, Aspects of particle production in charge asymmetric matter, Nucl. Phys. A **762**, 147 (2005), arXiv:nucl-th/0504032.
  - [169] T. Song and C. M. Ko, Modifications of the pion-production threshold in the nuclear medium in heavy ion collisions and the nuclear symmetry energy, Phys. Rev. C **91**, 014901 (2015).
  - [170] Z. Zhang and C. M. Ko, Effects of energy conservation on equilibrium properties of hot asymmetric nuclear matter, Phys. Rev. C **97**, 014610 (2018), arXiv:1712.03286 [nucl-th].
  - [171] A. M. Poskanzer and S. A. Voloshin, Methods for analyzing anisotropic flow in relativistic nuclear collisions, Phys. Rev. C **58**, 1671 (1998), arXiv:nucl-ex/9805001.
  - [172] L.-W. Chen, C. M. Ko, and Z.-W. Lin, Partonic effects on high order anisotropic flows in relativistic heavy ion collisions, Phys. Rev. C **69**, 031901 (2004), arXiv:nucl-th/0312124.
  - [173] L.-W. Chen, V. Greco, C. M. Ko, and P. F. Kolb, Pseudorapidity dependence of anisotropic flows in relativistic heavy-ion collisions, Phys. Lett. B **605**, 95 (2005), arXiv:nucl-th/0408021.
  - [174] G.-F. Wei and Y.-L. Zhao, Kaon production in the HADES experiment in Au+Au collisions at  $s_{NN}=2.4$  GeV, Phys. Rev. C **110**, 054615 (2024), arXiv:2402.13570 [nucl-th].
  - [175] G.-C. Yong, B.-A. Li, Z.-G. Xiao, and Z.-W. Lin, Probing the high-density nuclear symmetry energy with the  $\Xi^-/\Xi^0$  ratio in heavy-ion collisions at  $s_{NN}\approx 3$  GeV, Phys. Rev. C **106**, 024902 (2022), arXiv:2206.10766 [nucl-th].
  - [176] Q.-f. LI, Z.-x. LI, E.-g. Zhao, and R. K. Gupta, Sigma-/Sigma+ ratio as a candidate for probing the density dependence of the symmetry potential at high nuclear densities, Phys. Rev. C **71**, 054907 (2005), arXiv:nucl-th/0504065.
  - [177] Y. Ye, Y. Wang, J. Steinheimer, Y. Nara, H.-j. Xu, P. Li, D. Lu, Q. Li, and H. Stoecker, Cumulants of the baryon number from central Au+Au collision at  $E_{lab} = 1.23$  GeV/nucleon reveal the nuclear mean-field potentials, Phys. Rev. C **98**, 054620 (2018), arXiv:1808.06342 [nucl-th].
  - [178] Y. Wang, Q. Li, Y. Leifels, and A. Le Fèvre, Study of the nuclear symmetry energy from the rapidity-dependent elliptic flow in heavy-ion collisions around 1 GeV/nucleon regime, Phys. Lett. B **802**, 135249 (2020).
  - [179] Y.-Y. Liu, J.-P. Yang, Y.-J. Wang, Q.-F. Li, Z.-X. Li, C.-J. Xia, and Y.-X. Zhang, A perspective on describing nucleonic flow and pionic observables within the ultra-relativistic quantum molecular dynamics model, Nucl. Sci. Tech. **36**, 45 (2025).
  - [180] Z.-Q. Feng, Nuclear dynamics and particle production near threshold energies in heavy-ion collisions, Nucl. Sci. Tech. **29**, 40 (2018), arXiv:1802.10294 [nucl-th].